INFLUENCE OF OXIDE LAYERS ON THE MICROWAVE SURFACE RESISTANCE OF SUPERCONDUCTING NIOBIUM

A Thesis

Presented to the Faculty of the Graduate School

of Cornell University

in Partial Fulfillment of the Requirements for the Degree of

Doctor of Philosophy

by

Fred Lawrence Palmer

January 1988

INFLUENCE OF OXIDE LAYERS ON THE MICROWAVE SURFACE RESISTANCE OF SUPERCONDUCTING NIOBIUM

Fred Lawrence Palmer, Ph.D.

Cornell University 1988

We have measured the influence of oxide layers grown at room temperature on the microwave surface resistance of superconducting niobium by comparing the quality factors of oxidized and unoxidized cavities. We have also investigated the microwave and surface properties that are altered when oxide layers are heated to temperatures near 300°C. Auger spectroscopy was used to determine a procedure for producing clean oxygen-free surfaces by ultra-high-vacuum firing the niobium at 1100 - 1400°C. A special vacuum furnace was then constructed so that the 8.6 Ghz. niobium cavities could be fired at these temperatures and then taken to a cryostat for testing without any exposure to air. These cavities exhibited residual resistances of 6 - 12 nΩ. Exposure of niobium to oxygen at room temperature is known to create a ~15Å thick layer consisting mostly of Nb_2O_5. This layer changed the temperature dependent BCS resistance by less than 2%, and changed the low temperature residual resistance by less than 1.5 nΩ.

Several cavities were heated to 325° for 10 minutes to demonstrate that the "clean" cavities were not contaminated with oxygen. Heating an oxidized cavity causes the oxide layer to dissolve into the first ~1000

A of the bulk metal. The resulting oxygen-rich layers had ~20% less BCS resistance due to the reduced mean free path, and had residual resistances of 40 nΩ or more. The "clean" cavities were unaffected by heating, demonstrating that they were actually oxide-free.

Several other measurements were made on oxidized cavities that had been heated to temperatures near 300°. The RF critical temperature of these cavities was reduced by ~5%; the energy gap was unaffected (±1%); and the dependence of residual resistance on ambient magnetic field during cooldown was increased from ~0.4μΩ/gauss to ~1μΩ/gauss. Comparison of these cavities with the XPS data of Kirby et al. showed that the increase in residual resistance did not correlate with the presence of any specific oxide, but appeared to correlate with the concentration of dissolved oxygen near the surface.

BIOGRAPHICAL SKETCH

Fred Palmer was born on April 9, 1951 in Superior, Wisconsin. He attended Emory University and Georgia State University (both located in Atlanta) eventually receiving a B.S. from Emory in 1973. He then attended Cornell University from 1974 to 1978, and received an M.S. in theoretical physics (solid state) in May of 1978. He worked for three years on particle detectors at the Cornell Laboratory of Nuclear Studies but then returned to graduate school in 1981. He served a brief jail term in 1971 in connection with anti-war demonstrations, and was the treasurer of the local chapter of United Campuses to Prevent Nuclear War from 1983 to 1987. In 1987 he finally finished graduate school, married Elaine Nancy Schuler, and they lived happily ever after.

ACKNOWLEDGEMENTS

I would like to thank Maury Tigner for many years of advice, support, and careful editing, which has continued to the present time in spite of his demanding responsibilities with the Superconducting Supercollider. The day to day assistance and advice of Hasan Padamsee has also been extremely useful. I am indebted to Wilson Ho for many valuable conversations and for the use of his Auger spectrometer. The work of Bob Kirby and his research group has greatly enhanced our understanding of the material covered by this thesis. Conversations with Joe Amato, Vinay Ambegaokar, Peter Kneisel, Kathy Krafft, and Ron Sundelin have also been particularly useful. Much of the apparatus could not have been built without the advice of Joe Kirchgessner and Larry Phillips, as well as the assistance and expertise of Elsa Adrian, Gerhart Hellman, and Randy Miller. Finally I would like to thank Michael Pickup for tolerating me as an office mate for many years and for extensive help with computers and electronics, and Elaine Schuler for her endless patience and excellent banana bread.

TABLE OF CONTENTS

TABLE OF CONTENTS (CONTINUED)

TABLE OF CONTENTS (CONTINUED)

LIST OF TABLES

LIST OF FIGURES

LIST OF FIGURES (CONTINUED)

1. INTRODUCTION

1.1 Description of the problem

When a superconductor is cooled below its critical temperature (T_c), its DC electrical resistance drops immediately to zero, but, at radio frequencies (RF ~ 10^8 to 10^{10} cycles per second), the resistance never reaches zero. Instead, as the temperature goes below T_c, the resistance decreases rapidly as predicted by the BCS theory.{1,2} At much lower temperatures, the observed resistance approaches some constant value, while the theoretical value continues to decline toward zero. This sample-dependent empirical constant is called residual resistance or residual surface resistance, since, at high frequencies, electrical current in any good conductor is always confined to a thin layer near the surface. Known causes of residual resistance in niobium include surface defects such as dust, inclusions, chemical residues, and cracks or splatters from welds. Other likely contributors include grain boundaries, strain from forming or machining, or more fundamental mechanisms such as direct generation of phonons by the RF electric field.

The principal goal of this thesis is to determine the contribution of the native oxide layer to the surface resistance of niobium. Niobium oxidizes very rapidly when exposed to room temperature oxygen or air, forming a layer of mostly Nb_2O_5 that reaches 10 - 20 angstroms within seconds, and then grows more slowly to ~50 Å after several days. The

contribution to residual resistance from this layer is particularly important since its presence is almost unavoidable in many cases of practical interest.

1.1 Applications of Low Surface Resistance Superconductors

Most applications and even most measurements of RF superconductivity involve the use of resonant cavities. A cavity is a hollow structure inside which electric and magnetic fields oscillate at one or more specific frequencies. Lowering the surface resistance of a cavity reduces the amount of power needed to maintain fields of a given intensity in the cavity. It also improves the frequency stability and usually increases the maximum field which can be obtained before the cavity is driven into a normal (as opposed to superconducting) state. Presently, superconducting cavities can be operated continuously at fields of 5 to 25 megavolts per meter, while continuously operating copper cavities are limited to ~1 MV/m, although copper cavities can reach more than 100 MV/m for very short (10 - 100μs) pulses. Potential applications of superconducting cavities range from the most fascinating to the most deplorable of human activities. Cavities are being developed for use in particle accelerators for elementary particle or nuclear research, for free electron lasers with possible application ranging from neurosurgery to incendiary weapons, and for precision timers with applications in basic research or for spacecraft navigation.

A) Accelerators

Historically, superconducting cavities were developed in order to increase the efficiency of accelerators used in elementary particle or nuclear physics. Cavities have been used in accelerators at HEPL (Stanford), Stony Brook, and Argonne, and plans are underway to install them at CERN (Geneva), DESY (W. Germany), KEK, (Japan), and CEBAF (Virginia). Considerable effort is also underway to develop cavities for a ~TeV electron linac.{3} Assuming such a linac can be operated at its optimum electrical field, then both the capital cost and the power consumption are roughly proportional to $1/\sqrt{fQ}$, where f is the frequency, and Q is the (dimensionless) quality factor of the cavities. The quality factor is related to the surface resistance (R) by Q = G/R, where G depends only on the shape of the cavity. (For electron accelerator cavities, G is usually 250 to 300 Ω.) At $fQ = 10^{11}$ Ghz, the cost of a 1 TeV machine would be around 5 billion dollars, and the power consumption would be roughly 300 Mw. The optimum gradient, in megavolts per meter, is roughly $\sqrt{fQ/10^{9}\text{Ghz}}$, or 10 MV/m at $fQ = 10^{11}$. The values just listed for the gradient and fQ are about a factor of 2 to 5 above what can presently be achieved in mass production, and the costs estimates show that an additional factor of 10 in fQ (i.e. 10 times lower surface resistance) and a factor of 3 in the gradient would be highly desirable.

B) Free electron lasers

There is a small but expanding effort to use superconducting linacs as injectors for free electron lasers (FEL's).{4} Although it is too

early to be certain what applications this device may find, it is hard to make an comprehensive estimate that is completely encouraging. The brighter side of the story was the subject of the 1984 conference on the applications of free electron lasers.{5} Speakers at the conference stated that FEL's would be useful for several kinds of spectroscopy and for chemical catalysis, and that modest improvements in the treatment or surgical removal of certain types of tumors could be realized. Applications in fusion and uranium isotope separation were described as less likely.

Even though, at the time of the conference, four out of five of the operating FEL's were at least partially funded by military agencies, {4,6,7,8} there was almost no mention of possible military applications. The principal exceptions were the isotope separation paper, and a brief paper{9} which argued that FEL's were better suited for pulsed radar than for civilian communications. The void has been at least partially filled by the APS study of directed energy weapons{10}. Although the text of this study is rigorously confined to a discussion of unlikely applications in ballistic missile defense, the graphs showing power requirements and mirror diameters cover the range of activities that incendiary weapons are presently used for. The report concludes that additional research is necessary before the feasibility of ballistic missile defense can be determined. However, their discussion implies that devices that deliver several thousand watts per square centimeter at distances of several miles can probably be built.

Since most of the RF power in a FEL injector is consumed by the electron beam, the principal effect of using lower surface resistance

superconductors would be to increase the field strength and thus reduce the size of the device.

C) Other applications

Many other applications of superconducting cavities make use of their excellent frequency stability.{11} Superconducting-cavity-stabilized oscillators have achieved stabilities of $f/\Delta f = 10^{15}$ or more, making them useful as secondary time standards and for spacecraft navigation. Superconducting cavities have also been used to measure the loss tangents of very good dielectrics, and to detect extremely faint microwave signals. Open resonators made from superconductors can be used to measure mechanical motions of less than an angstrom.{12} These devices may be used to make accurate measurements of the gravitational constant or to search for gravity waves.

1.3 Description of Thesis

A) Research overview

The goal of this experiment was to measure the influence of oxide layers on the microwave surface resistance of superconducting niobium by comparing the quality factors of oxidized and oxide-free cavities. The first step was to use auger spectroscopy to determine a procedure for high-temperature removal of the oxide layer. We found that UHV firing at 1200 - 1400°C for a few minutes was sufficient to produce a clean surface if the niobium was sufficiently pure.

A cavity and furnace arrangement was constructed so that the cavity could be heated to 1400° under vacuum, sealed with an all-metal valve, and moved to a cryostat for testing without any exposure to air. Later, the valve could be opened, and the cavity exposed to controlled amounts of oxygen and retested.

Since it was found that exposure to oxygen affected neither the residual resistance (±1.5nΩ) nor the temperature dependent BCS resistance (±2%) of the cleaned cavities, and since the pressure inside the cavity could not be measured directly, making it hard to assess the contamination that occurred in between the cooldown from T > 1000° and the cryotest, it therefore was necessary to find a way to determine whether or not the cleaned cavities were actually oxide-free. The technique of heating the (evacuated) cavities to 325°C for 10 minutes was developed for this purpose. At this temperature, the surface oxides decompose, and the oxygen diffuses into the metal, creating an oxygen-rich layer which is a few thousand angstroms thick. This layer exhibits a reduced BCS resistance and an increased residual resistance. Oxide-free cavities were unaffected by this heat treatment, implying that the "clean" cavities were covered with no more than one or two monolayers of oxide.

Several experiments were done on cavities which had been oxidized and then heated to better understand the oxygen-rich layers and the processes by which they form. These experiments included measurements of the BCS resistance and the residual resistance, as well as measurements of the (radio frequency) critical temperature, the normal surface resistance, and the dependence of the residual resistance on the ambient magnetic field during cooldown.

B) Thesis outline

Chapter two describes the present state of knowledge about superconducting surface resistance. It begins with a description of the computer programs that have been written to calculate surface resistances based on the BCS theory. A couple of approximate formulas are also discussed. The next section describes experimental data, in particular, some typical values of residual resistance, as well as the minimum values achieved to date at several frequencies. Finally there is a discussion of various known or possible causes of residual resistance. The effect of oxide layers is deferred to the next chapter.

Chapter three discusses oxide layers on niobium. The primary emphasis is on layers which are grown at room temperature, although a description of layers grown at higher temperatures is included because of the influence which this information has had on the study of room-temperature oxidation. The effect of oxidation on the penetration depth, the critical temperature, and on the tunnel junction characteristics of niobium is also discussed. Several studies linking oxygen to residual resistance are described. The chapter ends with a summary of high temperature techniques for removal of oxide layers.

Chapter four is on experimental procedures. It begins with an overview of the entire project explaining the motivation behind the various experiments that were done. The remainder of the chapter describes specific procedures and the associated apparatuses.

Chapter five contains the experimental results. It begins with Auger studies which found a procedure for removing oxide layers from niobium. Next there is a comparison of the residual resistances of

oxidized and unoxidized cavities. These data are also organized to show separately the performance of chemical polished and UHV fired cavities. The effect of ambient magnetic fields on the residual resistance is shown primarily to estimate the errors induced by these fields, and the effect of niobium purity on the BCS part of the resistance is shown.

The chapter continues with results from cavities where the oxide layer had been heated to temperatures near 300C for a few minutes. This procedure was first used to measure the amount of oxide on the inner surface of the cavities, but the results are interesting in themselves. The dependence of these results on the temperature to which the layer was heated was studied, as well as the effect of this procedure on the RF critical temperature and the normal surface resistance. Data were analysed carefully to see if the energy gap was altered by any of the above procedures. All of these results are shown explicitly, although no significant change was observed in any case. Next is an account of XPS and other spectroscopic studies done by Kirby et al. on the behavior of oxide layers near 300 degrees, followed by a discussion which links the spectroscopic data and the RF data in a coherent picture of the behavior of oxide layers at these temperatures.

Chapter six summarizes the results of the thesis and discusses unanswered questions and possible directions for future research.

2. SURFACE RESISTANCE

2.1 BCS Theory of Surface Resistance

Calculations of the superconducting surface resistance based on the BCS theory{13} were done by Mattis and Bardeen{1}, who used the formalism of the original BCS paper,{13} and by Abrikosov et al,{14} who used the temperature-Greens-function formalism. Both calculations use a momentum independent gap with a temperature dependence given by the BCS formula. In either case, the surface resistance is a complicated multiple integral that depends on temperature and frequency as well as four material parameters: the mean free path,l; the fermi velocity, v_f; the temperature dependent energy gap, $\Delta(T)$; and the density of states at the fermi surface, N. Computer programs which evaluate these expressions were written by Turneaure and Weissman,{15} and by Halbritter.{16} Turneaure used the Mattis and Bardeen result, while Halbritter used that of Abrikosov. Since real materials do not precisely follow the BCS formula, $\Delta_o/T_c = 1.76$, both programs allow the BCS formula for Δ as a function of T to be rescaled so as to give the observed values of both the critical temperature and the zero temperature gap. The two programs were compared by Wilson{17} using parameters for lead and for niobium. Their output is practically identical over the range from 1.85° to 4.2° and from 1 to 11 Ghz. except that Halbritter's results are consistently 9 or 10 percent lower than Turneaure's.

Experimental measurements of superconducting surface resistance are in good agreement with calculated values over a wide range of temperatures and frequencies.{15,16} Although most of the input parameters for the programs cannot be independently verified to better than 10%, the "standard" values given earlier along with a reasonable estimate for the mean free path may be used to predict the surface resistance of niobium to within ~5%. Similar results can be obtained with lead. Measurements have been made from less than 0.1 Ghz to more than 10 Ghz without any significant deviation from theory, except at low temperatures where the residual resistance dominates. Some data are now available on the variation of surface resistance with mean free path, and these results are also in reasonable agreement with theory.{18}

There are two approximate formulae for BCS resistance which are frequently used in data analysis. The more accurate of these is the "Pippard limit" (infinite coherence length and mean free path) formula of Abrikosov:{2}

$$[2.1] \qquad \frac{R}{R_n} = \frac{4}{3\pi}\left(\frac{\hbar\omega}{\pi\Delta}\right)^{1/3}\left(\frac{\hbar\omega}{kT}\right)\ln\left(\frac{2.2\ kT}{\hbar\omega}\right)\ e^{-\Delta(T)/T}$$

where R_n is the normal surface resistance. Both Wilson{17} and Turneaure have compared this formula with computer calculations. They found that, for $T < \Delta_o/4$ and $1Ghz < f < 10Ghz$, this formula gives the "correct" temperature dependence to within ~5%. However, the frequency dependence is off by a factor of about $\omega^{1/3}$, and the absolute value at any one temperature and frequency may be off by an order of magnitude.

Another widely used approximation is the simple formula $R_{BCS} \propto (1/T)\cdot\exp(\Delta_o/T)$. For temperatures between $\Delta_o/15$ and $\Delta_o/5$, this formula

gives the same temperature dependence as the Pippard limit formula ± 2%, except that a different value of the zero temperature energy gap must be used in the simple formula. If a gap of 17° is used in the Pippard limit formula, the simple formula requires a gap of 17.3° at 0.35 Ghz., 17.8° at 8.6 Ghz., and 18.4° at 20 Ghz. The error increases to 10% if the temperature range is extended to $T = \Delta_o/4$.

2.2 Experimental Data and Residual Resistance

Experimental data on the low temperature residual resistance have been reviewed by several authors.{3,19,20} Common causes of residual resistance include contamination layers or inclusions of normal metal or lossy dielectrics, trapped magnetic flux, and cracks or splatters from welds. Other features that are associated with surface resistance include damage from machining, surface roughness, grain boundaries, and oxide layers that have been damaged by heat or electron impact. Residual resistances of 20 to 100 nΩ are usually obtained with carefully welded cavities made from good quality niobium that have been etched in an acid mixture to a depth of a few microns, thoroughly rinsed and dried in a dust-free atmosphere, evacuated, and cooled to cryogenic temperatures in a magnetic field of less than 10 milligauss. Lower residual resistances can be obtained by ultra-high-vacuum firing at temperatures greater than 1000°C, or by anodic oxidation of the cavity surface in a dilute solution of NH_4OH. (Anodized cavities are not used in high field applications because they are easily degraded by electron impact.){21} The lowest reported value is 1.5 nΩ at 10.5 Ghz. The

measurement was made in the TE mode of a cavity that had been machined from solid niobium, chemically polished, ultra-high-vacuum fired at 2200°C, and assembled in a glove box with a dry nitrogen atmosphere.{22} Values of ~2nΩ have been reported at 3.7 Ghz,{21} 1.5 Ghz,{23} and 0.1 Ghz.{24} The best results are usually obtained with TE mode resonators that have no electric fields perpendicular to the cavity wall. Residual resistances for TM modes, which have perpendicular E fields are typically a factor of two higher,{22,25,26} which suggests that lossy dielectrics may be present in the cavities.

Many researchers have used thermometer arrays to measure the spatial distribution of residual losses.{27} The usual finding is a few localized defects superimposed on a more smoothly varying background of losses. The background losses tend to have maxima in both the high current region and the high (normal) electric field region of the cavity. The results tend to depend on details such as the orientation of the cavity during rinsing and drying, but the losses in the high electric field region are generally comparable to or greater than the losses in the high current region.{28}

Although there is no frequency dependence in the best results described above, measurements made in several different modes of the same cavity show a frequency dependence of roughly ω^2.{26} In the next section, we show that this frequency dependence may result either from a very thin layer of metallic impurities, or from a layer of very lossy dielectric. It has been proposed that the lack of frequency dependence in the best results is just due to the fact that the lower frequency cavities are larger, and are therefore more likely to contain one or

more defects. These defects tend to cancel the ω^2 dependence that would otherwise have been observed.{19}

2.3 Theories of Residual Resistance

While the BCS Theory predicts that the surface resistance goes to zero at T = 0, experimentally, the low temperature value always remains finite. Since this residual resistance is frequently due to several different causes, it is unlikely that any theory will reproducibly predict its value in cavities which have been processed in such a way as to minimize these losses. However, theories can help to separate and identify the various mechanisms which are responsible for residual resistance. Mechanisms which have been described theoretically include normal conducting material or lossy dielectrics inside the cavity, magnetic flux penetrating the cavity walls, and direct generation of phonons by the electromagnetic field.

Probably the most common cause of residual resistance is the presence of normal conducting materials inside the cavity. These may be either localized defects, or thin layers of normal metals or lossy dielectrics. A few idealized cases are discussed below.

The simplest case is that of a large normal-metal defect whose dimensions exceed the skin depth of the defect material. The observed residual resistance will depend on the location of the defect, but, if there is a uniform distribution of such defects over the entire cavity, then the residual resistance is

[2.2] $\quad R = R_n \cdot F$

where R_n is the normal surface resistance of the defect, $(\mu_o\omega/2\sigma)^{1/2}$, and F is the fraction of the surface area covered by normal metal.

For normal layers with thickness less than the superconducting penetration depth, λ_s, the electric field in the layer will be roughly the same as the field just inside the superconductor. The (average) power loss per unit volume in the normal metal is σE^2, where E denotes the root mean square (rms) value of the electric field, which is related to the rms magnetic field by $E = \lambda_s \omega B$. The surface resistance, defined by $R = (P/A)\cdot(\mu_o/B)^2$ where P/A is the power loss per unit area, is

[2.3] $\quad R = \sigma t \lambda_s^2 \omega^2 \mu_o^2 \ (\cdot F)$

where t is the thickness of the layer. For "typical" values of $1/\sigma$ = 0.1 $\mu\Omega$-cm, λ_s = 300 angstroms and $\omega/2\pi$ = 3 Ghz., R/t comes out to about 50 nΩ/angstrom, which suggests that very thin surface layers can cause substantial residual resistances. If the fraction of surface coverage, F, is included, then this formula describes a uniform distribution of small defects. Note that this result is smaller than the large defect case (Eq. [2.2]) by a factor of $4\lambda_s^2 t/\delta^3$, where δ is the normal metal skin depth, $(2/\mu_o\omega\sigma)^{1/2}$. Using our "typical" parameters with t = 300 angstroms, this is a factor of 1/250.

An unresolved question is the extent to which thin surface layers will be driven superconducting by the proximity effect. This problem was described by Strongin{29} in 1971, but it has attracted little study since then. The calculation of McMillan{30} indicates that the surface layer will superconduct with an energy gap which is less than that of the superconducting substrate by a factor on the order of $(1-t/\xi_o)$, where ξ_o is the coherence length in the substrate. However, this

calculation describes the energy spectrum of electrons that travel back and forth between the superconductor and the normal layer. Since--especially if there is an anomalous skin effect--significant losses are due to electrons travelling almost parallel to the surface, it remains unclear whether or not the proximity effect can eliminate the residual resistance of a normal layer.

Another possible cause of residual resistance is a layer of lossy dielectric in the region of the cavity where there are large (perpendicular) electric fields. The displacement current, $J_d = \epsilon_o \omega E$, must pass through this layer, resulting in losses given by $\mathrm{Re}(\chi |J_d|^2)$, where the impedance, χ, describes both conduction and displacement currents in the dielectric.

$$\chi^{-1} = \sigma_1 + i\omega\epsilon\epsilon_o$$

So the power loss per unit volume is

$$\frac{P}{V} = \frac{(\epsilon_o \omega E)^2 \sigma_1}{\sigma_1^2 + (\omega\epsilon\epsilon_o)^2}$$

which is independent of ω for a low-loss dielectric, but has a dependence of ω^2 for larger values of σ_1. The term "surface resistance" is a misnomer in this case since these losses are not directly related to the surface magnetic field, but an effective surface resistance for the whole cavity can be obtained from the estimate, E = cB, which relates "typical" electric and magnetic fields in the cavity.

$$R = \left(\frac{P}{A}\right) \cdot \left(\frac{\mu_o}{B}\right)^2 = \frac{\omega^2 t}{c^2} \left[\frac{\sigma_1}{\sigma_1^2 + (\omega\epsilon\epsilon_o)^2} \right]$$

where t is the thickness of the layer. (This estimate is obviously invalid in a "TE" type cavity where the surface electric field is zero.) In a typical 3 Ghz accelerator cavity, this loss mechanism should be larger than the true surface resistance discussed earlier as long as $1/\sigma_1 > \sim 10^{-4}$ Ωm. These losses will vary as ω^2 unless $1/\sigma_1 > \sim 10$ Ωm, at which point the layer becomes a true dielectric with losses independent of ω. Note that formula [2.4], as a function of σ_1 has a maximum at $\sigma_1 = \omega\epsilon\epsilon_o \sim (10\ \Omega m)^{-1}$. At this conductivity, a "dielectric" layer will contribute on the order of 1 μΩ residual resistance per angstrom of thickness. This is at least an order of magnitude worse than is expected from a thin metallic layer.

Perhaps the most thoroughly documented cause of residual resistance is magnetic flux which is trapped in the cavity wall as it is cooled through the critical temperature.{20} For type I superconductors, this effect is particularly simple. Below T_c, the flux becomes concentrated into tubes which remain normal due to the local magnetic field which is equal to or slightly larger than the critical field, H_c. The radius of these tubes is likely to exceed the normal skin depth of the metal, so the surface resistance is just $R_n(B/H_c)$, where B is the average field penetrating the cavity.

The behavior of type II superconductors is more interesting. In this case, the field breaks up into individual flux quanta, whose normal cores are small enough to behave like "small" defects. (See equation [2.3]; the thickness is replaced by another factor of λ_s.) Conduction losses in the cores are thus reduced by at least a factor of 100 compared to the type I values. The principal loss mechanism in type II

superconductors appears to be the motion of the flux lines due to the Lorentz force, J x Φ. Gilchrist{31} has calculated losses from dissipative forces encountered by the moving flux lines. The dissipative forces were determined form DC measurements of flux creep. He obtained tolerable agreement with experimental data (±30%), but it is certainly possible that there are some other effects involved.

In many cases of practical interest, the preceding theory is difficult to apply because it is hard to determine what fraction of the ambient magnetic field actually gets trapped in the cavity surface. Lyenis{32} found that the magnetic field contribution to residual resistance could be reduced by an order of magnitude if the cavities were cooled very slowly (~10^{-3} deg/min) in order to facilitate flux exclusion. As a general rule, however, the observed magnetic contribution is on the order of $R = R_n(B/H_{c2})$, in rough agreement with the theory. For niobium at 3 Ghz, this is about 3 μΩ/gauss. The calculated frequency dependence is $\omega^{1/2}$, in good agreement with experiment.{26}

Another possible cause or residual resistance is the direct generation of phonons by the RF electric fields in the superconductor. This effect has been studied theoretically by Halbritter,{33} Passow,{34} Kartheuser and Rodriguez,{35} and Scharnberg{36} with each author including additional effects or correcting the previous calculation. The most recent calculations, due to Scharnberg, find less than one nΩ for frequencies less than 4 Ghz, regardless of the mean free path. However, for the case of most relevance to this thesis, f=10.5 Ghz and l = 900 angstroms, Scharnberg finds about 3 nΩ. This result

decreases more or less linearly with mean free path, but the resistance begins to saturate for $l > 1000$ angstroms, and never exceeds about 5 nΩ. Experiments near 10 Ghz frequently give this same order of magnitude for the residual resistance. (Values of less than 2 nΩ have been reported,{22} but the accuracy is questionable and the mean free path is unknown.) This theory might be more reliably tested at around 20 Ghz, since the maximum residual resistance (at $l = \infty$) varies with ω^2. However, the mean free path which is required in order to get close to the maximum resistance increases with $\sim\omega^3$ or ω^4, making it difficult to use substantially higher frequencies. At 20 Ghz, residual resistance measurements would probably have to be made at temperatures below 1.3°K.

3. OXIDE LAYERS

3.1 Structure and Growth of Oxide Layers

The oxidation of Nb has been studied almost continuously for the last several decades. No attempt is made here to summarize this vast literature, but instead to point out only a few studies which relate to the structure of layers grown at room temperature. Particular attention is given to the possible presence of lower oxides, especially NbO. This oxide behaves like a normal metal (Tc = 1.38 K) with a resistivity of ~2 $\mu\Omega$ cm at low temperatures.{37} The discussion begins with a brief description of oxide layers formed at temperatures near 1000°C. These relatively thick (~50 μm) structures were studied in the early 1960's and the results have significantly influenced and perhaps confused the more difficult investigation of the much thinner (< 100 angstroms) layers that typically form at room temperature. The next section describes studies of room temperature oxidation using X-ray photoelectron spectroscopy (XPS), ultraviolet photoelectron spectroscopy (UPS), and low energy electron diffraction (LEED). Finally there is a brief description of properties of oxide layers that may be inferred from tunnel junction characteristics.

A) High temperature studies

The oxidation of Nb at temperatures near 1000°C was studied by Inouye{38} and by Hurleen.{39} Both authors heated pieces of Nb under varying conditions of time, temperature, and oxygen pressure. Cross

sections of the oxidized metal were examined under a microscope and individual oxides were identified by a combination of chemical etches and X-ray diffraction patterns. Figure 3.1, drawn from a photograph in Inouye, shows a typical example of heavily oxidized niobium. There is an outer layer of Nb_2O_5, followed by a nearly continuous layer of NbO_2. Below that are grains of NbO and other lower oxides, some of which were unidentified. The niobium metal within ~50 μm of the interface contains a few atomic percent dissolved oxygen. The structure of heavily oxidized niobium reflects the process by which oxides grow on the surface. If the hot metal is oxidized only briefly, the oxygen simply dissolves into the bulk. Longer exposures at high temperatures result in the successive formation of NbO, NbO_2, and finally Nb_2O_5.

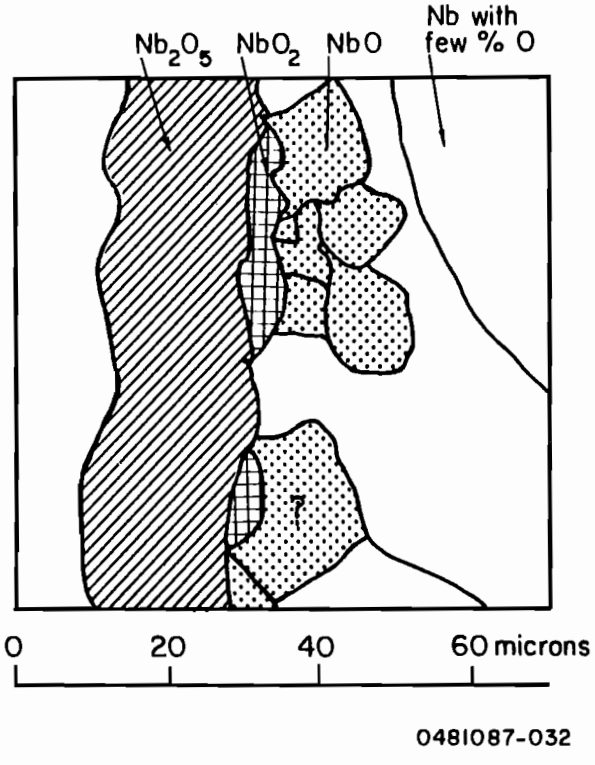

Figure 3.1 Profile of Niobium oxidized at 850°C from a photograph in Inouye.{38}

Although high temperature oxidation has served as a model for interpretation of experimental data on layers formed at room temperature, there are several aspects of room temperature oxidation that are qualitatively different. One such feature is the role of oxygen diffusion through niobium metal. Diffusion precedes the formation of oxides at high temperatures; but, at room temperature, the diffusion constant (extrapolated from values of a few hundred degrees) is less than one square angstrom per day,{40} which virtually eliminates this process. Another relevant process is the precipitation of NbO from saturated oxygen-niobium solutions. Solutions of several percent oxygen can be formed at temperatures greater than 1000°C, but at 600°, the solubility is less than one percent. This can result in the formation of grains of NbO when hot-oxidized niobium is cooled down to room temperature, but this process cannot occur if the oxidized metal is never heated.{41} A third feature of room temperature oxidation is the formation of amorphous Nb_2O_5.{42} At higher temperatures, depending on the details of temperature and pressure, one of several different crystalline forms{43} of Nb_2O_5 will be created as opposed to the amorphous form. All these processes suggest that oxide layers formed at or near room temperature need not be similar in structure to those formed at 800° or more.

B) Room temperature oxidation

Most of our present knowledge of room temperature oxidation comes from XPS investigations,{44,45,46} in particular the study by Grundner and Halbritter.{47} These authors studied niobium after oxidation in

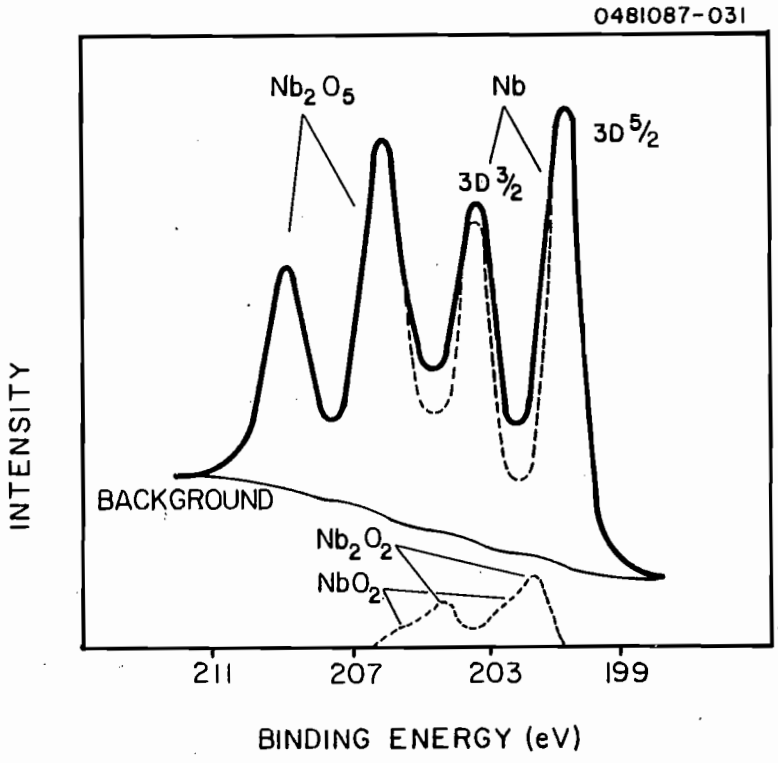

Figure 3.2 XPS spectrum of "typical" niobium oxidized at room temperature from Grundner,{47} showing technique for detection of lower oxides.

air, water, methanol, and dilute H_2O_2. They found that all of these oxide layers consist mostly of Nb_2O_5. Layers grown in air reach a thickness of 5 - 10 angstroms within a few minutes or less. The Nb_2O_5 layer eventually grows to 30 - 50 angstroms after several days. Wet prepared oxides generally grow somewhat thicker during the first few minutes, but aging in air eventually results in about the same structure in all cases. Grundner also noted that the impact of 1 kilovolt electrons converted some of the Nb_2O_5 to NbO_2, and that argon ions of the same energy quickly replaced most of the Nb_2O_5 with a mixture of

lower oxides. Unfortunately, XPS measurements cannot resolve stoichiometries to better than a few percent. As noted in section 3.2A, such a variation might have a substantial effect on the electrical properties of Nb_2O_5.

Figure 3.2 , taken from Grundner's paper, shows the difficulties which are encountered in trying to "assess the possible contribution of lower oxides" to the XPS spectrum. The figure shows the Nb 3d lines from a "typical" oxide. The peaks corresponding to Nb metal and Nb_2O_5 are clearly visible, but the existence of lower oxides is inferred from the modest discrepancies between the observed spectrum and a calculated one. Several difficulties interfere with such calculations: Effects such as localized charging, or photoelectron energy loss in the oxide layer may play a role; the spectrum for amorphous Nb_2O_5 may contain unexpected features due to the indefinite stoichiometry{48} of that material; and, since there is always enough time for background gases to contaminate the surface while the data is collected, no spectrum for clean Nb metal is available as a reference. This last problem is particularly important since these studies report negligible <u>growth</u> of the lower oxides. The full amounts are already present on the cleanest samples.

Grundner identified the lower oxides, Nb_2O, and NbO in his spectra, while Karulkar{45} and Sanz{46} found NbO and NbO_2. In every case, the average thickness of lower oxides is no more than 5 angstroms, which is less than two layers of NbO molecules. Much of this signal could be due to the mixed valence Nb atoms that must exist even at a "perfect" interface between the metal and the pentoxide.

C) Auger, UPS, and LEED studies

Several authors{47,49,50,51} have used Auger spectroscopy to monitor the oxygen concentration at the surface while the oxide layer was sputtered away with an argon ion beam. Many of these authors have reported transition regions as thick as 100 angstroms between the oxide and the metal. Because of the damage which the argon beam does to the surface, these results are only an upper limit for the thickness.

Ultraviolet photoelectron spectroscopy (UPS) and low energy electron diffraction (LEED) measurements are sensitive to the first two or three atomic layers on the surface. These techniques are useful during the early stages of oxidation in order to look for the successive formation of different phases which has been observed at higher temperatures.

Lindau and Spicer{52} made UPS measurements on oxides grown at temperatures from 23 to 700°C at pressures in the 10^{-7} torr range. Exposures ranged from less than one Langmuir to several thousand Langmuirs. (1L = 10^{-6} torr-sec ~ 1 monolayer of surface coverage.) At room temperature, as oxidation progressed, the conduction band in the metal was gradually replaced by a single energy level, indicative of only one oxide. In contrast, at 700°, at least two distinct energy levels were seen.

The results from LEED measurements are more complicated.{53,54,55} When the (110) face is exposed at room temperature,{54} one pattern appears after a few Langmuirs exposure, and additional features appear after about 100 L. Both patterns, especially the second are characterized by weak maxima and high background due to disorder. The

first pattern probably corresponds to a simple surface coverage, while the second pattern may be a true oxide. This second pattern could not be found on any sample that had been heated above a few hundred degrees. Additional coverage at room temperature resulted in deterioration of the pattern until, after ~ 1000 L, it was nearly invisible. Exposure of the (100) plane never produced any pattern other than that of the bare niobium. The image simply became more and more diffuse with additional exposure, indicating the formation of an amorphous oxide. It should be pointed out that the (100) planes of Nb metal and of NbO are almost identical in structure and size, so that this oxide would be hard to observe, although the existence of three dimensional NbO was "not proposed" by the experimenters.{53} Both faces showed several well defined structures at various stages of oxidation at higher temperatures, but these structures cannot be assigned to specific oxides with certainty. LEED measurements are capable of determining the type of structure and the spacing for the top two or three layers of atoms. It is not possible to determine the number or position of atoms within the unit cell.

Both the LEED measurements and the UPS measurements suggest that high temperature oxidation is a poor model for room temperature behavior. Although some evidence for multiple oxide layers was found by LEED measurements on the (110) face, the observed structures do not correspond to that of any known oxide.

D) Tunnel junction studies

The leakage current through tunnel junctions at voltages less than the sum of the appropriate energy gaps is often cited as evidence for the existence of a layer of NbO between the metal and the dielectric Nb_2O_5.{45} Although calculations{30} based on the proximity effect do predict leakage due to a normal layer at the interface, the actual relationship between these currents and XPS observations of lower oxides is very undependable. Other factors such as carbon contamination and the method of formation for the amorphous Nb_2O_5 seem to be equally important. Accurate modelling of junction leakage usually requires a theory with several adjustable parameters.{56}

Junctions formed by simple oxidation at room temperature have attracted little attention because of their high resistance and their tendency to short out. These two features in themselves, however, may indicate that the Nb_2O_5 contains relatively few oxygen vacancies, and that the surface coverage is very nonuniform.{57}

E) Conclusion

Niobium oxidizes quickly in air or water forming an oxide layer that reaches 10 to 15 angstroms within seconds, and then grows more slowly to ~50 angstroms after several weeks. XPS measurements show that this layer consists primarily of an oxide whose stoichiometry is roughly that of Nb_2O_5. Lower oxides, if present, have an average thickness of about one atomic layer. Since no LEED patterns have been seen except on very lightly oxidized surfaces ($< 10^{-3}$ torr-sec of O_2), the layer is assumed to be amorphous.

3.2 RF Superconductivity of Niobium-Oxygen Systems

Oxygen has been suspected of limiting the quality factors of RF cavities for a long time, although relatively little basic information is available about the electrical properties of niobium-oxygen systems. Much of the evidence linking residual resistance to the presence of oxygen is subject to multiple interpretation. This section contains a list of electrical properties of niobium containing dissolved oxygen and of several niobium oxides, followed by a description of experiments in which the RF surface resistance was altered by some process in which oxygen played a role.

A) Electrical properties of oxidized niobium

The most obvious change which occurs when oxygen is dissolved in niobium is the reduction in electron mean free path (l). This gives rise to several changes in the electrical properties. The normal resistivity increases by about 4.5 $\mu\Omega$ cm per atomic percent oxygen,{58} which is frequently the dominant source or resistivity at low temperature. Mean free path values less than the coherence length (ξ_o ~ 500 angstroms for Nb) cause an increase in the magnetic penetration depth of superconductors.{59} [For $l \ll \xi_o$, this relation is approximately $\lambda_s = 400\text{A}(l/\xi_o)^{-1/2}$.] Several authors{25,60,61} have observed increased penetration depths in niobium that was heated in an oxygen atmosphere, but it is unclear whether this is due to the mean free path or due to the field "penetrating" into serrations created by faceting or thermal etching which occurs during high temperature

oxidation. Changes in the mean free path can also alter the BCS part of the RF surface resistance by as much as a factor of two.{16} This effect is discussed in section 5.2E.

Dissolved oxygen also reduces the critical temperature by 0.93 degrees per atomic percent.{62} The reason for this is unclear, but comparison with the results for other solutes suggests that it is not simply a mean free path effect.{63}

Niobium forms a wide variety of oxides under different conditions of temperature and pressure.{43} The most common of these are NbO, NbO_2, and Nb_2O_5. NbO is a metallic oxide with a low temperature resistivity of around 2 $\mu\Omega$ cm., and a critical temperature of 1.38K. NbO_2 is a black oxide which has a resistivity that is many times higher than that of NbO, and which has no superconducting transition. Two phase mixtures of NbO and NbO_2 have roughly the same critical temperature as NbO, which suggests that NbO_2 is either an insulator or a semiconductor.{37} Nb_2O_5 is an insulator which occurs in several different crystalline and amorphous forms. Studies of anodic oxides provide some information about the amorphous forms. Thick (> 1000 angstroms) layers of amorphous Nb_2O_5 can be formed by anodization in a wide variety of solutions.{48} The exact stoichiometry and the dielectric constant depend on the choice of solution and the temperature. Anodic Nb_2O_5 is usually a few percent deficient in oxygen and has a dielectric constant between 20 and 60. Oxygen vacancies have significant effects on some crystalline forms of Nb_2O_5, causing it to become an n-type semiconductor with a dielectric loss tangent as large as one at 10^8 Hz.{64,65}

B) RF experiments

Although heretofore there have been no direct measurements, results reported in the literature provide an interesting collection of hints as to whether or not ordinary oxide layers grown at room temperature should be expected to contribute to residual resistance. Evidence pro and con is summarized below.

Perhaps the best known evidence indicating that oxide layers may cause residual resistance is the fact that UHV firing at 1800°C or more very frequently causes substantial improvements in the quality factors of niobium cavities.{22,66} While this procedure does remove the oxide layer, at least temporarily, it also causes other effects such as grain growth, bulk purification, stress relief, and removal of contaminants such as hydrocarbons and some particulates.

An interesting example is the work of Cepperly et al.,{67} who fired re-entrant 430 Mhz cavities at 1800°C, sealed the cavities under vacuum, and then tested them without exposure to air. They frequently obtained Q's in excess of 10^{10}, which corresponds to residual resistances of less than 10 nΩ. In one series of tests they exposed the cavity to air, which lowered the Q to ~10^{9}. Unfortunately, this large reduction was probably due to dust. Firing at 1000° did not improve the cavity, and firing at 1800° only brought the Q up to 6 x 10^{9}.

Evidence that oxide layers are not responsible for residual resistance come from the improvements in Q's that have been achieved by anodizing. Anodized cavities are covered with layers of amorphous Nb_2O_5 on the order of 1000 angstroms thick, and they exhibit an energy gap that is typically 10 percent lower than expected,{21} which, according

to McMillan's calculations of the proximity effect, could be due to a ~50 angstrom thick layer of NbO.{30} Anodized cavities can have Q's that are as high as those of fired cavities, but their performance is degraded by electron impact or by UHV bakeout at 100°C.{21,68,69} As noted in the previous section, both of these processes probably convert some of the dielectric Nb_2O_5 to conducting lower oxides.

Giordano et al.{25} attempted to measure the influence of bulk oxides on cavity performance by firing 8.6 Ghz cavities at 2100°C in an atmosphere whose oxygen pressure varied from $< 10^{-8}$ torr to 10^{-5} torr. The steady state concentration of dissolved oxygen under these conditions varies from one half of one percent to less than 10^{-3} atomic percent.{70} Unfortunately, the cavities were then cooled to room temperature in the same oxygen atmosphere. It is difficult to guess how severely this may have oxidized the surface. The cavities that were fired in the best vacuums had residual resistances of about 30 nΩ, while the oxidized cavities usually had about twice that amount.

3.3 High Temperature Removal of Oxide Layers

Oxygen is the most tenacious of the common gases that contaminate the surface of niobium. Nitrogen will cover the surface with only a single monolayer which can be removed by heating to less than 1000°C. Contaminants containing carbon, such as solvent residues or CO, usually disappear upon heating to 1000° or less, although they may leave oxygen behind.{71}

The problem of surface oxide removal is closely linked to the problem of bulk purification. Most papers describing the preparation of clean niobium surfaces recommend heating to temperatures between 1800° and 2400°C.{71,72} At these temperatures, oxygen escapes from the bulk metal as NbO vapor.{70} However, niobium purification can now be accomplished more easily{73} using solid state gettering techniques which were initially developed for Vanadium.{74} While oxygen is rarely seen on the surface of hot niobium above 1600°C, grains of NbO will precipitate to the surface if the bulk concentration exceeds one half of an atomic percent unless the metal is quenched very rapidly. At lower bulk concentrations, oxygen may precipitate to the surface, but the resulting layer will not be more than a single monolayer thick.

The ratio of surface coverage to bulk concentration at elevated temperatures has been examined by several authors, using a simple model to analyze the results. Pasternak{75} used an indirect measure of the sticking coefficient to measure surface coverage, while Farrell{71} and Hofmann{50} used Auger spectroscopy on the (100) surface and on a polycrystalline surface respectively. The surface is assumed to consist of independent sites which are either occupied or unoccupied. The fraction of occupied sites is θ. Oxygen leaves the surface and goes into the bulk at a rate $k\theta$ where k is a temperature dependent constant. The rate for the reverse process is proportional to the bulk concentration, c, and to the fraction of unoccupied surface sites, $(1 - \theta)$, with a proportionality constant, k'. At equilibrium these two rates are equal, so

$$k\,\theta = c\,k'\,(1 - \theta)$$

The quantity, (k'/k), is found experimentally to be thermaly activated:

$$\frac{k'}{k} = K_o \exp(T_o/T) = \frac{\theta}{1-\theta}$$

where T is in degrees Kelvin. Although this model ignores the faceting and other surface structures that have been seen in LEED measurements, it has nonetheless been partially successful. The exponential form is generally observed, at least over some restricted temperature range, but various authors disagree by more than a factor of two over the value of T_o, which implies substantial differences in observed coverages. The experimental details are different in each case, but the discrepancies are large enough that the results as a whole should be regarded as only semiquantitative. A reasonable value for T_o is around 8000°, and a typical coverage at 700°C is 25 percent for c = 0.1 % atomic. Hofmann found that K_o is almost proportional to 1/c, while the others found it to be reasonably constant. There are also differences in the observed range of validity for the equation. At low temperature, (k'/k) diverges so the coverage should approach unity, as reported by Hofmann. However, Farrell found that the coverage ceases to increase when the sample is cooled below 700°C, so that for concentrations below 0.1%, the surface remains relatively clean. In spite of the variety in the results, the exponential behavior which is observed does suggest that above 1000°, the surface coverage is at equilibrium with the bulk concentration. If this is true, then coverage at 1000° or more should depend only on the oxygen concentration in the adjacent metal and not on any other details of the thermal history of the sample.

One other important consideration is the diffusion rate of oxygen in niobium metal.{40} The distance which an oxygen atom will travel

during a time, t, at the (Kelvin) temperature, T, is approximately

$$x = Dt \quad \text{where} \quad D = 0.02 \exp(-13500°/T) \ (cm^2/sec)$$

This relation affects surface cleaning procedures in two ways. If an oxide layer which is several molecules thick is heated to only a few hundred degrees, the oxygen will be absorbed into a layer of metal whose thickness is limited by diffusion. This can result in a thin layer of metal that is severely contaminated. As a general rule, the surface should be kept hot long enough for oxygen to diffuse at least one million angstroms. This becomes practical at around 1000°C. On the other hand, for concentrations less than 0.01 atomic percent, the surface should be relatively clean at temperatures as low as 700°C. If the sample is cooled at a rate of 50°/sec, or more, very little oxygen will have time to reach the surface of the sample before being "frozen" into the metal.

In conclusion, niobium surfaces with one monolayer or less oxygen coverage can be made by heating to 1000°C in a vacuum if the metal contains 0.1 atomic percent oxygen or less. The heating time must be sufficient so that the oxygen can diffuse well into the bulk so as to avoid creating an oxygen-rich layer of metal near the surface. Heating to higher temperatures is useful only to aid diffusion, or to purify the bulk niobium.

4. EXPERIMENT

4.1 Overview of Experimental Strategy

The goal of this experiment was to measure the influence of oxide layers on the microwave surface resistance of superconducting niobium by comparing the surface resistance of oxidized and oxide-free surfaces. A procedure for cleaning the niobium was developed based on studies in the literature and on our own Auger measurements. The native oxide layer was removed from the surface by heating to 1100°C for 20 minutes. At this temperature, the oxygen was absorbed into the bulk; however, sulfur sometimes precipitated to the surface at the same time. The sulfur was removed by heating to 1400° for one minute. Surface resistance was measured by making a resonant cavity out of the niobium and measuring the quality factor of the cavity. The quality factor (Q) is related to the surface resistance (R) by a geometry factor, $G = RQ$, where $G = (\mu_o c)k_o L$, $\mu_o c/\pi = 120\Omega$, k_o is the free space wavenumber, and L is the ratio of the volume integral to the surface integral of $|B|^2$. For our cavities, $G = 270\Omega$.

A cavity and furnace arrangement was constructed so that the cavity could be heated to 1400° under vacuum, sealed with an all-metal valve, and moved to a cryostat for testing without any exposure to air. Later, the valve could be opened, and the cavity exposed to controlled amounts of oxygen and retested.

Upon finding that exposure to oxygen did not affect the RF performance of the cleaned cavities, it became necessary to make sure

that the cleaned cavities were actually oxide-free. There was little doubt that most of the native oxide was absorbed at 1100°; but, since the pressure inside the cavity could not be measured directly, it was hard to assess the contamination that occurred in between the cooldown from T > 1000°, and the cryotest.

The technique of heating the (evacuated) cavities to 325°C for 10 minutes was developed to get around this problem. At this temperature, the surface oxides decompose, and the oxygen diffuses into the metal, creating an oxygen-rich layer which is a few thousand angstroms thick. This layer exhibits a reduced BCS resistance and an increased residual resistance, while oxide-free cavities were unaffected by this heat treatment.

Several measurements were made on oxidized and heated cavities to verify the existence of the oxygen-rich layer and to better understand the process by which it forms. These include the usual measurements of the BCS resistance and the residual resistance, as well as measurements of the (radio frequency) critical temperature, and the normal surface resistance.

Measurements of the dependence of the residual resistance on ambient magnetic field during cooldown through the transition temperature were made in order to estimate errors due to this effect. Although these errors were small enough to be unimportant, it was interesting to note that the presence of heated oxides can magnify this effect by as much as a factor of 5.

4.2 Apparatus

A) UHV Furnace

Figure 4.1 shows the ultra high vacuum furnace with a cavity installed. A current of up to 350 amps passes through the feedthrough and the flexible bus bar, down the top cutoff tube, through the cavity and the lower cutoff tube, and out through the cavity flange. The 0.062" thick niobium sleeves around both cutoff tubes conduct heat and electricity so that the cavity becomes the hottest part of the furnace. The spring-supported flexible bus bar keeps the cavity from being crushed by thermal expansion.

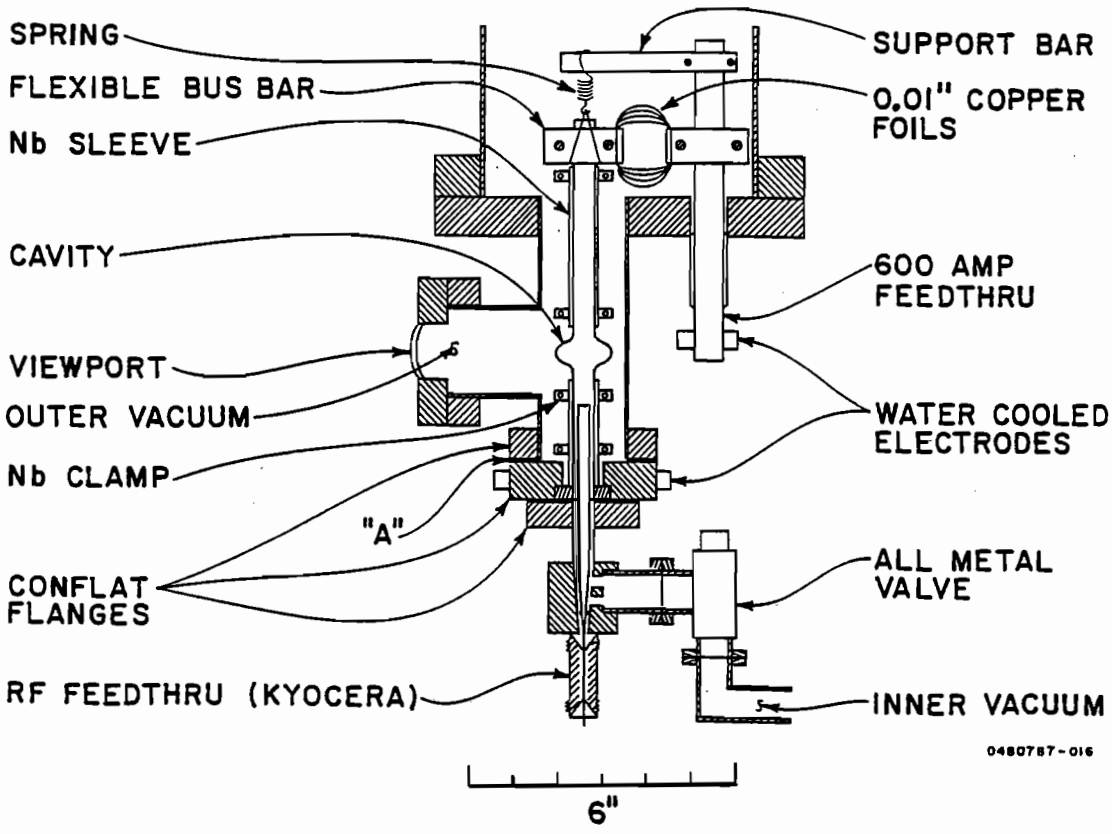

Figure 4.1 Ultra-high-vacuum furnace with cavity installed.

The cavities were cylindrically symmetrical with an "elliptical" profile{76}. Cavity halves, as well as the first quarter inch of the cutoff tubes were drawn from high purity 0.02" niobium sheet,{77} and electron beam welded together. Some of the later cavities were further purified by solid state gettering.{73} Cavities were fired at 1100°C for 20 minutes to remove the oxide layer, and at 1400° for one minute to remove sulfur. (The second step was sometimes omitted on cavities that had been previously fired.) After firing, the seal was broken at "A" (fig.4.1), the all metal valve was closed, and the cavity was taken to the cryostat for testing. Transfer from the furnace to the cryostat took about an hour.

The vacuum systems for the inside and the outside of the cavity were completely separate. Each was pumped by a sputter-ion pump with a pumping speed of 140 l/sec. for the inner vacuum, or 500 l/sec. for the outer vacuum. However, for points near the cavity, these pumping speeds were limited by geometrical obstructions to about one l/sec., and 10 l/sec., respectively.{78} Consequently, whenever the principal source of gas was near the cavity, the pressure there was on the order of 100 times higher than the pressure read by the pump. After a conventional bakeout at 100° to 200°C, both pumps read near their minimum values of 10^{-9} torr. During firing, the cavity was brought up to 1100° over a period of one or two hours, so that the outer pump always read less than 10^{-7} torr. The inner pump usually read about one fifth this much. A residual gas analyser showed that most of this gas was hydrogen, which desorbed from the cavity and other niobium parts. After heating above 800°C, niobium becomes an excellent getter for almost everything except

inert gases. During firing, at least half of the lower cutoff tube reached this temperature, so that it is unlikely that significant amounts of oxygen reached the inside of the cavity after cooldown. The situation outside the cavity was less ideal. Heat and hydrogen flux from the cavity liberated appreciable amounts of water and/or CO from the walls of the vacuum chamber. A good fraction of these gases were absorbed by the cavity degrading its purity. Since the reciprocal of the RRR is proportional to the amount of impurities in the niobium,{58} the change in cavity RRR due to firing may be described by the formula,

$$\frac{1}{RRR_f} - \frac{1}{RRR_i} = \frac{A}{600}$$

where the subscripts refer to the initial and final values. The number, "A", is proportional to the amount of oxygen, etc. absorbed by the cavity. Observed values of "A" ranged from 1 to 3, while a value of 0.3 corresponds to the absorption of 50 angstroms of Nb_2O_5 from each surface of the cavity.

B) Cryostat

The cryostat is shown in figure 4.2. The cavity is surrounded by three layers of "Co-netic" magnetic shielding. There are two 30-turn degaussing coils wound (in the same direction) around the inner shield, as well as a seven turn pickup coil (not shown) around the center of the shield. Prior to each cooldown, an AC current with amplitude decreasing from ~3 amperes to zero was passed through the degaussing coils. The voltage on the pickup coil was measured to make sure the shield was driven into saturation at peak amplitude. (The maximum voltage was ~0.2V rms.) A solenoid located just inside the innermost shield was

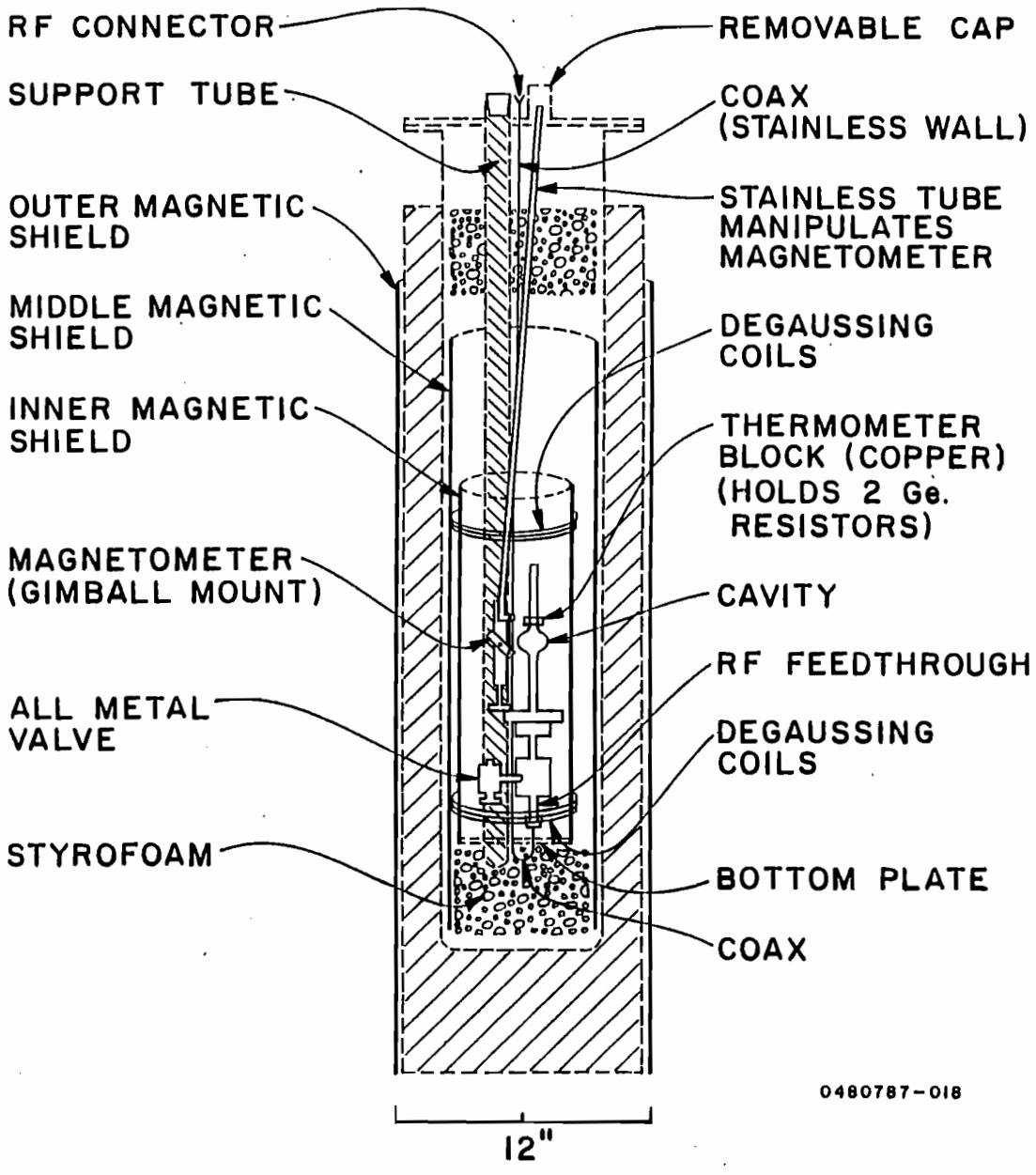

Figure 4.2 Cryogenic apparatus for measurements below 4.2°K.

used either to cancel out the remaining vertical field (~1 milligauss) or to create a magnetic field if one was required. The field near the cavity was measured with a single (Hewlett-Packard) fluxgate magnetometer. The magnetometer was mounted on a gimball and could be moved through several steradians by a long thin-walled stainless handle. This design allowed compensation of temperature dependent offsets as well as measurement of all three components of the field.

Temperature was measured with two germanium resistors set into a copper clamp just above the cavity. In addition, a carbon resistor (Allen-Bradley 100Ω, 1/8 watt) was attached to the bottom plate. All three thermometers usually agreed to within 0.01°K.

It was necessary to drill a hole lengthwise through the stem of the all-metal valve in order to keep helium from getting trapped below the threads and damaging the bellows.

C) Principles of single-probe cavity measurements

Measurements of cavity resonances require a power source, a circulator (or directional coupler), a cavity with a feedline and coupling probe, and a RF detector. (See figure 4.3.) The circulator separates power going into the cavity from reflected power coming out. Power travels from the source into port 1 of the circulator. It then comes out of port 2, and down the feedline to the probe in the cavity. Some of the power is then reflected back toward port 2 of the circulator, which sends it out port 3 to the detector.

If the power source is suddenly turned off, then stored energy (U) leaves the cavity as dissipated power in the cavity walls (P_o), and as

radiated power through the ("external") probe (P_e). The decay time is therefore

$$\tau = \left(\frac{P_o + P_e}{U} \right)^{-1}$$

The loaded Q (Q_L) is defined as $\omega\tau$, and the cavity Q (Q_o) and the external Q (Q_e) are similarly defined by their respective loss mechanisms.

$$Q_L = \omega\tau = \left(\frac{1}{Q_o} + \frac{1}{Q_e} \right)^{-1}$$

Q_o depends on the surface resistance of the cavity walls, while Q_e depends only on the geometry of the cavity and probe. The coupling parameter, β, is defined as

$$\beta = Q_o/Q_e = P_e/P_o$$

Now we consider a steady situation where the frequency of the incoming power exactly matches the resonance frequency of the cavity. The reflectivity at the probe tip is very close to unity, but this reflected power interferes destructively with P_e, which is emitted from the cavity. Setting the incoming power equal to one for convenience, the net reflected power is then

$$P_r = (1 - \sqrt{P_e})^2$$

By energy conservation, we must also have

$$1 - P_r = P_o$$

These two equations may be combined using $\beta P_o = P_e$ to give

$$P_r = \left(\frac{1 - \beta}{1 + \beta} \right)^2 \qquad \text{and} \qquad P_o = \left(\frac{4\beta}{(1 + \beta)^2} \right)$$

Finally, we note that if this steady state is suddenly interrupted by turning off the incoming power, then the power emitted by the cavity immediately after the shutoff will be

$$P_e = \beta P_o = \left(\frac{4\beta^2}{(1 + \beta)^2} \right)$$

D) Cavity and RF circuit

The cavities were of the "elliptical" design of Kneisel et al.,{76,79} scaled to 8.6 Ghz, with a cutoff tube diameter of 0.45", a magnetic geometry factor (Q times the surface resistance) of 270Ω, and a shunt impedance, Z/Q, of 6150 V/m. The RF power was coupled to the

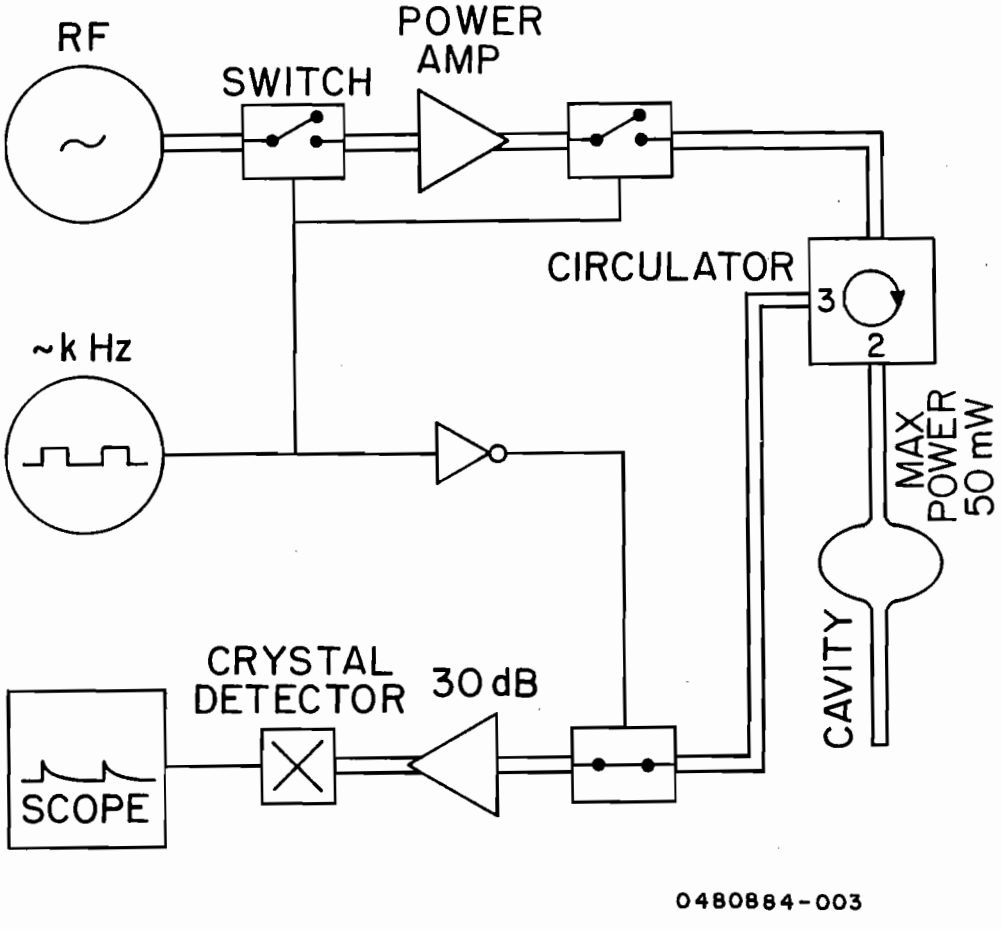

Figure 4.3 RF circuit used for measurements below 4.2°K.

cavity by a single coaxial probe. The external quality factor, Q_{ext}, could be adjusted only by changing the thickness of the copper gasket that sealed the cavity flange to the feedthrough/vacuum assembly. Values of Q_{ext} between $3x10^9$ and $3x10^{10}$ were necessary in order to make accurate measurements at low temperatures.

At higher temperatures, this coupling was too weak for the RF signal to be phase-locked to the cavity resonance, so a high-power pulse technique was used. The circuit for the RF is shown in figure 4.3. The RF is pulsed by diode switches on both sides of the power amplifier. A third switch is necessary to protect the 30 dB signal amplifier. When the pulse ends, this switch closes and the exponential decay of the emitted power from the cavity is seen on the oscilloscope. About 10 μw of emitted power was needed to get a clear decay curve, so the required input power was

$$P_{in} > 10\ \mu w \cdot (1 + \beta)^2/4\beta^2$$

where the coupling parameter, β, equals the cavity Q divided by the external Q. This power requirement restricted measurements to temperatures below ~3.3 degrees. (At low temperatures, where $\beta \sim 1$, about 5 mw of input power was still required due to FM noise in the RF supply.) The power dissipated by the cavity ranged from ~1 mw at 3.3°, to ~10 μw at 1.4°. Electric fields in the cavity were on the order of 100 kV/m. At low temperatures, β was close to unity, and conventional phase-locked measurements{20,80} were used to measure the external Q.

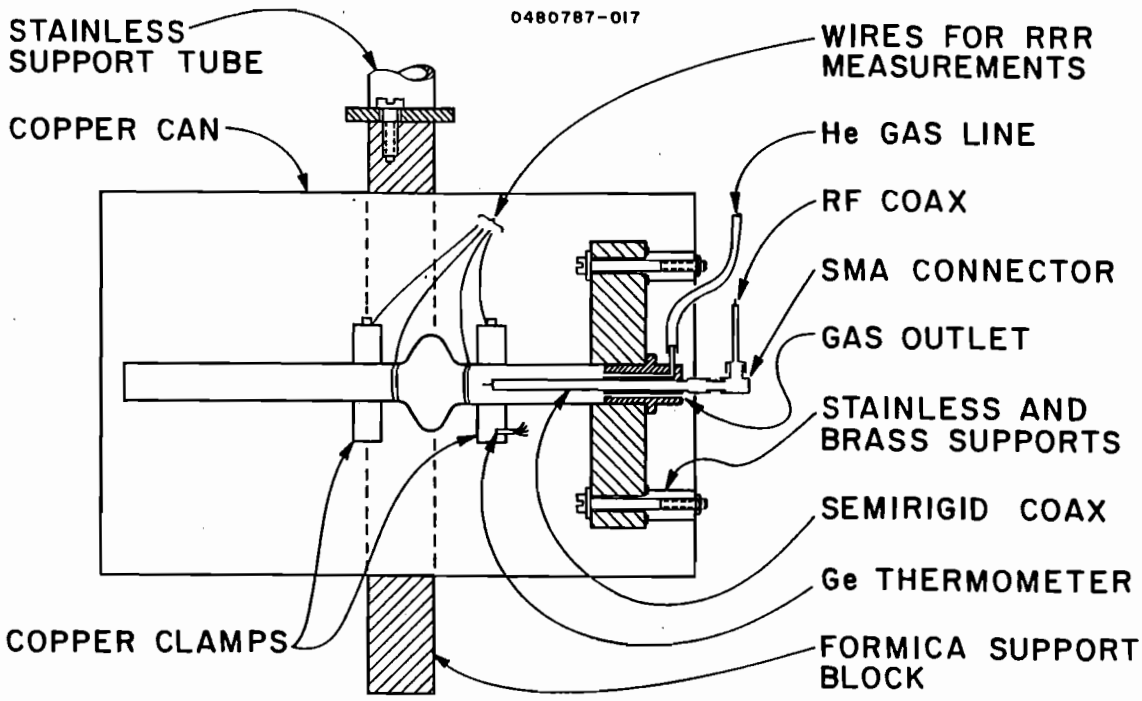

Figure 4.4 Cryogenic apparatus for measurements above 4.2°K.

E) Apparatus for measurements above 4.2°K

A simple but adequate apparatus for measuring DC resistivity and quality factors at temperatures between 7°K and room temperature is shown in figure 4.4. The cavity is mounted horizontally inside a copper can suspended above a small puddle of liquid helium inside the cryostat. Although not leaktight, the can has only a few small holes for the necessary wires, etc. to pass through. The cavity is attached to the can by thin stainless and brass mounts so that the helium atmosphere provides most of the thermal connection between the cavity and the can. Temperature was measured with a germanium resistor mounted in a copper

clamp next to the cavity, and was controlled by a ~10 watt heater coil wrapped around the can, or by raising and lowering the can in the cryostat.

Current for measuring the DC resistivity of the cavity was introduced through the heavy copper clamps, while the voltage leads were just two turns each of copper bus bar twisted tightly around the cutoff tubes. The maximum current used was ± 3 amperes; and a typical room temperature resistance for the cavity was ~250 $\mu\Omega$.

The RF probe is a short piece of semi-rigid coax with 1/8" of the center conductor exposed. The other end of the probe is connected to an RG58 cable which goes to a circulator outside the cryostat. The (off resonance) reflected power (measured at port 3 of the circulator) varied by more than a factor of 5 depending on the frequency, indicating the presence of substantial reflections and attenuations in the feedline.

Quality factors were determined from measurements of the reflected power as a function of frequency. A typical signal is shown in figure 4.5. The reflected power near the resonance frequency is given by the absolute square of the sum of two terms:

$$P_r = |R + A/(1-2izQ_L)|^2$$

where $z = (f-f_o)/f_o$ and f_o is the resonance frequency. The first term (R) is the sum of all the attenuated reflections (including the reflection at the probe tip), while the second term is the attenuated wave that is emitted from the cavity. As long as the off resonance reflected power does not vary significantly over frequency intervals as narrow as the resonance width, R and A are just complex constants.

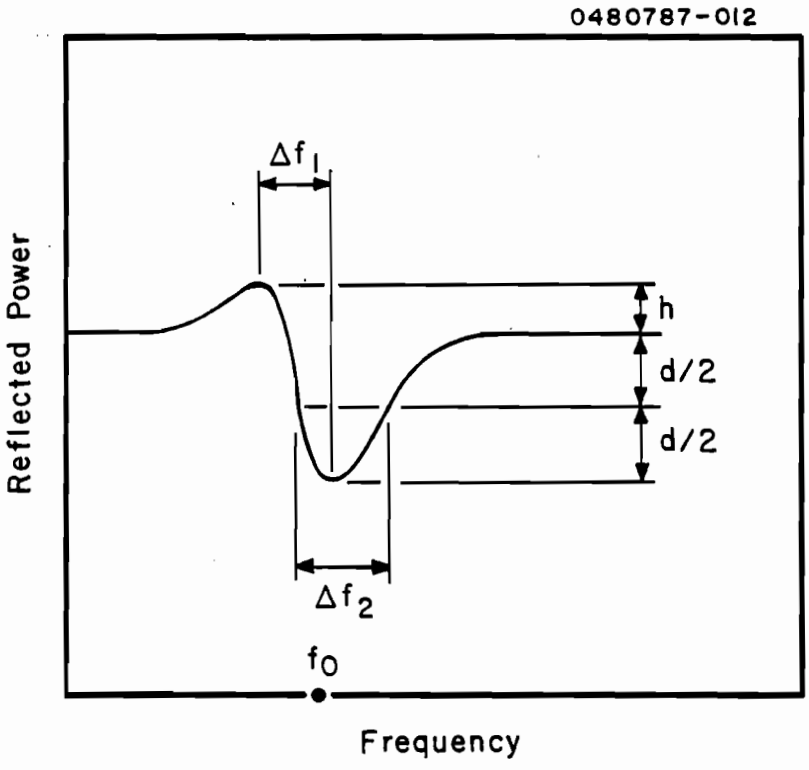

Figure 4.5 Reflected power as a function of frequency for a system with attenuations and reflections in the feedline.

Their phases and magnitudes are generally unknown, but if the feedline contains no reflections, then $R/A = 2\beta/(\beta+1)$. It is straightforward but tedious to show that the loaded Q, $Q_L \equiv (1/Q_o + 1/Q_{ext})^{-1}$, is given by

$$Q_L = \frac{f_o}{\Delta f_1} \cdot C_1$$

where f_o is the resonance frequency, Δf_1 is the frequency difference between the points of maximum and minimum reflectivity, and C_1 is a correction factor that depends of the ratio, h/d. (See figure 4.5)

Some values of C_1 are given in table 4.1. If h/d is too small for this technique to be convenient, then the usual "full width half maximum" formula,

$$Q_L = \frac{f_o}{\Delta f_2} \cdot C_2$$

may be used, where C_2 is another correction factor (table 4.1), and Δf_2 is defined in figure 4.5. The external Q was determined by cooling the cavity well below the transition temperature so that the cavity Q (Q_o) was very large, and $Q_L \sim Q_{ext}$. This estimate may be undependable, especially in the presence of temperature dependent attenuations, so cavity Q measurements were generally used only if $\beta \equiv Q/Q_{ext} < 0.5$, making small errors in the external Q relatively unimportant.

TABLE 4.1

Correction factors

h/d	0	0.1	0.2	0.5	1	2	5	10
C_1	-	1.7	1.3	1.1	1	1.1	1.3	1.7
C_2	1	1.1	1.2	1.4	1.7	-	-	-

5. RESULTS

5.0 Introduction

Results are presented in almost the same order in which the experiments were done. The first section describes a set of Auger spectroscopy measurements which were done in order to find an annealing temperature at which the natural oxide layer can be removed from niobium by absorbing the oxygen into the bulk. We found that 1100°C is hot enough to remove oxygen, but that a layer of sulfur sometimes appears, which can be removed at 1400°.

The second section begins with a description of the formula to which the superconducting surface resistance data were fit. This formula is the sum of a temperature independent residual resistance, and a temperature dependent BCS resistance, R_{BCS}. The BCS resistance consists of a function which varies roughly as $\exp(-\Delta/T)$, (where Δ is the energy gap,) multiplied by a prefactor which depends on the frequency and on the electron mean free path. The remainder of this section compares the residual resistance of ordinary chemical polished cavities with those that have been cleaned by UHV firing as described in section 1, and with fired cavities that were reoxidized by exposure to controlled amounts of oxygen. The residual resistance drops considerably when the cavity is fired, but it is not affected by subsequent oxygen exposures. It is also noted that the BCS resistance at 2° depends on the (bulk) purity of the niobium.

The third section describes the increases in residual resistance and the decreases in BCS resistance which occur when oxidized cavities are heated to temperatures near 300°C. These changes, presumably caused by the thermal breakup of the oxide layer, were initially monitored in order to show that the fired cavities were not contaminated with oxygen. An upper limit of one or two monolayers was established for the contamination. A slight decrease in the RF transition temperature and an increase in the normal surface resistance just above T_c were also observed on oxidized and heated cavities. Further studies showed how these changes depend on the temperature to which the cavity was heated.

Section four contains energy gap measurements. The gap is independent of all the preceding surface treatments, as well as the bulk purity of the niobium.

Section five describes XPS, Auger, and secondary yield measurements done on oxidized niobium during and after the heat treatments used in section three. These measurements show that the oxide layer remains intact until the temperature reaches 200 to 250°. However, by 300°, almost all of the oxygen has left the 20 angstrom thick surface layer where these measurements are sensitive.

The discussion section describes the process by which the oxide layers are absorbed at temperatures near 300°, based on the XPS measurements, and on the measurements of BCS resistance.

5.1 Auger Studies

An Auger electron spectroscopy study was done to find the temperature at which oxide layers are removed from the niobium material out of which we have made our cavities. It is well established that oxide layers disappear from niobium surfaces above 800°C, but, if the bulk concentration exceeds 0.1 atomic percent, some oxygen will precipitate back to the surface upon cooling. Temperatures in excess of 1800° are necessary to remove oxygen from the bulk by evaporation of NbO, however, this can now be accomplished by solid state gettering at lower temperatures.{73} Our study covered the temperature range between 800° and 1800° at which the oxide layer dissolves into the bulk metal. Since our material is about 100,000 thicker than the oxide layer, this degrades the purity of the metal only slightly.

We studied both a rolled strip of .020" thick sheet as received from Ames Laboratory,{77} which had a residual resistance ratio (RRR) of ~150 (Oxygen concentration < .03% atomic), and a .020" thick single crystal (1,0,0) which had been made from the same material, but which had been decarburized at 1600°C in 10^{-6} torr of oxygen and then degassed at 2100° to an RRR of ~1000. Samples were polished in a mixture of HNO_3, HF, and water,{81} and then rinsed in water, and methanol prior to insertion into the Auger apparatus. Inside the apparatus, they were heated to successively higher temperatures, and an Auger spectrum was taken during and after each cooldown. Each heating cycle lasted long enough for oxygen to diffuse through the thickness of the sample. Typical vacuum pressure was 5×10^{-10} torr while measurements were being

made. The pressure rose by as much as an order of magnitude while the sample was being heated.

Prior to heating, the contamination layer was so thick (> 30 angstroms) that the Auger spectrum showed mostly oxygen and carbon, but little or no niobium. However, a niobium signal was plainly visible after degassing for 30 minutes at a temperature well below the minimum which could be measured with the optical pyrometer.

The results are shown in figure 5.1. The pure crystal showed negligible oxygen coverage immediately after heating to 1200°C or more. The coverage rose steadily with time until it reached ~1 monolayer after

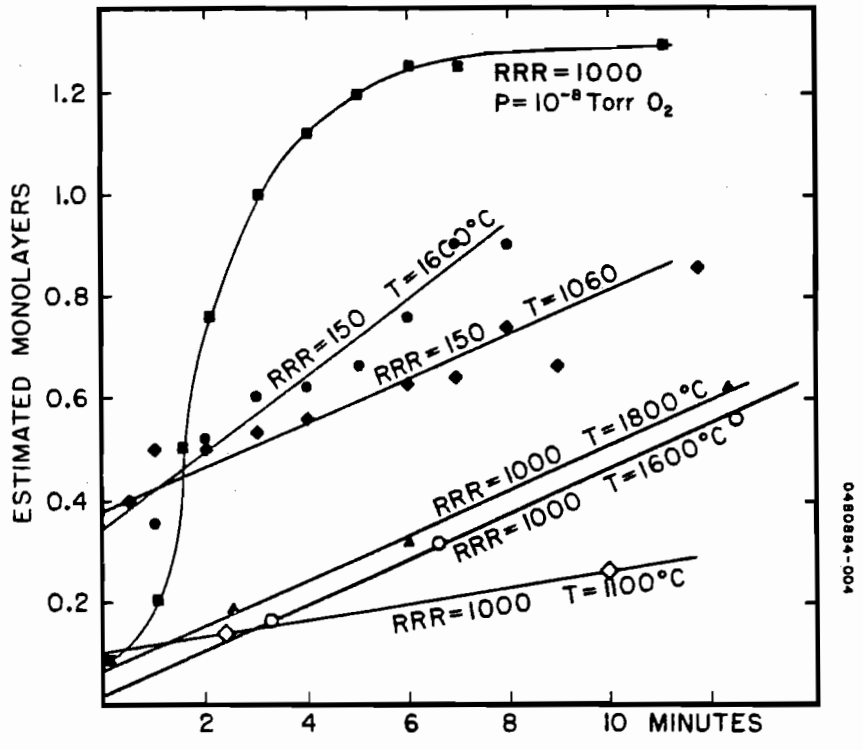

Figure 5.1 Oxygen coverage vs. time after heating to indicated temperature for polycrystaline (RRR=150), and single crystal (RRR = 1000) Nb. Slopes of straight lines are presumably due to background pressure (~10^{-9} torr) of CO or water.

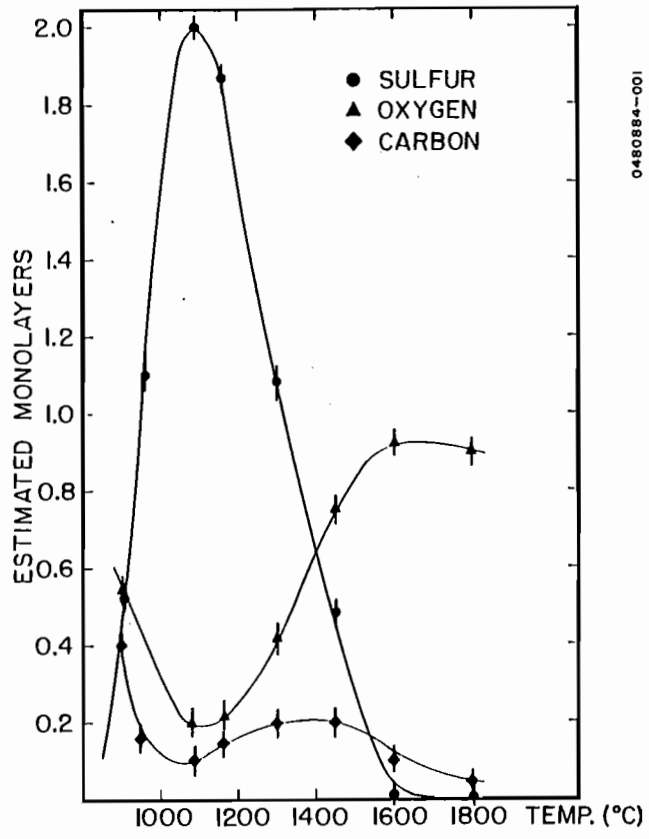

Figure 5.2 Coverage measured 10 minutes after cooldown from indicated temperature for polycrystaline Nb.

~10 minutes. This coverage is probably due to adsorption of ambient gases. The apparent temperature dependence on the rate of coverage is loosely correlated with increased background pressure due to heat. The results for the as-received rolled strip were similar to those for the single crystal except for two details: (1) When this sample was heated to 1200-1300°, it became covered with a few monolayers of sulfur, which apparently prevented oxygen from accumulating on the surface (Figure 5.2). This sulfur could be removed by heating to 1400°. Reheating this sample to temperatures of 1060° or more did not result in

reappearance of the sulfur. (Similar contamination was seen at the University of Geneva. They also found that the sulfur reappeared whenever the sample was heated to 800°.){82} (2)An initial coverage of ~ 1/3 of a monolayer of oxygen was observed immediately after heating. This oxygen probably precipitated out of the bulk. The spectrometer was calibrated to within a factor of two by exposing a clean sample to 10^{-8} torr of oxygen. The rate of coverage drops when one monolayer is reached.

We concluded that niobium can be cleaned by heating to 1100° if the initial purity of the metal is adequate.

5.2 Surface resistance of Chemical Polished, Fired, and Oxidized Cavities

Surface resistances at temperatures below 4K were fitted to a three parameter curve,

[5.1] $$R = A \cdot R_{BCS}(\Delta,T) + R_{res}$$

The free parameters are the constant, A, the energy gap, Δ, and the residual resistance, R_{res}. For the function, $R_{BCS}(\Delta,T)$, we used the Pippard limit formula for superconducting surface resistance. To a first approximation, this formula is proportional to $\exp(-\Delta/T)$. The exact formula is given by the right hand side of eq.[A.1](appendix). Wilson {17} has shown that this formula gives almost the same temperature dependence as the more detailed computer programs by Halbritter {16} or Turneaure {15} over a wide range of frequencies. Our own comparison, using Halbritter's program and parameters with a mean

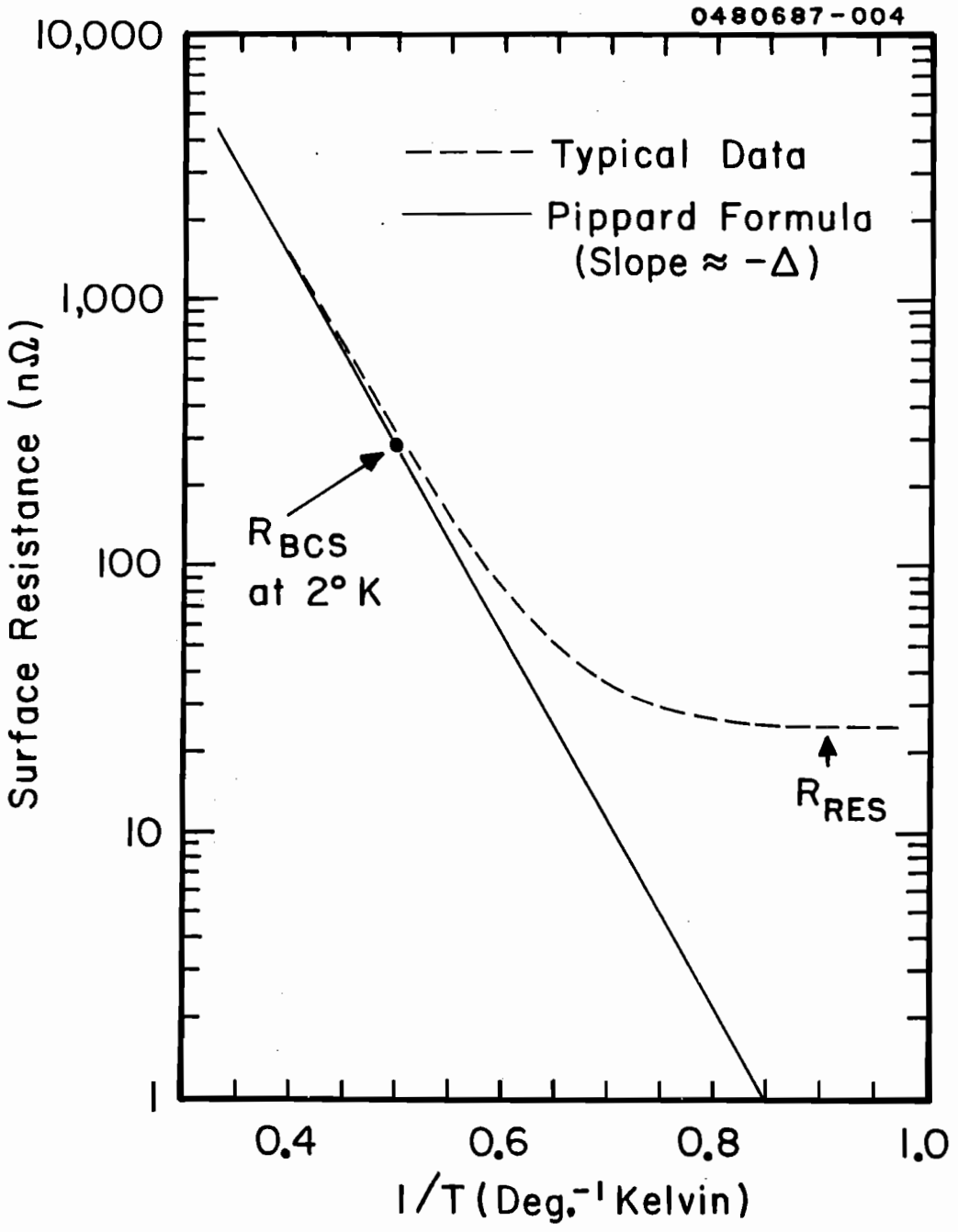

Figure 5.3 Surface resistance of a typical Niobium cavity at 8.6 Ghz. Pippard formula for BCS resistance is approximately exponential with a slope of - Δ.

free path of 2000 angstroms and a frequency of 8.6 GHz., show that the Pippard formula underestimates the gap by about 0.1 degree. Small variations in the determination of Δ result in fairly large changes in the value of R_{BCS}, which requires compensating changes in the value of A. Consequently, rather than reporting A explicitly, we have chosen to report the BCS resistance at 2K, $A \cdot R_{BCS}(\Delta,2)$, which can be measured directly. Figure 5.3 shows the results from a typical cryotest, indicating the significance of these three parameters.

A) Exposure to oxygen

The first group of measurements were done in order to determine the influence of oxide layers on residual resistance. Cavities were UHV fired at $T > 1100°C$ in order to remove the oxide layer, and then repeatedly exposed, first to argon as a control, and then to oxygen. Each pair of exposures was of greater duration and/or pressure than the preceding pair; and each exposure, as well as the initial firing, was followed by a cryotest. The results are shown in Table 5.1. With the exception of one measurement, there is no evidence of any change. There is good reason to suspect that the high value obtained on run 16 was due to a leak in the cavity. On the next test, after chemical polishing and firing, this cavity exhibited strange nonexponential decay curves. A few thermal cycles later, a leak was found with a helium leak detector.

In order to find an upper bound for the infuence of oxygen exposure on residual resistance, we have compared the residual resistance of all the fired cavities before and after their first exposure to oxygen. These data are shown in Table 5.2. Wherever multiple measurements are

TABLE 5.1

Residual resistance as a function of successive surface treatment

Cavity # 2

Run#	Surface Condition	Residual Resistance	RRR
9	BCP, Fired @ 1400C	6.2 n-ohms	42
10	Exposed .02 torr Ar for 2 min.	5.9	"
11	Exposed .02 torr 0 for 2 minutes	8.4	"
12	.1 torr Ar - 1hr	7.5	"
13	(same as 12 - retest)	9.6	"
15	.1 torr 0 - 1hr	7.1	"
16	.1 toor 0 - 45hr	21.2 (leaked?)	"

Cavity # 4

19	BCP, Fired @ 1400C	7.6	160
20	.1 torr Ar - 16hr	5.8	"
22	.1 torr 0 - 16hr	7.7	"
23	.1 torr Ar - 48hr	8.6	"
24	.1 torr 0 - 48hr	7.3	"

available, their average (weighted $1/\sigma^2$) is used. The method for determining the error margins is described in section A.3 (appendix). Our final conclusion is that these oxide layers contribute less than 1.5 nΩ to the residual resistance.

B) Chemical polished cavities

The chemical cleaning process prior to UHV firing consisted of etching the cavities in buffered chemical polish, followed by rinses in

TABLE 5.2

Change in R_{res} after first exposure to O_2

Run #'s		Exposure	Change
Unexposed	Exposed	to Oxygen	(nΩ)
9,10	11	1 min. at 0.02 torr	+2.4 ± 2.6
19,20,21	22	16 hr. at 0.1 torr	+0.6 ± 3.0
32,33	34	16 hr. at 0.2 torr	+1.1 ± 2.0
45,47,48	55	2 hr. at 0.1 torr	-1.1 ± 1.7
60	64	2 hr. at 0.15 torr	-1.9 ± 2.1
Average (weighted: $1/\sigma^2$)			-0.1 ± 1.5

water, acetone, and HPLC grade methanol. Cavities were not always cryotested after this step, and many of the tests that were done occurred before our best testing procedures were developed; however, a few observations can be made. The residual resistance of chemical polished cavities was usually about 50 nΩ. The best result was 26 nΩ, obtained on cavity #4 after several cycles of firing, oxidation, and chem polishing. On the other hand, cavities #5 and #6, which were annealed in yttrium vapor and soaked overnight in 50% HNO_3 prior to chemical polishing showed more than 100 nΩ even though cavity #6 performed acceptably (~12 nΩ) after firing. (Cavity #5 was never fired.)

C) Fired cavities

After chemical polishing, cavities were UHV Fired at T > 1100°C for ~20 minutes, and then tested without exposure to air. A total of six

firings were done using 3 different cavities. The residual resistance was measured after each firing, and a few additional measurements were made after argon exposures or other processes which probably had no effect. Table 5.3 lists these results. Most of the values fall between 6 and 12 nΩ, and much of the variation might be due to experimental uncertainties.

TABLE 5.3

Residual Resistance of Fired Cavities

Run #	Cavity	R_{res}	Surface Treatment	RRR
9	2	6.2 ± 2.5	Fired 1400°C	50
10	2	5.9 ± 2.5	Exposed to Argon (after run 9)	50
19	4	7.6 ± 3.1	Fired 1400°	160
20	4	5.8 ± 3.1	Exposed to Argon (after run 19)	160
21	4	8.3 ± 3.1	Retest after 2 weeks	160
32	4	11.1 ± 1.9	Fired 1100°	115
39	4	7.1 ± 1.9	Fired 1100°	98
45	6	11.3 ± 1.6	Fired 1400°	280
60	6	13.1 ± 1.6	Fired 1400°	180

D) Dependence of residual resistance on ambient magnetic field. Measurements were made on two cavities to determine the contribution to residual resistance from magnetic flux which is trapped in the walls of the cavity as it cools down through the transition temperature. Figure 5.4 shows residual resistance of two different cavities as a function of ambient magnetic field during cooldown. The results are only

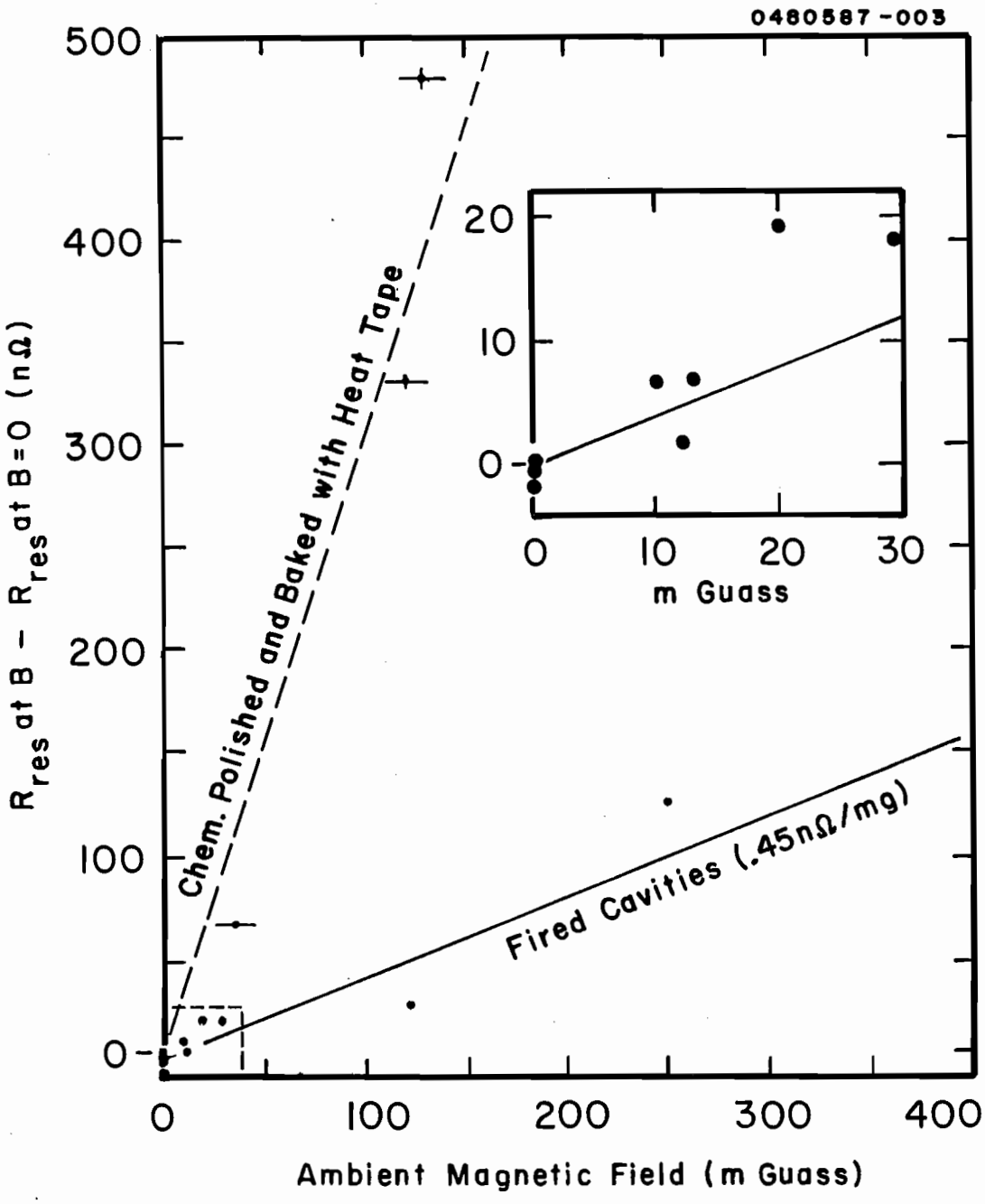

Figure 5.4 Increase in residual resistance due to ambient magnetic field applied during cooldown. Poorly reproducible data have a slope between 0.3 and 0.6 nΩ/mg for fired cavities, and a much higher slope for chemical polished baked cavity (baking temperature unknown). Inset shows points near origin.

reproducible to about ± 40%, but they show two distinct curves, both of which are roughly linear. The lower curve, with a slope between 0.3 and 0.6 nΩ/milligauss, was measured on cavity #6, which had an RRR of 280 and an oxide free (fired) surface. The upper curve, with a slope of about 3 nΩ/milligauss, is some early measurements on cavity #2. This cavity, which had an RRR of about 100, had been chemical polished and rinsed, and then evacuated and baked out overnight at an unknown temperature (maybe 200°C). Section 3 B of this chapter contains additional evidence suggesting that the bakeout caused this higher slope.

Lyenis{32} found that the magnetic field contribution to residual resistance could be substantially reduced if the cavity was cooled inside a vacuum chamber so that cooling occured only by thermal conduction. On many of our measurements, the cavity was cooled as slowly as possible (< 0.5 degree/min.) in a helium atmosphere, surrounded by a copper container in order to reduce thermal gradients. However, our procedure was not effective. The results were no different than those obtained when liquid helium was transfered directly onto the cavity.

E) Effect of niobium purity on BCS resistance

A simple measure of niobium purity is the residual resistivity ratio (RRR) which is the ratio of the DC resistivity of the cavity at room temperature divided by the resistivity at 10°K.{58} Figure 5.5 shows the BCS resistance at 2°K for several cavities as a function of the RRR of the cavities. (The point marked with an "X" is a heated

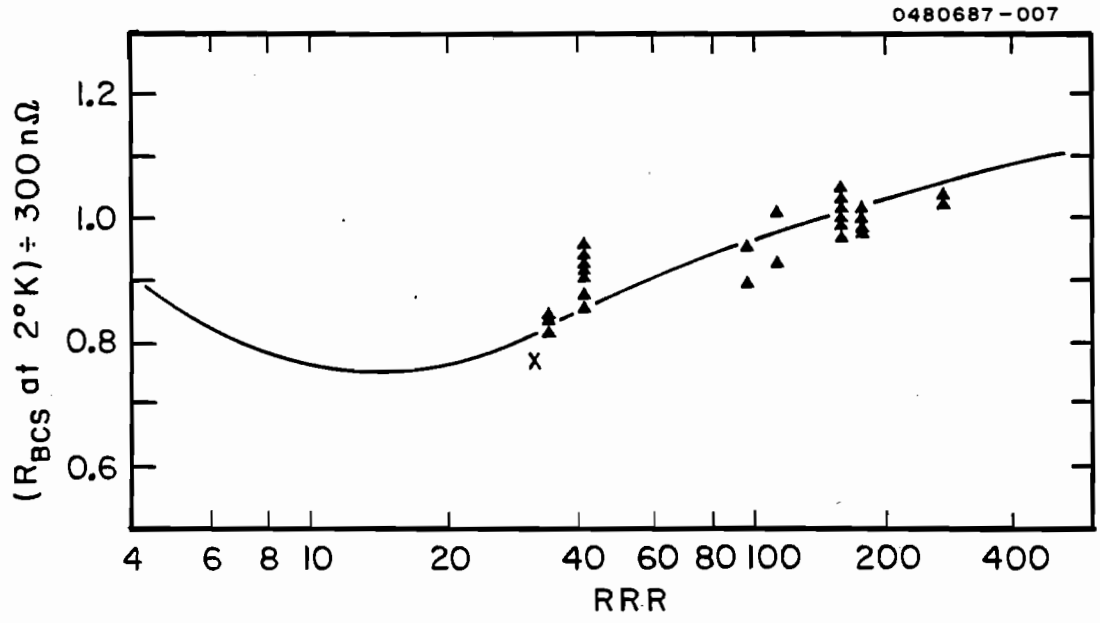

Figure 5.5 BCS resistance at 2°K as a function of niobium purity (RRR).

cavity discussed in section 3 D.) Figure 5.6 shows the same effect at 4.2° and at 1.33°. The results are essentially the same, although the accuracy is somewhat reduced since most of these results are extrapolated from data in the temperature range between 1.35° and 3.3°.

The curves drawn through figures 5.5 and 5.6 were calculated with the program by Halbritter,{16} which uses the single gap Green's function expression {2} for the current density. (We have used the estimate, l = (20 Angstroms)·(RRR), for the mean free path. Other material parameters for niobium are identical to those used by Halbritter.) The main features of these curves can be derived from a simple description of the anomolous skin effect. The expression for power loss per unit volume in an ordinary conductor is $E^2 \cdot ne^2\tau/m$, where,

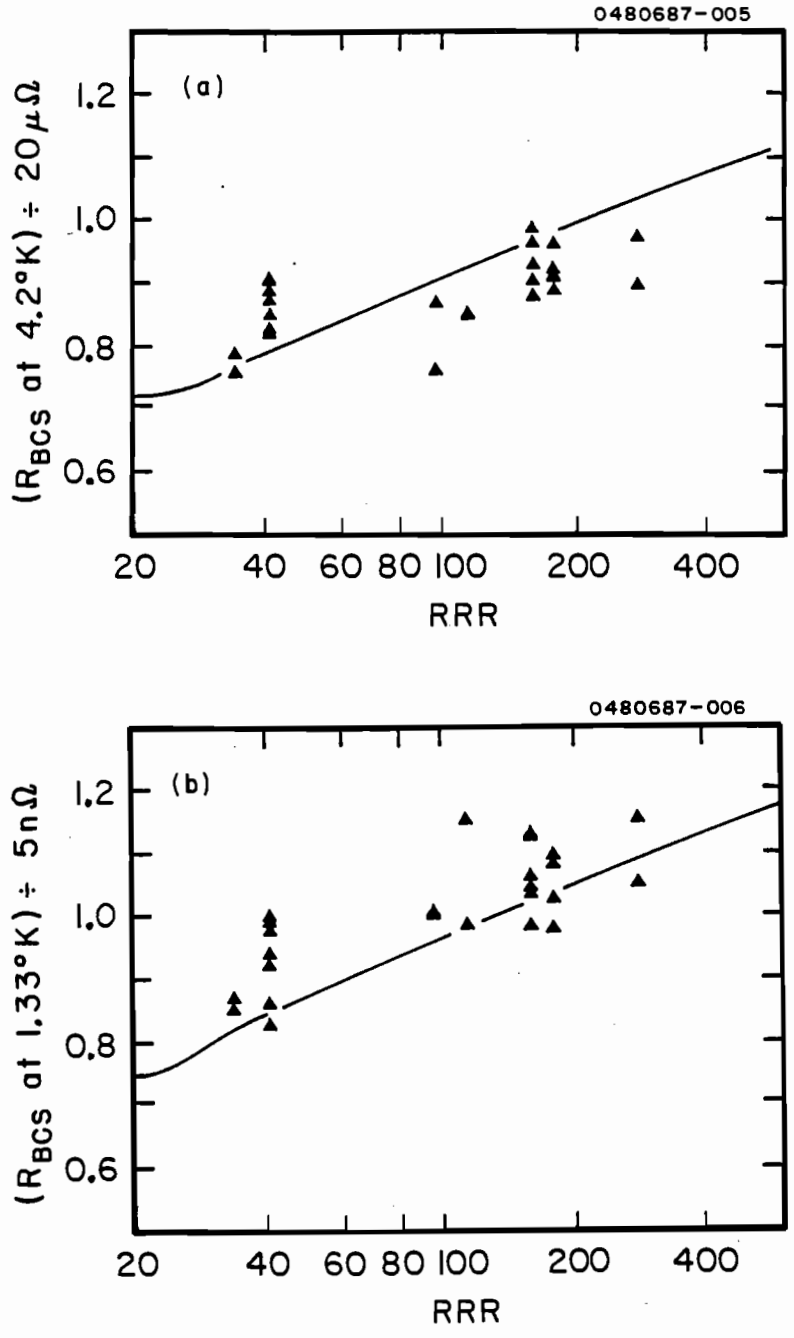

Figure 5.6 BCS resistance as a function of niobium purity, extrapolated to 4.2°K (A) for comparison with other work, and to 1.33° (B) since uncertainty in the values at this temperature contributes to errors in residual resistance.

in this case, n is the density of "normal" electrons. The relaxation time, τ, is related to the mean free path, l, by $\tau = l/v$, where the average thermal velocity, v, is typically about one half the fermi velocity. If l is less than the penetration depth, λ, then the penetration depth is proportional to $l^{-1/2}$. Maxwells equations give $\int E^2\, dz \sim \lambda^3$, so the surface resistance, R, is proportional to $l^{1/2}$. For $l >> \lambda$, the penetration depth is constant, and the factor of l in the conductivity is replaced by the average distance, l_{eff}, which the electron travels inside the penetration layer.

$$l_{eff} = \frac{1}{4\pi} \int L(\theta)\, d\Omega$$

where θ is the angle beween the electron trajectory and the normal to the surface, and $d\Omega = 2\pi \sin\theta\, d\theta$. If the electron travels parallel to the surface ($|\theta - \pi/2| < \lambda/l$), the local expression is correct, and $L(\theta) = 1$. For other angles, the anomolous expression is approximately $L(\theta) = \lambda/\cos\theta$, so the surface resistance is proportional to

$$l_{eff} = \int_{\pi/2}^{\pi/2+\lambda/l} l \sin\theta\, d\theta \;+\; \int_{\pi/2+\lambda/l}^{\pi} \lambda \tan\theta\, d\theta \;\sim\; \lambda\,(\,1 + \log(l/\lambda)\,)$$

If the relaxation time is greater than the RF period, further increases in l are unimportant. The anomolous term, which dominates l_{eff} is unchanged except that the range of integration becomes $|\theta - \pi/2| > \lambda\omega/v$ instead of $|\theta - \pi/2| > \lambda/l$. The local term goes to zero for very long l, since these electrons simply oscillate in the absence of scattering.

F) Possible effect of niobium purity on residual resistance.

Figure 5.7 shows the residual resistance of UHV fired (unoxidized) cavities as a function of niobium purity (RRR {58}). The curve drawn through (or below) the data is interpolated from the graphs by Scharnberg,{36} of calculated residual resistance due to direct generation of phonons by the RF electric field. [We assume that the mean free path is given by $l = 20\text{Å} \cdot (\text{RRR})$.] The data and the theory do at least have the same order of magnitude, and possibly the same sign for the slope, but the errors are almost as large as the data, so these similarities could easily be coincidental. Scharnberg's theory predicts a strong ($\sim\omega^2$) frequency dependence for the residual resistance of high-purity (RRR > 100) niobium. At frequencies below 4 Ghz, the prediction is well below the observed values, but verification of this theory might be possible at higher frequencies.

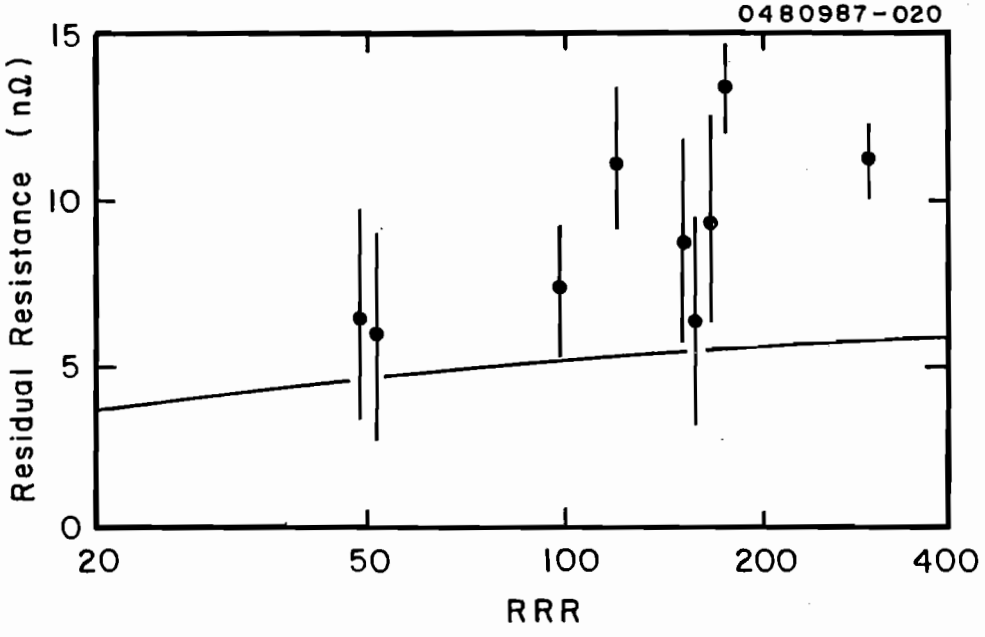

Figure 5.7 Residual resistance as a function of niobium purity. Curve is interpolated from theory of Scharnberg.

5.3 Effect of Heating Cavities to ~ 300°C

When an oxidized niobium surface is heated to 300°C for 5 to 10 minutes, most or all of the Nb_2O_5 surface layer dissolves into the metal, creating an oxygen-rich layer whose thickness is limited to a few thousand angstroms by the diffusion rate of oxygen in niobium. The oxygen concentration within this layer should be a few atomic parts per thousand. Oxygen - niobium solutions have several known properties: The residual resistivity ratio (RRR) is given by 3.5/c, where c is the oxygen concentration in atomic percent; the BCS resistance decreases slowly with increased oxygen concentration, at least for concentrations of less than 0.1 %; and the critical temperature declines by .93 degrees per atomic percent.{62}

Numerous measurements were made on both oxidized and unoxidized cavities which had been heated in this manner. Although quantitative comparisons are difficult, all of the above properties were observed on oxidized heated cavities. We also found that these cavities exhibited increased residual resistance, and an increased dependence of that residual resistance on ambient magnetic field. The first set of measurements used this heating technique as a tool to measure the extent of contamination of the "unoxidized" surfaces. Later experiments investigated various properties of surfaces which had been oxidized before heating.

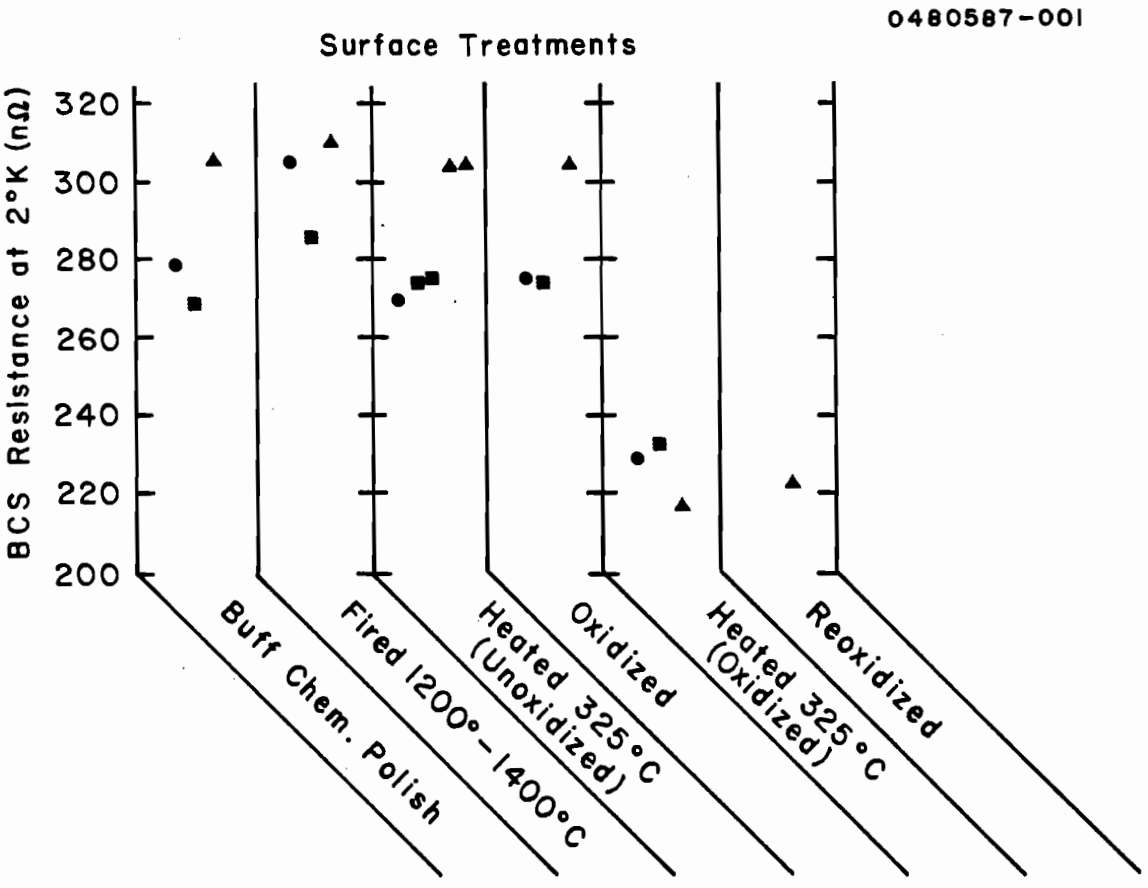

Figure 5.8 BCS resistance at 2°K as a function of successive surface treatments. ●: cavity 4 runs 31 through 37; ■: cavity 4 runs 38 through 43, and ▲: cavity 6 runs 44 through 58.

A) Surface resistance of cavities heated to 325°C

Three cycles of measurements were made to compare the surface resistance of oxidized and unoxidized cavities, which had been heated. Each cycle consisted of the following surface treatments, with a cryotest following each treatment: buffer chemical polish and rinsing, oxide removal by firing at 1200 - 1400°C, heating to 325° for 10 minutes, exposure to 0.1 torr oxygen for 2 to 16 hours (the time doesn't

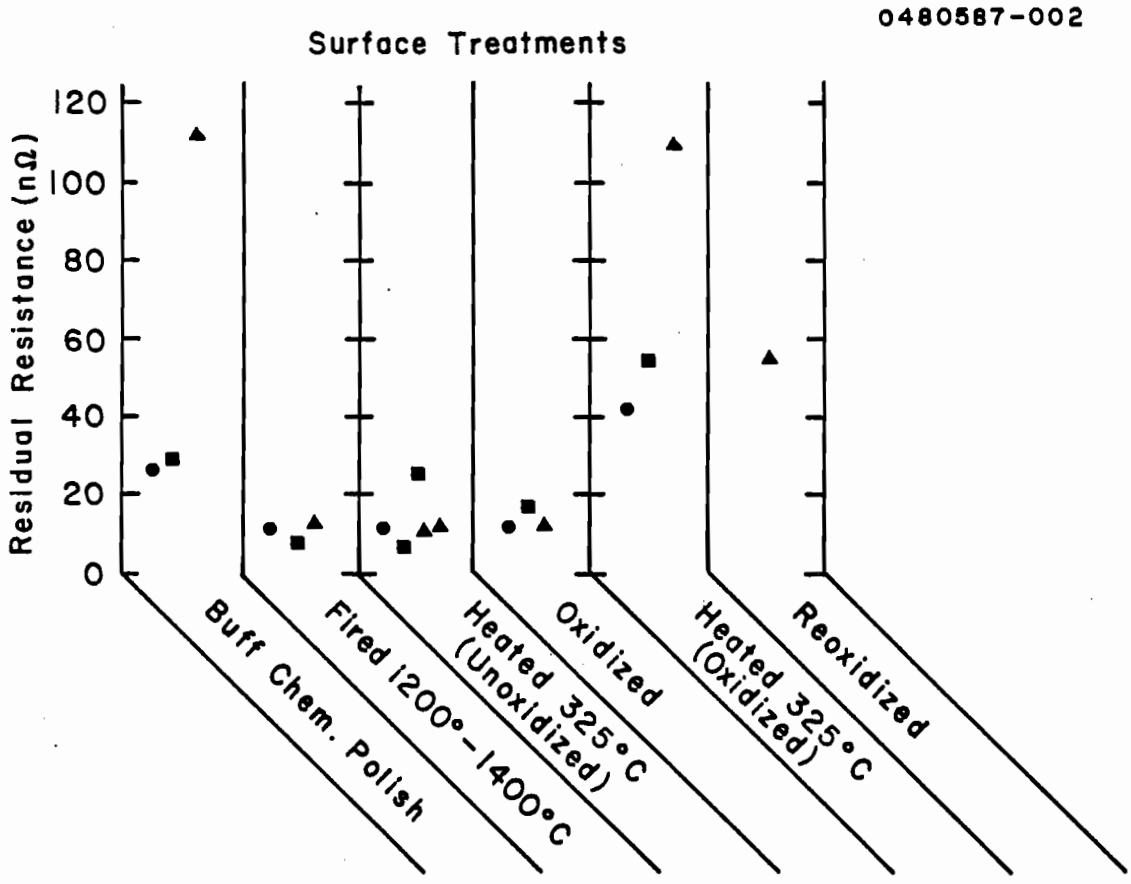

Figure 5.9 Residual resistance as a function of successive surface treatments for the same cavities shown in figure 5.8.

seem to matter), and reheating to 325°. The unoxidized cavities were sometimes heated twice in order to collect additional data.

Figures 5.8 and 5.9 show the effects of these treatments on the BCS resistance at 2°K, and on the residual resistance. When oxidized surfaces are heated to 325°C, the BCS resistance decreases by about 20%, but the residual resistance increases by about 50 nΩ. These two effects cancel each other near 2 degrees . The oxide-free cavities were usually not affected by this heating. Since the oxidized cavities were probably

covered with about 15 angstroms of Nb_2O_5, this implies that oxygen contamination of the UHV fired surfaces probably does not exceed one or two monolayers.

The last column of figure 5.9 shows a single measurement in which a final exposure to oxygen reduced the residual resistance of a cavity which had been first oxidized and then heated. This might suggest that the residual resistance of the heated cavity was due to a layer of suboxides that was then converted to the dielectric, Nb_2O_5, by exposure to oxygen. However, no such layer was found by Kirby et al.,{83} using XPS measurements. Their investigation is described in section 5 of this chapter.

B) Dependence of RF properties on heating temperature

A single cycle of measurements was made in order to determine the effects of heating to different temperatures. While the reproducibility of single measurements has not been checked, at least some of the trends in the data are probably correct. The cavity was first cold polished and fired, then oxidized, and then heated to successively higher temperatures with two cryotests following each of these procedures. The first cryotest was done in the usual way with the ambient magnetic field screened to less than two milligauss. The cavity was then warmed above 20°K; and a magnetic field of 120 milligauss was applied while the cavity was cooled and retested.

Figure 5.10-a and 5.10-b show the BCS resistance at 2 degrees, and the residual resistance after firing and oxidation, and after heating to three successive temperatures. The curve drawn through 5.10-a is

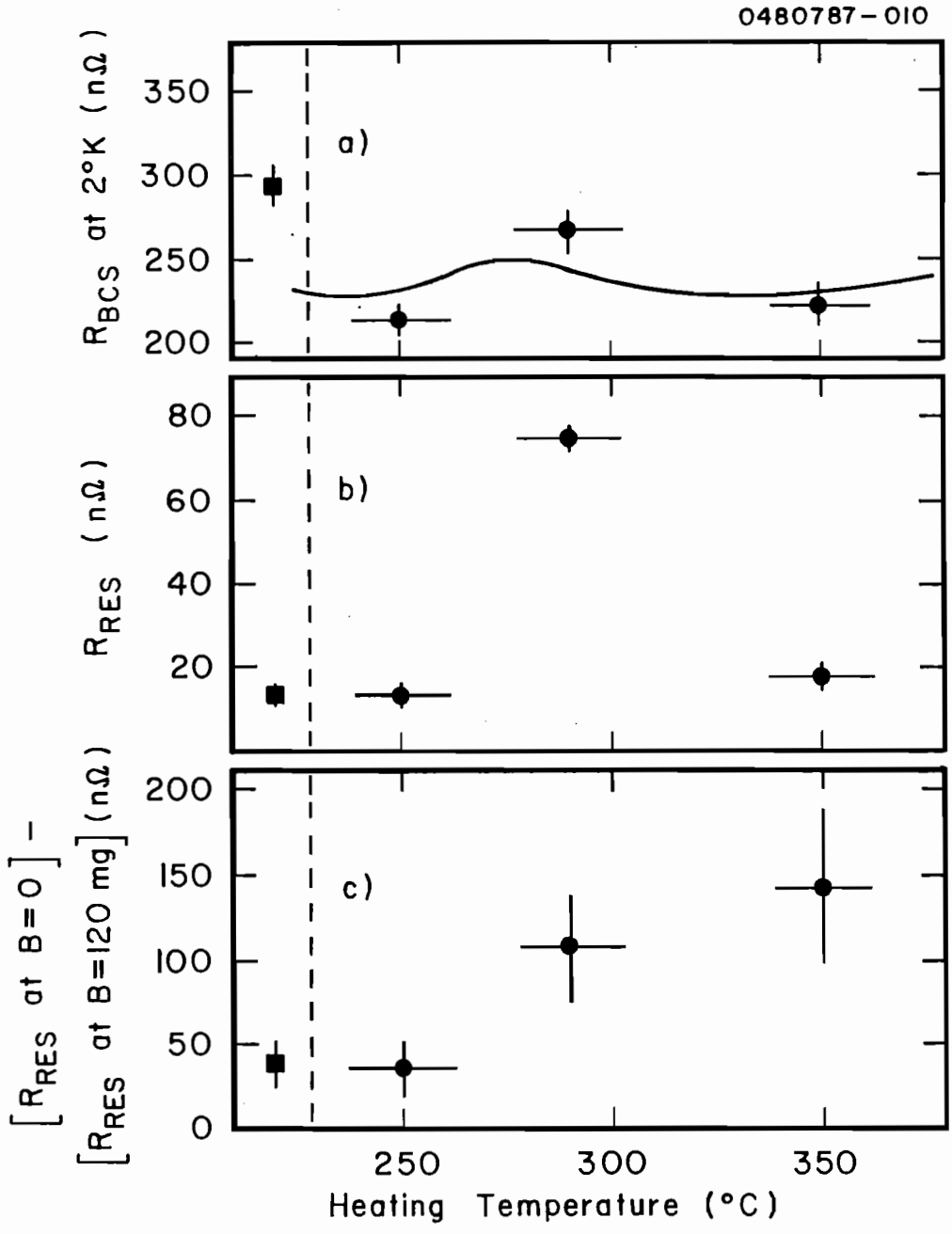

Figures 5.10 BCS resistance at 2°K (a), residual resistance (b), and enhancement of residual resistance from a 120 mg magnetic field applied during cooldown (c) for an oxidized niobium cavity after heating in vacuum to successively higher temperatures. Square points show values prior to oxidation.

calculated from equation [5.4]. Figure 5.10-c shows the increase in residual resistance caused by application of a 120 milligauss magnetic field following these same treatments. This increase is probably due to some nonuniformities in the surface where magnetic flux lines are trapped as the cavity cools. Kneisel et al.{60} observed a similar phenomenon on niobium cylinders which had been cooled to room temperature very slowly (~12 hr.) after UHV Firing. The effective penetration depth measured as a function of DC magnetic field, showed an irreversibility due to trapped flux. This effect was much smaller on samples that had been cooled roughly three times faster.

C) RF transition temperature

Heating an oxidized cavity typically reduced its RF transition temperature (T_c) by a few tenths of a degree. Although it is well known that the superconducting transition temperature of Nb declines by .93 degrees per atomic percent of dissolved oxygen,{62} the quantitative significance of our RF data is less clear. The influences of concentration gradients and proximity effects are not known, but it does seem safe to assume that RF measurements sample a depth no greater than the normal skin depth, which, in this case, is equal to 2 μm/(RRR)$^{1/2}$, where RRR is the local residual resistivity ratio. It was necessary to expose the cavities to air in order to make these measurements.

Since the RF surface resistance is continuous at T_c, we have arbitrarily defined the RF transition temperature as is shown in figure 5.11. Just below the transition, the Q of the cavity increases fairly linearly with decreasing temperature. We have defined T_c as the

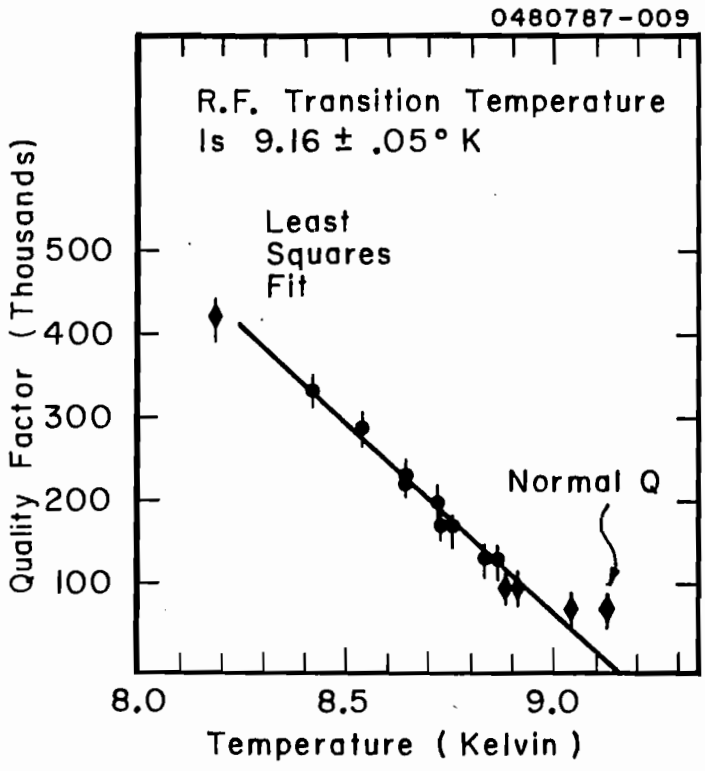

Figure 5.11 Quality factors for a typical cavity near T_c, showing the definition of the RF transition temperature. Diamond-shaped data points were not used due to high β or value within noise level of normal Q.

extrapolation of this line to Q = 0. Transition temperature measurements were typically reproducible to within a tenth of a degree.

The RF transitions for several cavities are shown in figure 5.12. All of the cavities which were oxidized and heated have T_c values below 9°. Two of these cavities were then chemical polished to remove the oxygen-rich layer, after which the T_c was remeasured. These pairs of points are indicated by identically shaped data points. Several other chemical polished or heated cavities are indicated by round dots. The

temperature calibration may contain an offset of a few tenths of a degree, but the changes in temperature should be accurate to within a tenth of a degree or less.

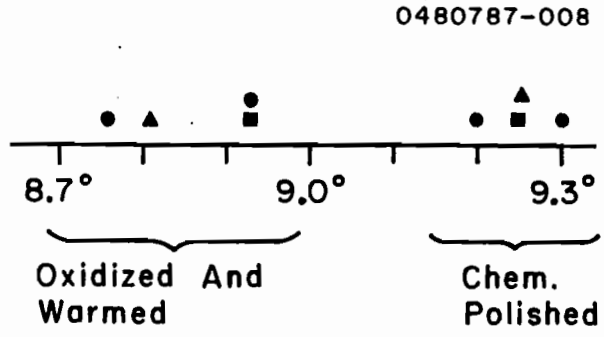

Figure 5.12 RF transition temperatures for several cavities after oxidation and heating to temperatures near 300°C, and after chemical polishing. ■: Cavity #4 after run 43. ▲: Cavity #6 after run 58.
●: Other cavities.

D) Normal surface resistance

The normal surface resistance of a non-magnetic metal with (local) resistivity, ρ ,is given by

$$[5.2] \qquad R = \frac{1}{2}\sqrt{\frac{\omega\ \mu_0\ \rho}{2}} \qquad \text{(MKS)}$$

For our cavities, this implies $Q = 27000/\rho$, where ρ is in units of μohm-cm. There are two likely reasons for this formula to fail. One is the anomalous skin effect, which occurs only if the resistivity is low enough for the electron mean free path to be comparable to the RF skin depth. The other is that the metal near the surface may have a

different resistivity from the bulk value which is obtained from DC or low frequency measurements.

Figure 5.13 shows normal Q's for two different cavities as a function of their measured DC resistivity. The latter was varied by cooling the cavity from ~100K down to 10K. Cavity #5 was a chemically polished cavity that had never been heat treated except for the initial annealing in Yttrium vapor during manufacture. Its RRR was about 400, which implies a bulk resistivity of .04 μohm-cm at 10°K. The Q of this cavity agrees with the simple theory at least for $\rho > 0.2$ μohm-cm, indicating that, for resistivities in this range, the anamolous skin effect is not important.

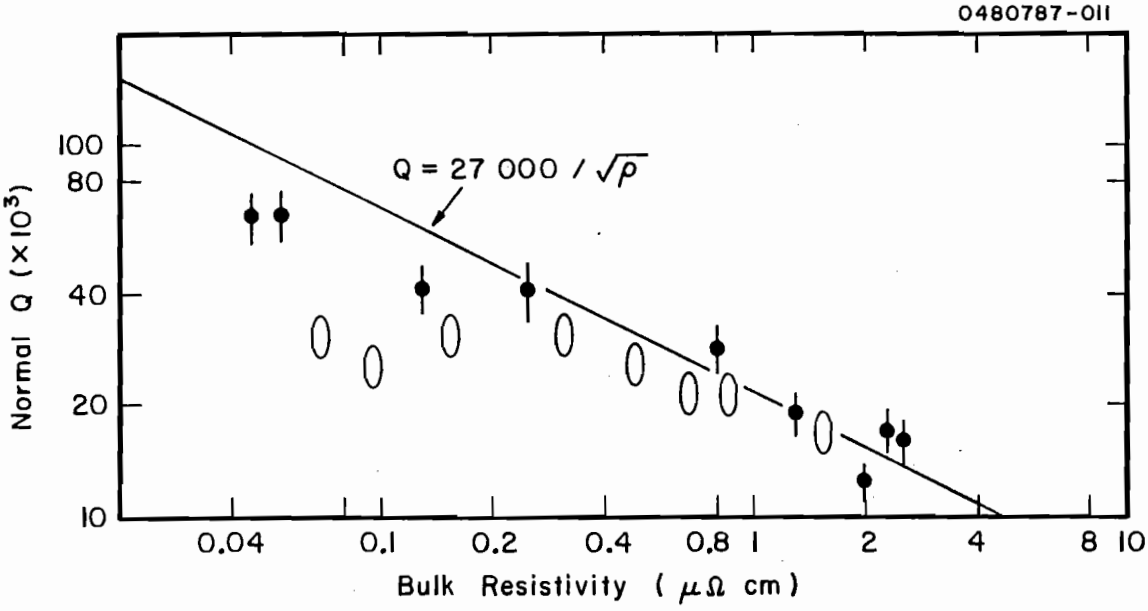

Figure 5.13 Normal quality factors for two cavities at 10°K < T < 100°K as a function of the DC resistivity of the cavity. ♦: Chemical polished cavity. O: Oxidized and heated cavity.

Cavity #6 had a bulk RRR of 180. It had been oxidized and then heated to a maximum of 350°C, as described in section 3 B of this chapter. The normal Q of this cavity never exceeded 10,000, which corresponds to ρ = .5 μohm-cm, or RRR = 30. This result is consistent with the value of the BCS resistance at 2°K which had been measured earlier. The relationship between the RRR of unheated cavities and their BCS resistance at 2° is shown in figure 5.5. The point corresponding to this cavity is marked with an X. After the normal Q measurements were made, this cavity was cooled below the transition temperature. The Q increased rapidly, as expected, indicating that the normal Q had not been limited by dead flies or similar foreign matter in the cavity.

5.4 Energy Gap

It is surprising that no significant variations in the superconducting energy gap temperature (Δ) were observed. Variations have been reported in the literature under similar circumstances,{84} and might have been expected from the BCS theory. The simplest form of this theory predicts a constant ratio, $\Delta = 1.76\ T_c$, between the gap and the transition temperature, which was seen to vary by several per cent. A possible explanation has to do with the relative scales of length. For $T < T_c/2$, the coherence length, $\hbar v_f/\pi\Delta$, is less than the mean free path unless the metal is very dirty (RRR < 20). This implies that the oxygen atoms act as localized defects which do not affect most of the superconductor, so the low temperature gap is unaffected. Near the

transition temperature, the gap approaches zero, making the coherence length much larger than the mean free path, so that scattering may limit the ability of the system to form a coherent state. The depression of the critical temperature by interstitial oxygen is probably not a simple mean free path effect, since some impurities can even raise T_c.{63} But, the change in the coherence length may explain why T_c is altered while the gap remains unchanged.

We have looked for correlations between the energy gap and several parameters, each of which is discussed briefly below. In most cases, changes in the gap were found to be well under one percent.

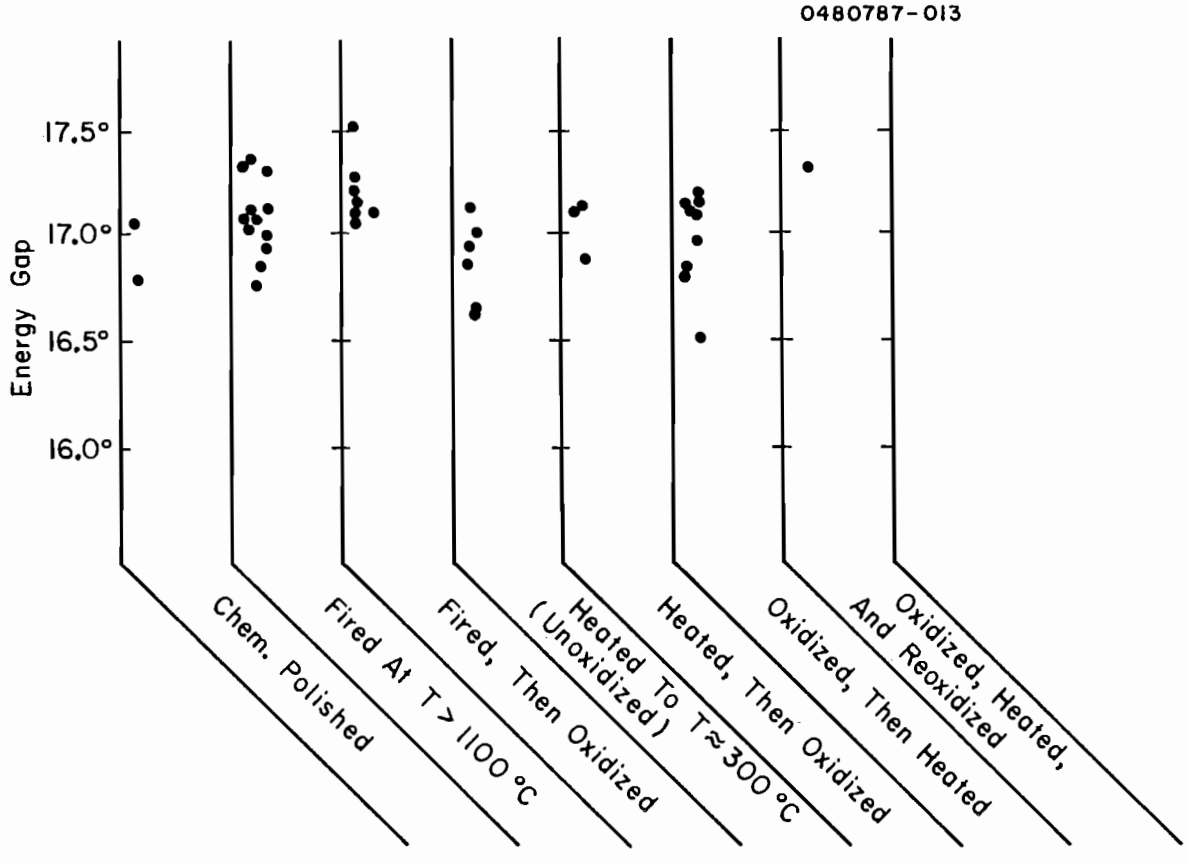

Figure 5.14 Energy gap for cavities with various surface treatments (error bars not shown).

A) Surface treatment

Figure 5.14 shows gap values grouped according to the surface preparation of the cavities. These treatments include chemical polishing, and three types of heat processes: UHV Firing at T > 1000°C, heating to T ~ 300°C without exposure to oxygen ("clean"), and heating to ~300° after exposure to oxygen. For each heat treatment there are two groups of data depending on whether or not the cavity had been exposed to oxygen after the treatment. The analysis of these data is summarized in figures 5.15 and 5.16. Figure 5.15 shows the mean and

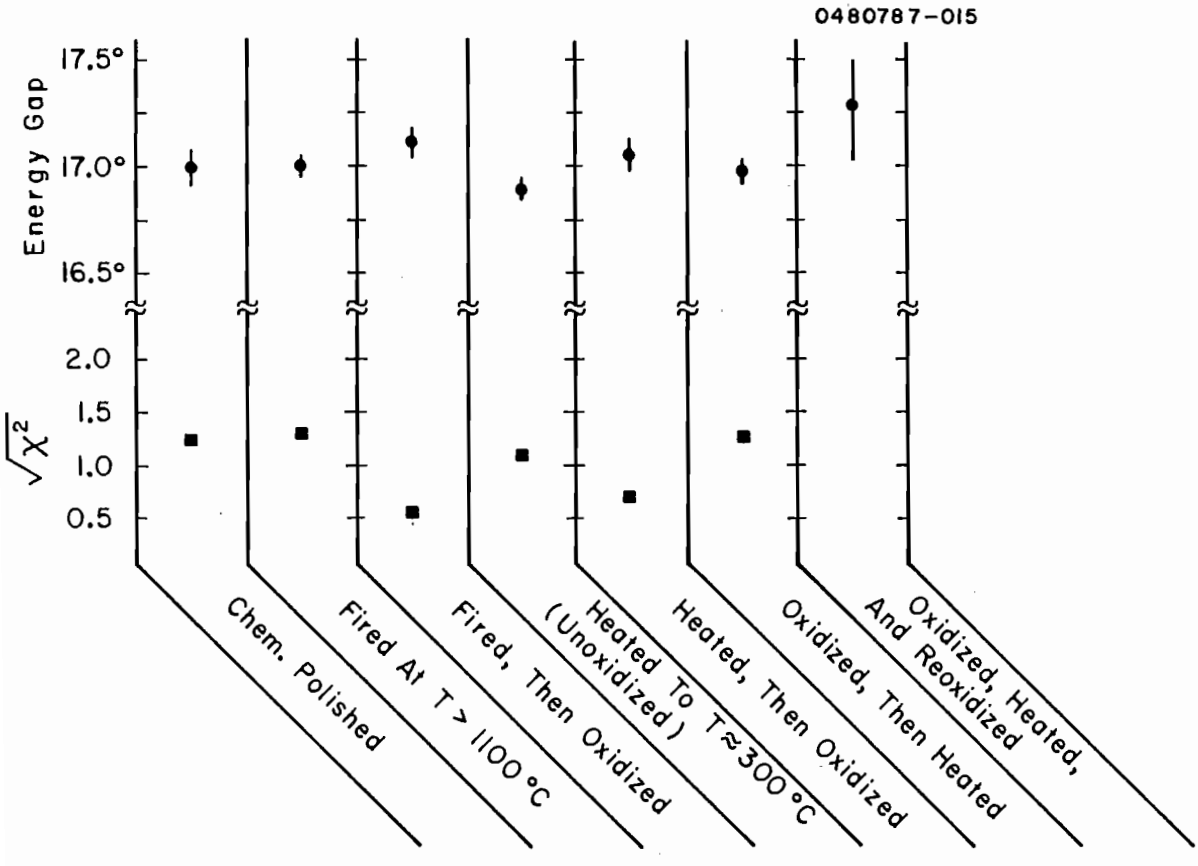

Figure 5.15 Average energy gap for same surface treatments shown in 5.14, with error estimates for averages and normalized goodness of fit parameter, χ^2.

standard deviation for each of these groups, while in figure 5.16, the oxidation immediately prior to testing is assumed to have no effect, so that there is only one group for each heat treatment. The "goodness of fit" parameter, χ^2 is also shown. It is defined by

$$\chi^2 = \frac{1}{N-1} \cdot \sum_{i=1}^{N} \left[\frac{(\Delta_i - \bar{\Delta})}{\sigma_i^2} \right]^2 \quad , \text{ where } \quad \bar{\Delta} = \frac{\Sigma\, \Delta_i/\sigma_i^2}{\Sigma\, 1/\sigma_i^2}$$

where N is the number of measurements in the group, and the σ's are the estimated accuracies for each measurement. The method for determining σ's is described in section A.1 (appendix). χ^2 should be expected to differ from 1 by no more than about $(N-1)^{-1/2}$.

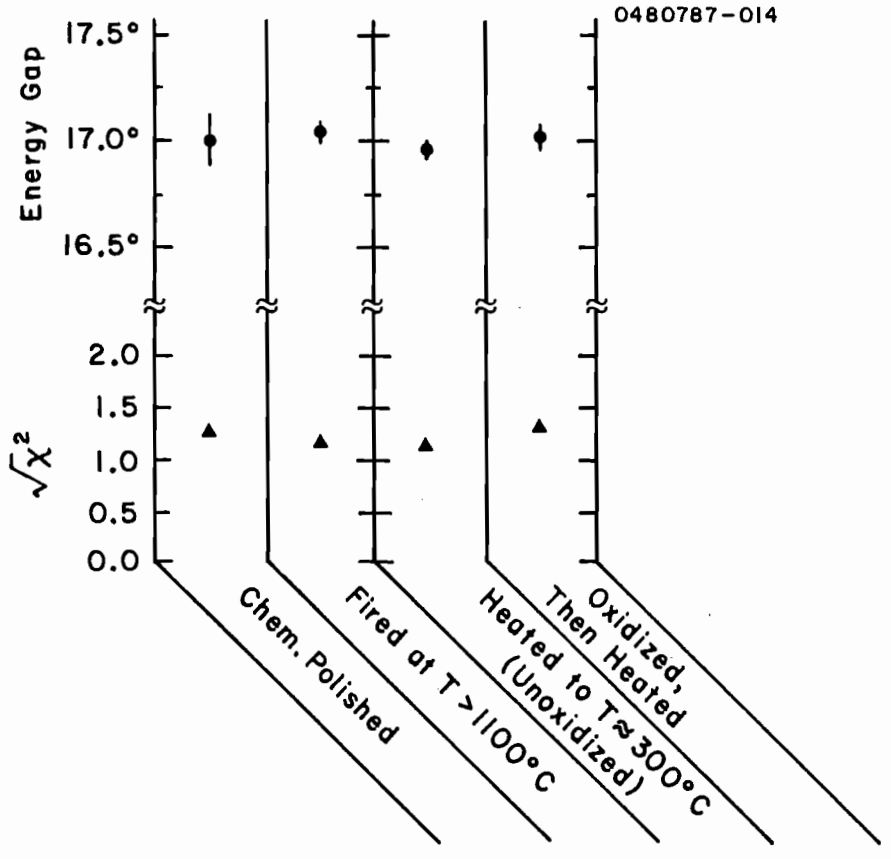

Figure 5.16 Average energy gap for same surface treatments as 5.15 with data from oxidized and unoxidized cavities merged.

B) Niobium purity

Figures 5.17 shows the gap as a function of the residual resistivity ratio (RRR) of the cavity. All cavities with RRR > 90 had been purified by annealing in Yttrium vapor. The other cavities did not receive this treatment. Cavities which had been exposed to oxygen and then heated are not used here.

C) Magnetic field

Figure 5.18 shows the Gap as a function of the ambient magnetic field during cooldown. The fields have been truncated to the nearest 10 milligauss. Values for χ^2 are listed if more than one measurement was made at the same field. No significant trend was expected or observed.

D) Time

Figure 5.19 is provided for completeness. It shows all gap values as a function of run number (chronological order). The RRR values are also shown so that separate measurement cycles can be easily identified.

5.5 Surface Studies of Oxide Layers Near T = 300°C

Kirby et al.{83} have conducted XPS, Auger and secondary electron emission studies in parallel with our superconducting RF studies of oxide layers which have been heated to temperatures near 300°C. This study used niobium samples from the same materials that were used in cavity manufacture and followed our procedures as closely as possible.

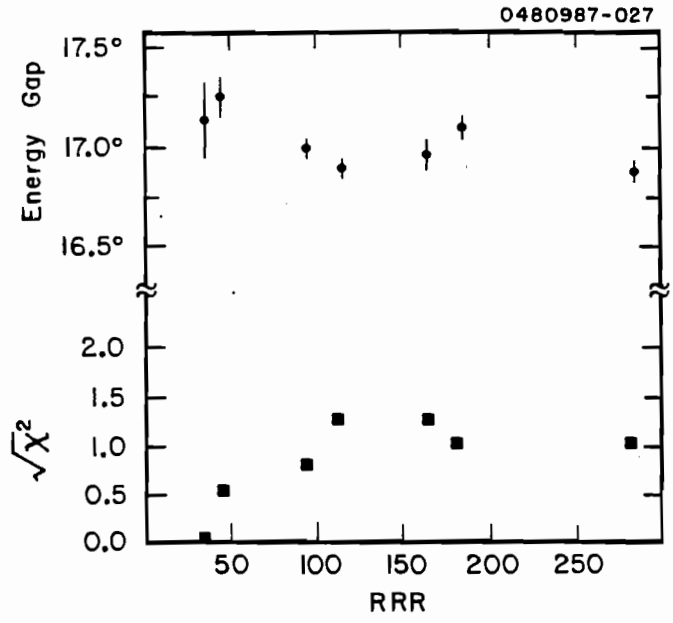

Figure 5.17 Average energy gap as a function of niobium purity (RRR). (χ^2 is normalized goodness of fit parameter.)

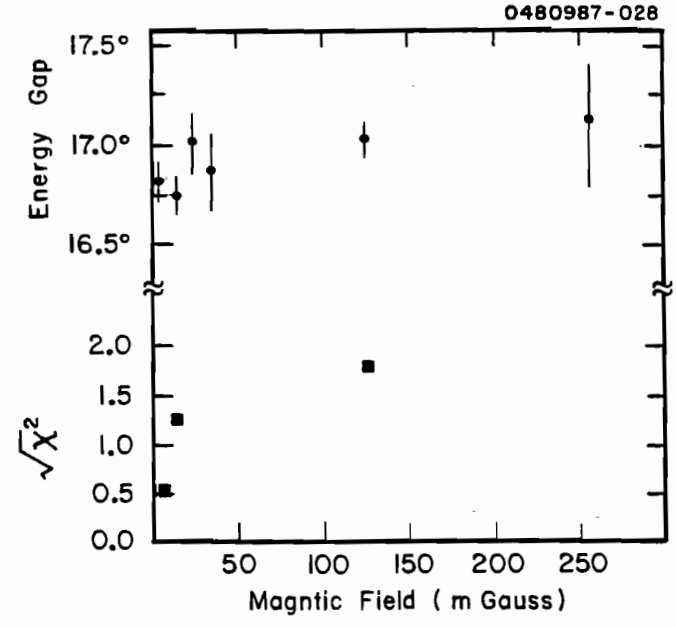

Figure 5.18 Energy gap as a function of ambient magnetic field during cooldown. χ^2 values are shown if more than one measurement was made at same field.

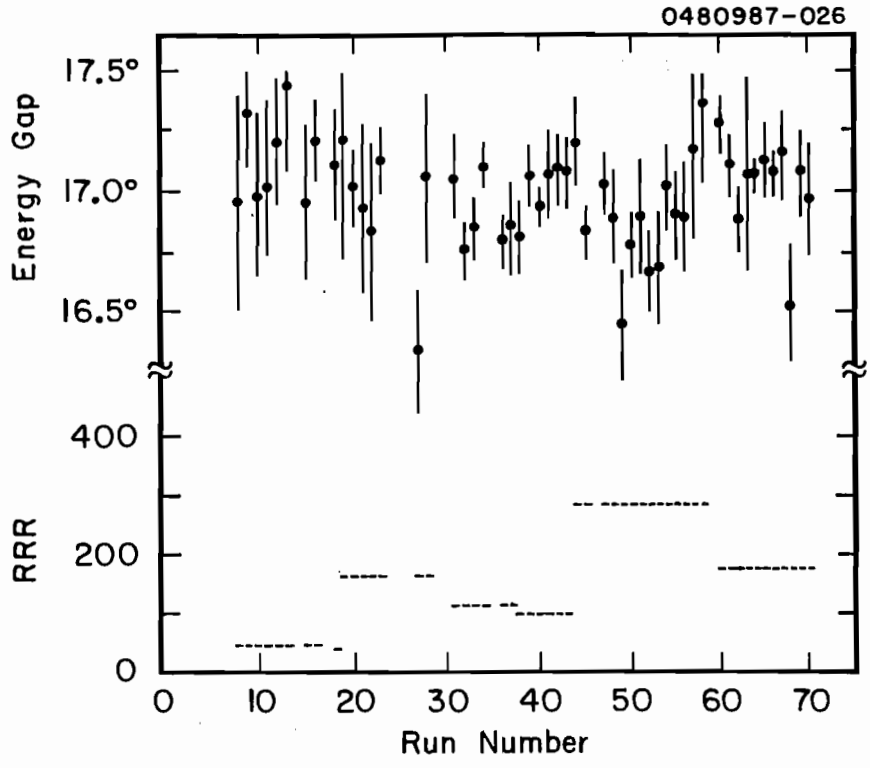

Figure 5.19 Complete listing of all measured energy gaps. Cavity RRR is also shown.

The samples, which had RRR values between 100 and 150, were fired in an RF furnace at 1200° for 20 minutes and then raised to 1400° for one minute. They were then transferred, under vacuum, to the chamber where the spectrometers were located. Samples could be heated in the spectrometer chamber to 300° or more with an electron beam incident on the back of the sample. An adjoining chamber was used to expose the sample to 0.1 torr of oxygen for two hours. As with the RF study, the first measurements looked at niobium which was fired, oxidized, and heated to 300° for 10 minutes. Later measurements studied the dependence of these results on the temperature of the final heating.

The principal observation from the first part of this study was that measurements made after high temperature firing, exposure to oxygen, and heating to 300°C were practically indistinguishable from measurements made immediately after firing. The fired niobium was covered with roughly one monolayer of oxygen, which was probably due to to a combination of precipitation from the bulk during cooldown, and contamination during transfer to the spectrometer chamber. After exposure to oxygen, the XPS showed a 13 angstrom thick layer of Nb_2O_5, which contained about five times more oxygen than was originally seen. The 300° heating drove most of this oxygen into the metal leaving roughly the same coverage as before. It was not possible to associate any particular stoichiometry with the single monolayer coverages.

The Auger spectrometer detected both sulfur and phosphorus contamination on some of the samples, but there is no evidence that these elements had any major effect on the RF results. The total secondary yield was not significantly affected by oxidation or heating. It remained between 1 and 1.2 over the range of incident energies from 100 to 1400 volts.

Some particularly interesting XPS data were taken while a piece of niobium was slowly heated up to 350°. The temperature as a function of time for these measurements is shown in figure 5.20. The times during which each spectrum was made are indicated with solid lines, and identified with numbers. Figure 5.21 shows the Nb 3d and the oxygen 1s lines from these spectra. The signal for niobium metal is the two main peaks at binding energies of 202 and 204.5 ev. If the niobium is

oxidized, these peaks are shifted in proportion to the valence of the niobium.{85} The two small peaks in curve (A) are due to Nb_2O_5 (valence = 5).

As the temperature approaches 250°, The Nb_2O_5 breaks up into a mixture of oxides with valences from 4 to 5, however the Nb metal peaks, as well as the oxygen peak at 531 ev remain at the same height, indicating that almost all of the oxygen remains within the ~ 20 angstrom surface layer from which the photoelectrons can escape. Seven minutes later, and 40 degrees warmer, most of the oxygen has left the surface and diffused farther into the bulk. Above 300°, the XPS spectrum changes only slightly as the remaining traces of oxygen continue to diffuse into the bulk.

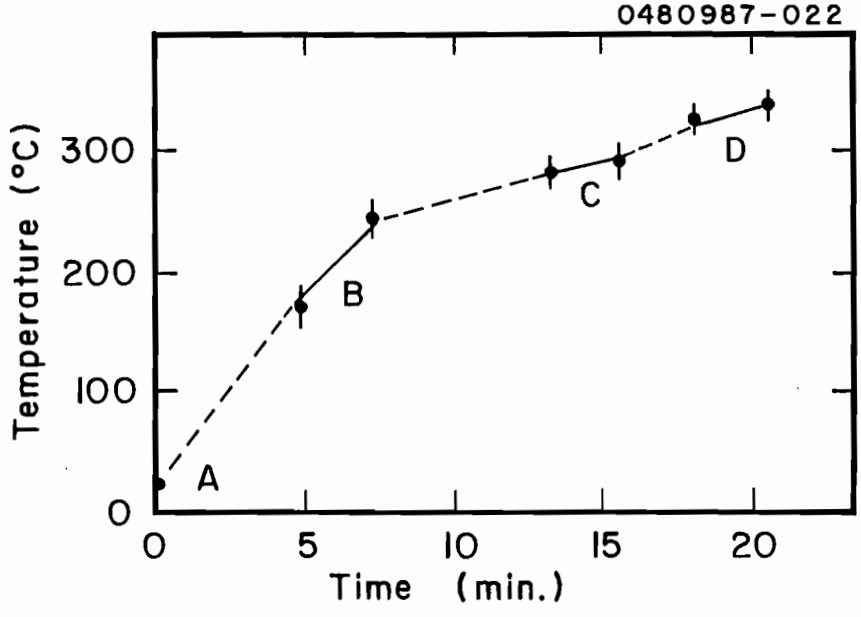

Figure 5.20 Temperature vs. time for niobium sample. Solid lines show when XPS data were taken. (See figure 5.21.)

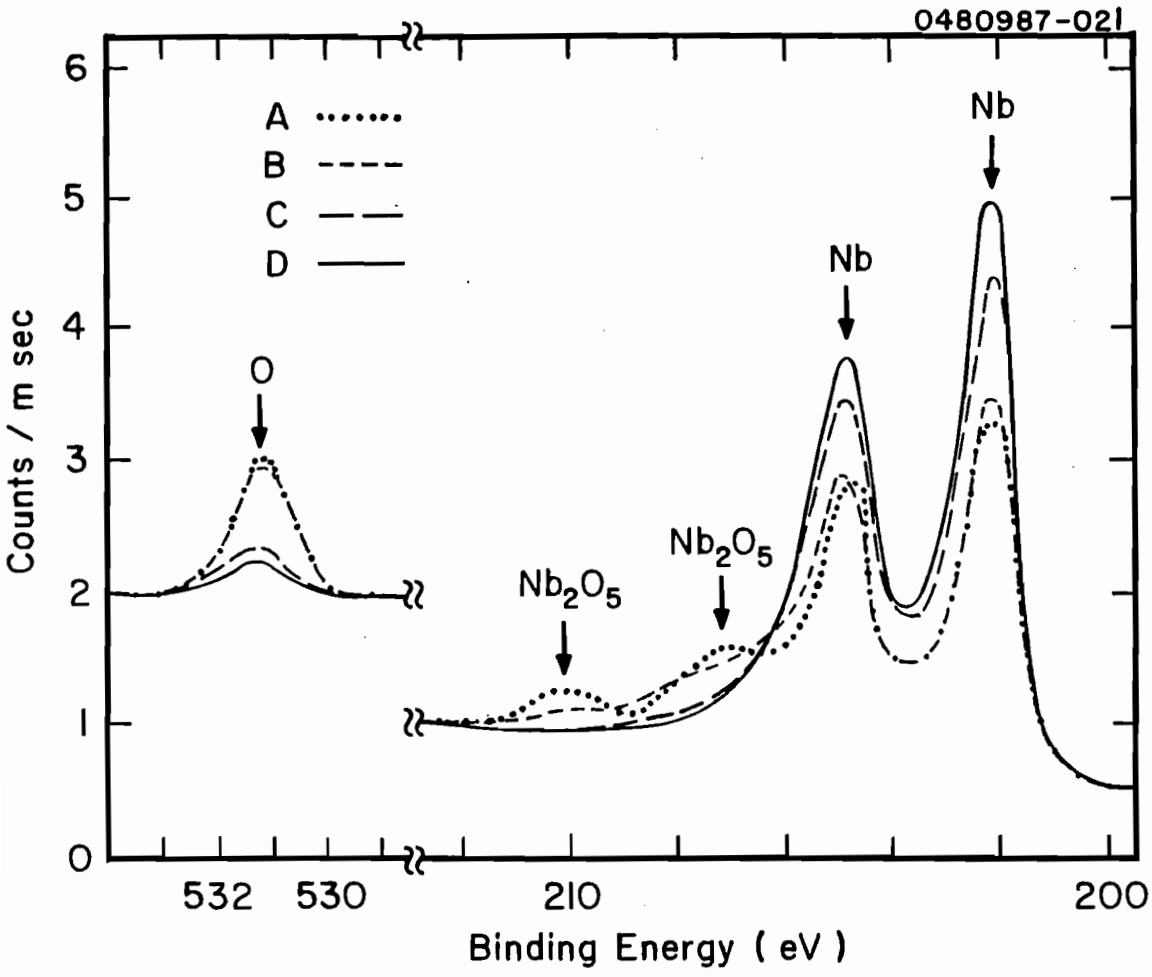

Figure 5.21 XPS spectra taken while oxidized niobium was heated form 23° to 350°C. Different curves correspond to temperature ranges shown in figure 5.20.

5.6 Discussion

The sensitive temperature dependence of both XPS and RF data near 300°C makes it difficult to establish connections between these two types of measurements, however, a tentative description of the

dissolution of the oxide layer can be made based on these results and on the diffusion rate of oxygen in niobium.

Dissolved oxygen moves through niobium metal according to the diffusion equation,{40}

$$\frac{\partial c}{\partial t} = D(T)\ \frac{\partial^2 c}{\partial x^2}$$

where c is the oxygen concentration, x is the distance from the surface, and D is the diffusion constant, which depends only on the (Kelvin) temperature.

$$D(T) = 0.02 \cdot \exp\left[\frac{13500}{T}\right]\ \left[\frac{cm^2}{sec}\right]$$

A particularly useful solution to the diffusion equation is

$$[5.3] \qquad c = \frac{A}{\delta\sqrt{\pi}}\ \exp\left[\frac{-x^2}{4\delta^2}\right]$$

where δ^2 is the time integral of the diffusion constant, $\int D\ dt$; and A is the total amount of oxygen per unit area, $\int_0^\infty c\ dx$.

Figure 5.22 shows this solution to the diffusion equation for niobium which has been heated to successively higher temperatures for 5 minutes at each temperature. Although these heatings are cumulative, the diffusion rate increases so quickly with temperature that most of the diffusion has always occurred at the most recent temperature. The concentration which is plotted is the ratio of the density of oxygen atoms in solution to the density of niobium atoms in pure metal. The total amount of oxygen present corresponds to a 13 angstrom layer of

Nb_2O_5 on the surface. At t=0, the initial value of δ is set to 5 angstroms, so that most of the oxygen is within 15 angstroms of the surface.

After heating to 150°C, the diffusion model predicts that the oxygen will be spread out over a region at least 100 angstroms thick, but the XPS measurements show that this is not the case. The oxygen remains within 20 angstroms of the surface, with the valence of the oxidized niobium still roughly equal to its original valence in the Nb_2O_5. This suggests that the interface between the metal and the oxide

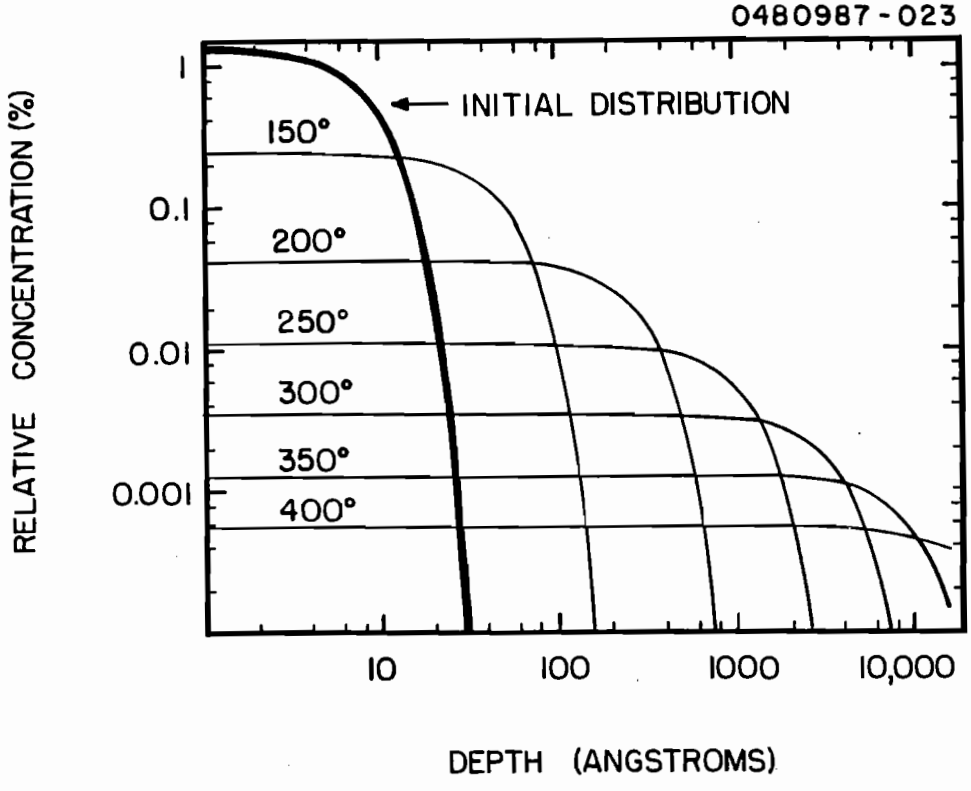

Figure 5.22 Calculated oxygen concentration as a function of distance from surface after heating for five minutes at each successive temperature. Bold curve is the assumed initial concentration.

is fairly sharp. Any oxygen which escapes into the metal can diffuse rapidly away from the surface, leaving relatively pure metal next to the oxide.

When the oxide finally decomposes at around 250°C, the oxygen quickly spreads out into a layer which is on the order of 1000 angstroms thick. Since the magnetic penetration depth is between 400 and 800 angstroms, this oxygen should be expected to influence the BCS resistance. The concentration in this layer rises as the oxide decomposes, reaches a maximum around 300°, and then declines at higher temperatures as the oxygen diffuses farther into the bulk. After heating at 350°, the concentration is down to about 0.1 percent, which corresponds to an RRR of 35, in good agreement with the value determined from the normal Q measurements.

The curve in figure 5.10A is an approximate calculation based on the previous discussion. The fraction (f) of the oxide layer that dissolved into the bulk was assumed to be given by the fermi-type function,

$$f = \frac{1}{1 + \exp\left(\frac{265°C - T}{15°}\right)}$$

in reasonable agreement with the XPS measurements. The oxygen concentration was found by multiplying f by equation [5.3].

$$[5.4] \qquad c = \frac{f\,A}{\delta\sqrt{\pi}} \quad , \quad \text{where } \delta^2 = D(T) \cdot 200 \text{ sec.}$$

The time of 200 seconds was chosen instead of 5 minutes to allow some time for the oxides to decompose. The exponential term in [5.3] was ignored since the important values of x are less than the penetration

depth, which is less than δ. The concentration was then converted to an RRR value ($c \cdot RRR = 0.035$), and the BCS resistance was taken from figure 5.5. The local maximum at 275°C in figure 5.10-a corresponds to the maximum in oxygen concentration near the surface, which is about one half of an atomic percent. The concentration exceeds 0.25 percent from $230° < T < 335°$, which is in reasonable agreement with the oxygen concentrations derived from critical temperature measurements.

The peak in residual resistance also seems to correspond to the peak in dissolved oxygen concentration. It is important to note that, at these high concentrations and at temperatures below 1500°, niobium - oxygen solutions are probably unstable against formation of NbO.{41} Although this transition was not seen below 600°, some kind of clustering may take place at lower temperatures, or these super saturated solutions may simply not form at 300°. The XPS shows no evidence of low valence oxides, but, if these precipitates were scattered throughout a ~ 1000 angstrom layer, the amount near the surface would be too small to detect.

6. CONCLUSION

6.1 Research Summary

We have developed a technique for removing the native oxide layer from the surface of niobium by ultra high vacuum (UHV) firing at 1100°C. Final coverages of less than a monolayer can be achieved provided that the initial purity of the bulk metal is sufficient, and that both the length of time at high temperature and the thickness of the metal are large enough for the oxygen to diffuse into the bulk without excessively degrading the purity of the metal near the surface. A coverage of about one half of a monolayer was obtained on a sample whose bulk oxygen concentration was between 100 and 200 ppm atomic. Data from the literature indicate that at 1000 ppm, the coverage is around one monolayer, and that, for concentrations less than 100 ppm, coverage varies linearly with bulk concentration. The precipitation of sulfur and phosphorus to the surface was observed on some, but not all of the samples. Precipitation of sulfur can be avoided or even reversed by heating to 1400°C or more. Very low partial pressures of oxygen ($< 10^{-10}$ torr) are necessary to maintain clean surfaces over periods of hours, but these conditions were apparently met inside the UHV-fired niobium cavities.

Niobium cavities were manufactured, cleaned as described above, and then tested without exposure to air. The residual resistance of these cavities varied from 6 to 12 nΩ, which is almost an order of magnitude less than the values observed on cavities cleaned by the usual chemical

methods. Exposing the oxide free cavities to ~0.1 torr of pure oxygen for a day or more altered neither the temperature dependent (BCS) resistance nor the residual resistance. Variations of the BCS resistance with bulk purity of the niobium were in reasonable agreement with the values calculated by Halbritter's program. We noted that this dependence of BCS resistance on electron mean free path can be qualitatively explained by a simple semiclassical model.

The technique of heating cavities to 325°C for 10 minutes was initially developed in order to determine whether or not the fired cavities were actually oxide free. As described below, several RF properties of the oxidized cavities were altered by heating in this manner. Since none of these changes were observed when "oxide free" cavities were heated, we concluded that oxygen coverage on the "oxide free" cavities did not exceed one or two monolayers.

A picture of the behavior of oxide layers near 300°C was constructed based on the XPS studies of Kirby et al., on the diffusion rates for oxygen in niobium, and on our RF measurements. Upon heating for a few minutes at temperatures below 275°C, the composition of the oxide layer changes from mostly Nb_2O_5 to a mixture of Nb_2O_5 and NbO_2. Most of the oxygen, however, remains within 20 angstroms of the surface. At around 300°, the oxide layer can dissolve into the bulk within a minute or two, creating an oxide-rich layer at least 1000 angstroms thick. The oxygen then gradually diffused farther into the bulk.

Several changes were observed in the RF properties of oxidized cavities after heating to temperatures near 300°. The BCS resistance declined by 15 - 30 percent, as expected from the reduced mean free path

in the oxygen-rich layer. The residual resistance increased by as much as 100 nΩ. Efforts to correlate high values of residual resistance with particular oxides seen by XPS were unsuccessful. The largest values of R_{res} were obtained under conditions where most of the oxygen had probably dissolved into the first one or two thousand angstroms of the bulk. The residual resistance was affected more strongly by the presence of a magnetic field during cooldown through the transition temperature. The increase seen on oxide-free cavities was about one half of a nΩ per milligauss, while the increase for oxidized and heated cavities was two to five times larger. The RF transition temperature was typically a third of a degree lower, as expected from other measurements of T_c as a function of oxygen concentration.

No change in the energy gap was observed as a result of any of the processes described above. Upper limits of around one percent were determined for the changes due to chemical polishing, UHV firing, oxidation, and heating to 325°C. The gap was also independent of both the bulk purity of the niobium, and the ambient magnetic field in the cryostat.

6.2 Questions and Possibilities for Future Research

A) High field measurements

The high field performance of oxide-free cavities would be of interest to the accelerator community. Breakdown fields of these cavities may exceed 1000 gauss, since the low residual losses would not create excessive heat at these fields. The principal experimental

problem would be to construct a variable coupler for the sealed cavities so that high powers could becoupled efficiently into the cavity. One drawback is that the RRR of the oxide-free cavities is limited to about 300 by the absorption of gases, surface oxides, and other contamination while the cavity is hot. However, measurements and calculations by Padamsee{86} show that increasing the RRR above 300 causes only very small increases in the breakdown field. DC field emission studies suggest that UHV firing at 1400°C may significantly reduce electron loading in the cavities in addition to removing the oxide layer. Field emission is likely to depend on the extent to which sulfur is eliminated from the surface, either by the selection of good starting material for cavity manufacture, or by increasing the firing temperature to 1500° or 1600° degrees.

Kneisel et al.{68} found that electron impact degrades the Q of niobium cavities, and that the degradation is worse on anodized cavities than on cavities with thinner oxide layers. It would be interesting to see if this problem occurs on oxide-free cavities.

B) Residual resistance studies

A particularly interesting question which remains unanswered is whether the 6 - 12 nΩ which was observed on our best cavities is due to some fundamental effect such as the direct generation of phonons by the RF electric field, or whether it is due to some kind of contamination or morphological defect. Construction of a cryogenic thermometry system to look for localized defects would be a useful first step toward resolving this question. If local defects are found, it would be very useful to

design a cavity in such a way that the defects could be examined with an electron microscope or XPS analyser without destroying the cavity. Whether such defects are found or not, measurements made in other (higher frequency) modes should provide some useful information. Comparison of TE and TM modes can separate metallic losses from dielectric losses. As noted in chapter 2, the frequency dependence may provide information about the morphology of metallic defects, or about the loss tangent of dielectrics.

If few localized defects are found, further investigations into the residual resistance on niobium might proceed in several different directions. One approach is to try to guess the cause of the 6 - 12 nΩ residual found on the cleanest cavities, and to perform experiments in which the proposed cause is either eliminated or controlled. Such experiments might include studies of thicker walled cavities, which should have fewer grain boundaries after firing, or perhaps a careful examination of the residues of solvents or acids present on the cavity either before or after firing. In any case, a cryogenic thermometry system for locating losses during testing would be a useful improvement to the apparatus. While this approach may be the shortest route to the production of cavities with higher quality factors, it has the disadvantage that if the new procedures result in less than a factor of two improvement, the time required to collect statistically significant data may be prohibitively long.

An alternate approach is to try to determine why cavities that were fired and then oxidized performed better than chemical polished cavities or cavities that had been oxidized and heated to 300°C. Exposing fired

cavities to water vapor or methanol vapor either with or without an initial exposure to oxygen might provide information about the oxides and other forms of contamination on chemical polished surfaces. In fact, a study of Nb_3Sn tunnel junctions has shown that the electrical properties of niobium oxides can depend on the choice of oxidizer.{87} Studies of heated oxide layers could be made more precise if spectroscopic measurements were done on the cavities themselves. This could be accomplished with muffin tin or TE type cavities if suitable spectrometers were available. This type of experiment--done on imperfect surfaces--has a reasonable likelihood of producing reproducible data. A better understanding of oxygen and other contaminants may lead to improved processing methods for mass production, or possibly even to better procedures for making superconducting alloys.

It would also be very interesting to test the theory of Scharnberg, {36} which calculates the residual resistance due to direct generation of phonons by the RF electric field. A useful comparison of theory and experiment might be possible at 15 to 20 Ghz, using materials with RRR values varying from a few hundred to a few thousand. Unfortunately, the expected residual resistances would have to be measured at temperatures between 1.25 and 1.3°K.

APPENDIX: DATA ANALYSIS

Introduction

Energy gaps and residual resistances were calculated using the Pippard limit formula{2} (infinite coherence and mean free path) for the BCS resistance:

$$[A.1] \qquad R \propto \frac{1}{T} \, LN(46 \cdot T/f) \; e^{-\Delta_0 \cdot G(T)/T} \qquad (\; f = \text{frequency - Ghz} \;)$$

The Gap function, G(T), is defined by $\Delta(T) = G(T) * \Delta_0$. The temperature dependent gap is the solution to: {13}

$$[A.2] \qquad 1 = NV \int_0^{\theta} \frac{1}{(\xi^2 + \Delta(T)^2)^{1/2}} \cdot [\; 1 - 2 \, f(\sqrt{\xi^2 + \Delta(T)^2}\;) \;] \, d\xi$$

Where θ is the Debye temperature and $f(x) = (1 + \exp(x/T))^{-1}$. In the limit as T goes to 0, the solution to [A.2] is

$$G(T) - 1 = \sqrt{\frac{2\pi T}{\Delta_0}} \cdot e^{-\Delta_0/T} = .60 \sqrt{T} \; e^{-\Delta_0/T} \quad (\text{for } NV << 1)$$

However, we have used

$$G(T) = 1 - 0.82 \cdot \sqrt{T} \cdot e^{-\Delta_0/T}$$

which is slightly closer to the exact solution over the temperature range of interest. The gap is found by rewriting [A.1] as a straight line,

$$[A.3] \qquad y = \Delta \cdot x + b$$

where $y = \log[R \cdot T/\log(46 \cdot T/f)]$, $x = G(T)/T$, and b is a constant. The best fit to [A.3] is found by minimizing the error function,

$$[A.4] \qquad E^2 = \frac{\sum_i w_i \cdot (y_i - \Delta \cdot x_i - b)^2}{\sum_i w_i}$$

where the y_i's and x_i's are the measured values of y and x, and the w_i's are weighting factors whose purpose is to avoid using data which are dominated by external Q or residual resistance in the determination of Δ. We have used

$$w_i = |x_{i-1} - x_{i+1}| \cdot \frac{R_{BCS}}{R_{BCS} + R_{res} + 270/Q_{ext}}$$

although several other formulae were tried on selected sets of data without any significant change in the result. The best value of Δ and b can be found directly by differentiating [A.4], while the optimum value of R_{res} must be located by trial and error.

The remainder of this appendix consists of error estimates. The most attention is paid to errors in the energy gap. The errors are found to come from two sources: errors due to random fluctuations in the data (σ_f), and errors due to thermometer drifts, (σ_{ct}). A simple formula is derived for calculating σ_f from the data. The thermometer drifts are more difficult to estimate. They appear as consistent errors during the course of a single measurement, but tend to drift randomly from day to day. A minimum estimate for σ_{ct} is determined from discrepancies between pairs of thermometers. The actual spread in observed gap values suggests that the preceding estimates are low by a roughly factor of two. A simulation using computer-generated data shows that the calculated values for σ_f are actually low by almost this much.

It is certainly plausible, but hard to prove, that σ_{ct} is also an underestimate. Our final estimate for the error in an individual gap measurement is twice the quadratic sum of σ_f and σ_{ct}. The analysis of errors in BCS resistance is very similar to the analysis of errors in the gap. Errors in residual resistance come from errors in the BCS resistance, errors due the limited accuracy with which the oscilloscope can be read, coupling problems, and also from magnetic fields in the cryostat.

In all of the error analyses, we have used the convenient approximation,

[A.5] $R_{BCS} \propto \exp(-\Delta/T)$

so that $y = -\log(R_{BCS})$ and $x = 1/T$. These formulae are adequate for estimating the importance of various sources of error; however, wherever actual results are given, the Pippard limit formula has been used.

A.1 Measurement of the energy gap

A) Statistical analysis of fluctuations

A simple estimate of uncertainties in Δ can be made by assuming that each data point, (x_i, y_i), satisfies

[A.6] $y_i = \Delta_o x_i + b_o + e_i$

where $-y_i$ is the log of the BCS resistance, x_i is $1/T_i$, Δ is the gap, and b is a constant. The subscript, o, identifies the true values of Δ and b as opposed to the observed values. The errors, e_i, are assumed to be independent, and to have an expectation value, $\langle e_i \rangle$, of zero, and a

variance of $\langle e^2 \rangle$, so that $\langle e_i e_j \rangle = \delta_{ij} \langle e^2 \rangle$. The observed value is found by minimizing E in equation [A.4]. The result is

$$[A.7] \qquad \Delta = \frac{1}{V_x} \left\{ \frac{\sum_i w_i \cdot x_i \cdot y_i}{\sum_i w_i} - \bar{x} \cdot \frac{\sum_i w_i \cdot y_i}{\sum_i w_i} \right\}$$

where $\bar{x} = \frac{\sum w_i \cdot x_i}{\sum w_i}$, and $V_x = \frac{\sum w_i \cdot x_i^2}{\sum w_2} - \bar{x}^2$

are the mean and variance of the input variables, x_i. Substituting [A.6] into [A.7] gives:

$$[A.8] \qquad \Delta = \Delta + \frac{1}{V_x} \cdot \frac{\sum w_i \cdot (x_i - \bar{x}) \cdot e_i}{\sum w_i}$$

The w's and the x's are assumed to be "correct", so the expectation value and standard deviation of Δ are:

$$[A.9] \qquad \Delta = \Delta_o \pm \sigma_f \quad , \quad \text{where} \quad \sigma_f^2 = \langle e^2 \rangle \cdot \frac{\sum w_i^2 \cdot x_i^2}{(\sum w_i \cdot x_i)^2}$$

The standard deviation becomes more recognizable if we replace one of the factors of w_i in the numerator with its mean value, $(\Sigma w_i)/N$, so

$$[A.10] \qquad \sigma_f^2 = \frac{\langle e^2 \rangle}{N \cdot V_x}$$

(This approximation typically changes σ_f by less than 15%.)

One may then either deduce $\langle e^2 \rangle$ from knowledge of the apparatus, or use the experimental value, $\langle e^2 \rangle \sim E^2$ from [A.4].

B) Temperature measurement errors

Equation [A.5] has the solution:

$$\Delta_o = - \frac{\partial(\log(R_{BCS})}{\partial x_o}$$

If, instead of the true (reciprocal) temperature, x_o, we use an observed temperature, x, the observed Δ becomes:

$$\Delta_o \cdot \left(\frac{\partial x_o}{\partial x} - 1 \right) = \sigma_{ct} \pm \sigma_{ft}$$

The only way we have of estimating the magnitude of $(\partial x_o/\partial x - 1)$ is to compare 2 thermometers, and use the derivative of one temperature measurement with respect to the other. The expectation value and the uncertainty in $\partial x_o/\partial x$ can then be calculated by the least squares method described in section A.1A. For future reference, we denote these consistent errors and their uncertainties as:

[A.11] $$\Delta_o \cdot \left(\frac{\partial x_o}{\partial x} - 1 \right) = \sigma_{ct} \pm \sigma_{ft}$$

If the thermometers were "well behaved", the value of $\partial x_0/\partial x$ would not differ from one by much more than the calculated uncertainty; however, this is frequently not the case. The origin of these consistent errors is incompletely understood, although one source is probably the heating of individual resistors by stray RF in the cryostat. This phenomenon has frequently been noticed and measured. Two features are worth noting. Although the temperature dependence of this heating at a given RF level is in reasonable agreement with the $1/T^3$ law for the heat capacity of solids, the typical RF level in the cryostat varies with temperature in a manner that may be similar to T^3

so that the actual temperature dependence of these errors is unpredictable. Fortunately, the spatial distribution of the RF is very nonuniform. The resistor leads probably act as antennas with arbitrary impedances. As a result, the degree of RF heating of two different resistors will be substantially different even if the resistors are located very close together. This makes σ_{ct} a useful estimate of the magnitude of this effect.

C) Observed and expected errors in the data

The most obvious source of random errors is the limited accuracy with which time constants, τ, can be read from the oscilloscope. Following the notation of [A.6], we have, (ignoring the external Q and residual resistance),

$$y = \log(\tau) + \text{const.}$$

the differential of which is

$$dy = \frac{d\tau}{\tau}$$

The accuracy of oscilloscope measurements is limited to about 2% by the thickness of the line which is observed on the screen, so $(\langle e^2 \rangle)^{1/2}$ should be about 0.02.

Equation [A.10] converts $\langle e^2 \rangle$ into errors in the energy gap. A typical value of $N^{1/2}$ is ~4.5, and V_x is roughly one third of the range of reciprocal temperatures, or about 0.1 deg^{-1}. Figure A.1 is a histogram of the calculated errors in the gap due to fluctuations. There is a peak near 0.04 degrees, as expected, but also a substantial tail toward higher values, indicating that other errors sometimes occur.

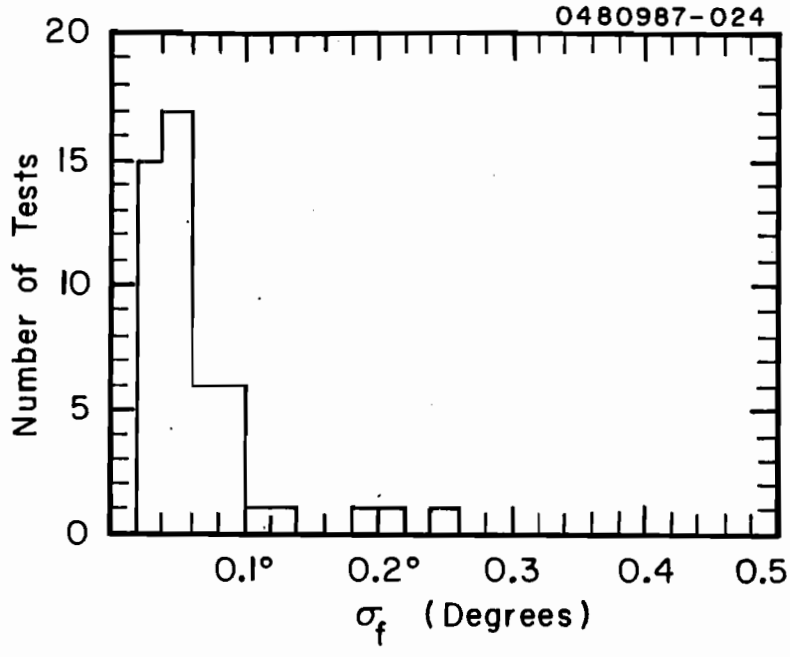

Figure A.1 Histogram of predicted errors in energy gap based on observed fluctuations in the data.

Germanium resistors can be read quite accurately. Most measurements are recorded to within one or two parts in a thousand, including errors resulting from the time which elapses between measurements of time constants and temperatures. Using the approximate relations, $\tau \propto \exp(\Delta_o x)$,and $x \propto \Omega^{1/2}$ where Ω is the resistance of the Ge resistor, we get

$$\frac{\partial \tau}{\tau} = \left(\frac{\Delta_o \cdot x}{2} \right) \cdot \frac{\partial \Omega}{\Omega} \sim 5 \frac{\partial \Omega}{\Omega}$$

So a 0.2% error in thermometer resistance is roughly equivalent to a 1% error in time constant. Random fluctuations in temperature measurements have been monitored by comparing separate resistors, and they usually

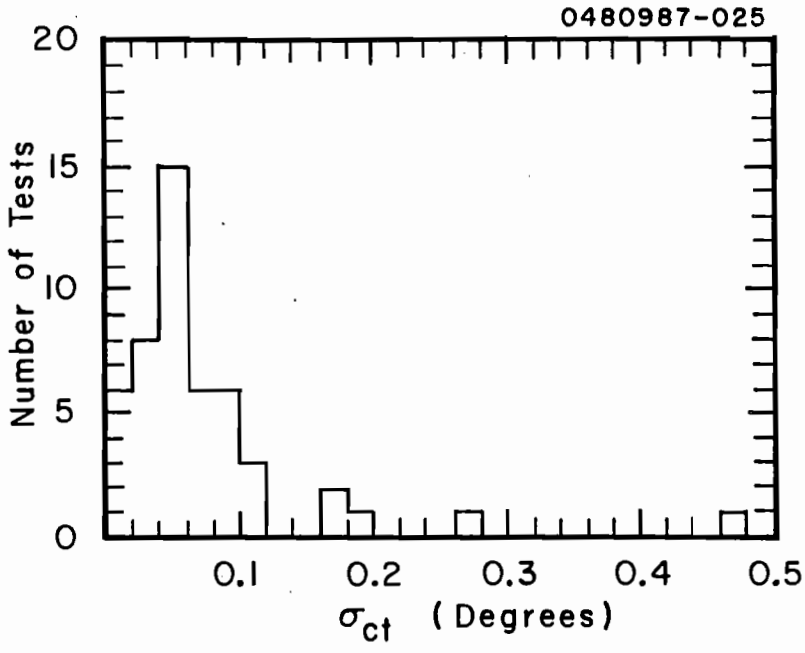

Figure A.2 Histogram of predicted errors in energy gap based on systematic discrepancies between thermometer measurements.

have a standard deviation of about 0.1%. In any case, these fluctuations are already included in σ_f , which is shown in figure A.1.

Consistent temperature errors, σ_{ct} (see eq.[A.9]), are shown in figure A.2. Comparison with figure A.1 shows that the consistent errors are at least as important as the errors due to fluctuations of individual data points. The absence of a peak at $\sigma_{ct} = 0$ suggests that this formula may substantially exaggerate the reliability of the thermometers in those cases where σ_{ct} happens to be less than 0.02 degrees. The quantity,

$$[A.12] \quad \sigma_c = (\sigma_{ct}^2 + 0.001\ (\text{deg}^2))^{1/2}$$

is probably a better estimate of the effect of thermometer errors on the gap.

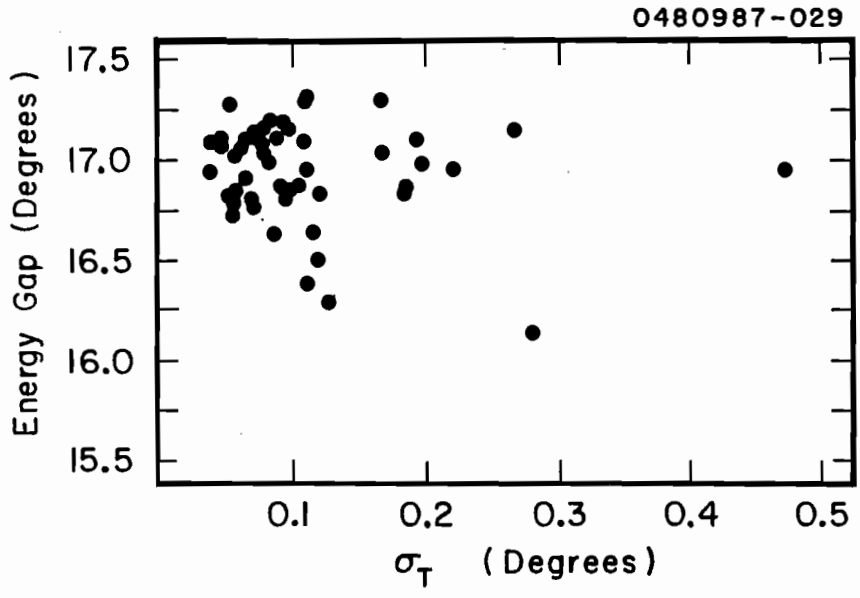

Figure A.3 Energy gap values (without error bars) as a function of predicted total errors, showing increased spread in data with increased σ_T.

Comparison of predicted errors with scatter in the values of Δ:

Error analysis of energy gap measurements is particularly convenient since no evidence has been found to indicate that the gap actually changes from test to test. Figure A.3 is a scatter plot which shows the measured values of Δ as a function of the sum of the predicted errors,

[A.13] $$\sigma_T = (\sigma_{ct}^2 + 0.001 \text{ deg}^2)^{1/2}$$

In figure A.4, these data have been divided into groups according to the value of σ_T. The error bars show the mean gap value and RMS deviation for each group as a function of the average σ_T. Since there are roughly 10 points in each group, the lengths of these error bars are significant

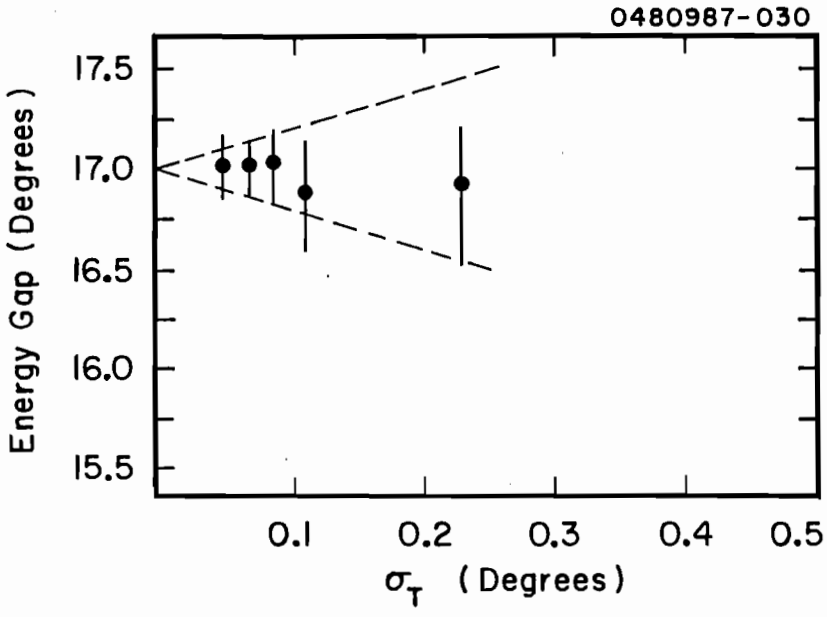

Figure A.4 Mean value and RMS deviation of energy gaps. Data separated into groups of 10 according to predicted errors, σ_T. Dashed lines are $\Delta = 17°K \pm 2\sigma_T$.

to ± 30%. The error bars fit reasonably well within the region bounded by $\Delta = 17°K \pm 2\sigma_T$. The origin of this factor of 2 is partially understood. Both components of σ_T, σ_f and σ_{ct}, are probably low estimates. Computer simulations (section 4D) show that σ_f underestimates the effect of fluctuations by a factor of ~1.7 ± 0.2 ; σ_c is just the minimum believable error for the thermometers. In any case, figure A.4 is empirical evidence that

[A.14] $\sigma = 2\sigma_T$

is a reasonable estimate for the accuracy of individual gap measurements.

A.2 Measurement of BCS Resistance at Specified Temperatures

Measurement of $R_{BCS}(T)$ requires evaluation of the constant, b, which minimizes E (Eq. [A.4]). The result which corresponds to equation [A.8] is

$$[A.15] \quad b = b_o + (\Delta_o - \Delta)\cdot\bar{x} + \frac{\Sigma\, w_i \cdot e_i}{\Sigma\, w_i}$$

which contains both explicit errors, e_i, and implicit errors in Δ. The observed value of $R_{BCS}(T)$ is

$$[A.16] \quad -\log(R_{BCS}(T)) = \Delta\cdot(\tfrac{1}{T}) + b = \Delta\cdot x + \Delta(\tfrac{1}{T} - \bar{x}) + \frac{\Sigma\, w_i \cdot e_i}{\Sigma\, w_i}$$

If T is chosen to be nearly equal to $1/\bar{x}$, then the errors in Δ are unimportant. For our data, this occurs near T = 2K. The analog to [A.9] is then

$$-\log(R_{BCS}(T)) = \Delta\cdot(\tfrac{1}{T}) + b = \Delta\cdot\bar{x} + \Delta\cdot(\tfrac{1}{T} - \bar{x}) + \frac{\Sigma\, w_i \cdot e_i}{\Sigma\, w_i}$$

Since $(\langle e^2 \rangle)^{1/2}$ is usually around 2%, we conclude that fluctuations typically account for an error of ~ 1/2 % in $R_{BCS}(2)$.

A larger uncertainty arises from the consistent errors in temperature measurement. Again, our only way to estimate this error is to compare data from two different germanium thermometers. The mean value of the difference between two thermometer readings during a typical test is in the range of 0 .002 degrees. Since

$$R_{BCS} \propto e^{-\Delta/T} \quad \rightarrow \quad \frac{d\, R_{BCS}}{R_{BCS}} = \frac{-\Delta}{T} \cdot \frac{d\, T}{T}$$

this difference leads to an error of at least 2% in $R_{BCS}(2)$.

The data in figures 1.3, 1.4, and 1.5 are in reasonable agreement with this analysis. At 2°K, the typical spread in BCS resistance for a given RRR is plus or minus 3 or 4 percent. At 4.2° or at 1.33° these errors have grown to almost ± 10 percent.

A.3 Measurement of Residual Resistance

Residual resistance is determined from the last few (lowest T) data points in each test. The time constant measured on the scope is given by

$$[A.17] \quad \frac{4.6}{\tau} = R_{res} + R_{BCS} + \frac{270}{Q_{ext}}$$

where τ is in seconds, R is in nΩ, and Q is in units of 10^9. The differential of this is

$$-4.6 \cdot \frac{d\,\tau}{\tau^2} = d\,R_{BCS} + d\,R_{res} + \frac{270}{Q_{ext}^2} \cdot d\,Q_{ext}$$

or

$$[A.18] \quad d\,R_{res} = \frac{-4.6}{\tau} \cdot \left[\frac{d\,\tau}{\tau}\right] - R_{BCS} \cdot \left[\frac{d\,R_{BCS}}{R_{BCS}}\right] + \frac{270}{Q_{ext}} \cdot \left[\frac{d\,Q_{ext}}{Q_{ext}}\right]$$

The relative error, $d\tau/\tau$, is about .02, and $d(R_{BCS})/R_{BCS}$ can be seen from figure 1.4 to be about 0.1. The external Q is determined from the coupling constant, β, by the formula, $Q_{ext} = w\tau \cdot (1+1/\beta)$. A typical value for β at low temperatures is $\sim 12/Q_{ext}$. The actual value can be measured to ± 10%, so, ignoring errors in τ, the relative uncertainty in external Q is

$$\frac{d\,Q_{ext}}{Q_{ext}} = \frac{1}{1+\beta}\cdot\left[\frac{d\beta}{\beta}\right] \sim \frac{0.1}{1+12/Q_{ext}}$$

Using [A.17] for the value of τ, and adding independent errors in quaduature,

$$\text{error in } R_{res} = \sqrt{\left[(R_{res}+R_{BCS}+\frac{270}{Q_{ext}})\cdot(0.02)\right]^2+\left[0.1\cdot R_{BCS}\right]^2+\left[\frac{27}{Q_{ext}+12}\right]^2}$$

Since both R_{BCS} and R_{res} are roughly equal to 10 nΩ in the region of interest, the error in residual resistance is

$$\sqrt{(0.4+\frac{5}{Q_{ext}})^2+(1n\Omega)^2+\{1n\Omega\}^2+\left[\frac{27}{Q_{ext}+12}\right]^2}$$

where the Q's are in units of 10^9. The one nΩ in curly brackets is an estimate of the effect of magnetic field in the cryostat. The term in square brackets is the uncertainty in the coupling, which affects the absolute values of residual resistance, but does not affect the differences between successive measurements on the same cavity unless the RF probe has been moved.

A.4 Simulation of Error Propagation

Due to limited confidence in our analytical estimates of error propagation, we have done several computer experiments to determine the effect of random errors in time constant measurements on the final results. For each experiment, nine simulated runs were generated and then analyzed. Data for each run consisted of 18 reciprocal temperatures spaced evenly between 0.37 and 0.71 (deg^{-1}). The time constants for these temperatures were calculated from the Pippard limit

TABLE A.1

Simulation Results

Exp	Qext	R_{res}	R_{BCS}	Gap	f
1	3 E9	10.5±.6	5.01±.19	17.24±.13	.069±.010
2	3 E9	10.2±.8	5.13±.13	17.17±.075	.069±.014
3	1 E10	10.3±.3	5.04±.07	17.21±.046	.040±.006
4	1 E10	9.9±.4	5.13±.09	17.16±.051	.043±.006
5	3 E10	10.1±.5	5.08±.13	17.19±.088	.032±.004
6	3 E10	10.0±.3	5.10±.09	17.07±.054	.033±.004
7 (4)	1 E10	10exact	5.10±.07	17.17±.049	.045±.005
8 (5)	3 E10	10exact	5.12±.05	17.17±.036	.037±.004

formula and then multiplied by (1 + 0.02·e) where e is a pseudorandom number between -1 and 1. The parameters used to calculate the time constants were $\Delta = 17.2°$, $R_{BCS}(1.33°K) = 5n\Omega$, and $R_{res} = 10\ n\Omega$. The external Q varied from experiment to experiment. The analysis of each run gave "observed" values for four parameters: R_{res}, $R_{BCS}(1.33°)$, Δ, and σ_f. Table A.1 shows the mean values of these parameters for each experiment. The uncertainty listed for each parameter is the RMS spread in the results, which is an estimate of the reproducibility of individual measurements.

The first three pairs of experiments show simulated results at three different external Q's. Experiments were done in pairs in order to illustrate the effects of different random number seeds. The results are about as expected, except that the actual errors in Δ consistently exceed the predicted errors, σ_f. For these six experiments as a whole, the ratio of actual to predicted errors in Δ is ~1.7 ± 0.2.

Measurements at $Q_{ext} = 3 \times 10^9$ are not as accurate as those at $Q_{ext} = 1 \times 10^{10}$, but little is gained from further increases in external Q. The simulated errors are generally much smaller than the scatter in the real results, but this may only reflect the absence of consistent errors in the simulations.

Experiments 7 and 8 reanalyzed the data from experiments 4 and 5, using the correct residual resistance, 10 nΩ, instead of searching for the residual that gave the best fit. The search procedure necessarily lowers σ_f, but only slightly. Searching also contributed to errors in Δ and $R_{BCS}(1.33K)$, possibly accounting for much of the difference between σ_f and the actual errors in Δ.

A.5 Conclusion

Errors in the prefactor of the BCS resistance and in the energy gap have very similar origins. The are due to the limited accuracy of oscilloscope readings and to drifts in temperature measurements. The drifts are imperfectly understood, but there is adequate statistical evidence to indicate that these errors are only slightly larger than those associated with the oscilloscope.

Errors in the residual resistance are due to errors in the BCS resistance, errors in reading the last few time constants from the oscilloscope, errors in measuring the coupling constant, and magnetic flux in the cryostat. All of these sources contribute similar amounts to the total error.

In general, the errors that were observed were rarely much more than twice the minimum values which are inherent in this experimental technique, and in the quality of standard laboratory equipment.

REFERENCES

1. D. Mattis and J. Bardeen, "Theory of the Anomalous Skin Effect in Normal and Superconducting Metals," Phys. Rev. 111, 412 (1958).

2. A. Abrikosov, L. Gorkov, and I. Khalatnikov, "A Superconductor in a High Frequency Field," Soviet Phys. JETP 8, 182, (1959).

3. M. Tigner and H Padamsee, "Superconducting Microwave Cavities in Accelerators for Particle Physics--A Review," in Physics of High Energy Particle Accelerators, SLAC Summer School--1982, M. Month, ed., AIP Conf. Proc. 105, 801 (1983).

4. "TRW Using Superconducting Materials to Boost Radio Frequency FEL Power," Aviat. Wk. & Space Tech. 125 No. 7, 73 (1986).

5. D. Deacon and A. Angelis, ed., "Proceedings of the Workshop on Applications of Free Electron Lasers," Nuc. Inst. A 239, 371-439 (1985).

6. B. Newman, R. Warren, J. Goldstein, and C. Brau, "The Los Alamos Free Electron Laser Oscillator: Optical Performance," Nuc. Inst. A 237, 187 (1985).

7. W. Barletta, J. Boyd, A. Paul, and D. Prono, "Brightness Limitations in Multi-Kiloampere Electron Beam Sources," Nuc. Inst. A 237, 318 (1985).

8. G. Elias, J. Hu, and G. Ramain, "The UCSB Electrostatic Accelerator Free Electron Laser: First Operation," Nuc. Inst. A 237, 203 (1985).

9. J. Walsh, "Application of Free Electron Lasers in Communication," Nuc. Inst. A 239, 383 (1985).

10. G. Pake, ed., "Science and Technology of Directed Energy Weapons," Rev. Mod. Phys. 59 No. 3 Part 2, p. S33 (1987).

11. S. Stein and J. Turneaure, "Superconducting Resonators: High Stability Oscillators and Applications to Fundamental Physics and Metrology," in Conference on Future Trends in Superconducting Electronics AIP Conf. Proc. 44 192 (1978).

12. H. Piel, "Non-Accelerator Applications of RF Superconductivity," Proceedings of the Third Workshop on RF Superconductivity, (Argonne Ill. 1987).

13. J. Bardeen, L. Cooper, J. Schrieffer, "Theory of Superconductivity," Phys. Rev. 108, 1175 (1957).

14. A. Abrikosov, L. Gorkov, R. Dzyaloshinski, Quantum Field Theoretical Methods in Statistical Physics, 315, (Pergamon Press, 1965).

15. J. Turneaure, and I. Weissman, "Microwave Surface Resistance of Superconducting Niobium," J. Appl. Phys. 39, 4417 (1968).

16. J. Halbritter, "Comparison between Measured and Calculated RF Losses in the Superconducting State," Z. Physik 238, 466 (1970).

17. P. Wilson, "Theoretical Surface Resistance for Superconducting Lead and Niobium at High Frequencies," SLAC-TN-70-35 (Stanford, 1970).

18. B. Arnolds-Meyer and W. Weingarten, "Comparative Measurements on Niobium Sheet and Sputter Coated Cavities," IEEE Trans. Mag. MAG-23, 1620 (1987).

19. J. Turneaure, "Status of Superconductivity for RF Applications," Proceedings of the 1972 Applied Superconductivity Conference, IEEE Pub. No. 72CH0682-TABSC, 621 (1972).

20. J. Pierce, "Superconducting Microwave Resonators" in Methods of Experimental Physics, Vol. 2, R. Coleman, ed. (Academic Press, N.Y.,1974).

21. P. Kneisel, O. Stoltz, and J. Halbritter, "On the Variation of RF Surface Resistance with Field Strength in Anodized Niobium Cavities," Proc. Appl. Superconductivity Conf., H. Long and W. Gauster, ed., IEEE Pub. 72CH0682-5-TABSC, 657 (1972).

22. M. Allen, Z. Farkas, H. Hogg, E. Hoyt, and P. Wilson, "Superconducting Cavity Measurements at SLAC," IEEE Trans. Nuc. Sci. NS18-2, 168 (June, 1971).

23. P. Kneisel, private communication.

24. J. Fricke, B. Piosczyk, J. Vetter, and H. Klein, "Measurements on Superconducting Helically Loaded Resonators at High Field Strengths," Part. Accel. 3, 35 (1972).

25. S. Giordano, H. Hahn, H. Halama, C. Varmazis, and L. Rinderer, "Influence of Solute Oxygen and Nitrogen on Superconducting Niobium Cavities," J. Appl. Phys. 44, 4185 (1973).

26. P. Kneisel, O. Stoltz, and J. Halbritter, "Investigation of the Surface Resistance of a Niobium Cavity at S-Band," IEEE Trans. Nuc. Sci. NS-18, 158 (1971).

27. G. Muller, "Diagnostic Techniques and Defect Classification," Proceedings of the Second Workshop on RF Superconductivity, H. Lengeler, ed., 377 (CERN, Geneva, 1984).

28. P. Bernard et al., "New Results with Superconducting 500 Mhz Cavities at CERN," Nuc. Inst. Meth. 206, 47 (1983).

29. M. Strongin, "The Sensitivity of the Q of Superconducting RF Cavities to Surface Conditions," J. Appl. Phys. 42, 4105 (1971).

30. W. McMillan, "Tunneling Model of the Superconducting Proximity Effect," Phys. Rev. 175, 573 (1968).

31. J. Gilchrist "Microwave Surface Resistance of Type II Superconductors," Proc. Roy. Soc. A295, 399 (1966).

32. C. Lyenis, Ph.D. Dissertation, Stanford University, Stanford, California, (1974).

33. J. Halbritter, "Surface Resistance of High-Q Superconducting Resonators," J. Appl. Phys. 42, 82 (1971).

34. C. Passow, "Explanation of the Low-Temperature High-Frequency Residual Surface Resistance of Superconductors," Phys. Rev. Let. 28, 427 (1972).

35. E. Kartheuser and S. Rodriguez, "Effect of Acoustic Generation on the Residual Surface Impedence of Superconductors," J. Appl. Phys. 47, 700 (1976).

36. K. Scharnberg, "Comment on the Residual RF Surface Resistance of Superconductors," J. Appl. Phys. 48, 3462 (1977).

37. J. Hulm, C. Jones, R. Hein, and J. Gibson, "Superconductivity in the Ti-O and Nb-O Systems," J. Low Temp. Phys. 7, 291 (1972).

38. H. Inouye, "The Oxidation of Columbium at Low Oxygen Pressures" in Columbium Metallurgy, AIME Metallurgical Society Conference, Vol. 10, D Douglass and F. Kunz ed., (Interscience, N.Y. 1961).

39. T. Hurleen, "Oxidation of Niobium," J. Inst. Met. 89, 273 (1961).

40. R. Powers and M. Doyle, "Diffusion of Interstitial Solutes in Group 5 Transition Metals," J. Appl. Phys., 30, 514 (1959).

41. L. Van Torne, and G. Thomas, "Phase Transformation in Niobium Involving Interstitials," Acta Mett. 12, 601 (1964).

42. M. Strongin, H. Farrell, H. Halama, O. Kammerer, and C. Varmazis, "Surface Condition of Niobium for Superconducting RF Cavities," Part. Accel. 3, 209 (1972).

43. N. Terao, "Structures des Oxydes de Niobium," Jap. J. App. Phys. 2, 156 (1963).

44. W. Bauer, A. Citron, G. Dammertz, M. Grundner, L Husson, H. Lengeler, and E Rathgeber, "Studies of the CERN-Karlsruhe Superconducting RF Particle Separator," IEEE Trans. Nuc. Sci. NS22, 1144 (1975).

45. P. Karulkar and J. Nordman, "Study of Thin Nb Oxide Films," J. Vac. Sci. Tech. 17 262 (1980).

46. J. Sanz and S. Hoffman, "AES and XPS Studies of the Oxidation of Polycrystalline Ta and Nb at Room Temperature and Low Oxygen Pressures," J. Less Com. Met. 92, 317 (1983).

47. M. Grundner and J. Halbritter, "XPS and AES Studies on Oxide Growth and Oxide Coatings on Niobium," F. Appl. Phys. 51, 397 (1980).

48. F. Kover and M. Musselin "Anodic Oxide Films on Titanium, Niobium, and Tantalum," Thin Solid Films 2, 211 (1968).

49. A. Joshi and M. Strongin, "Surface Segregation of Oxygen in Niobium-Oxygen and Tantalum-Oxygen Alloys," Scr. Metall. 8, 413 (1974).

50. S. Hofmann, G. Blank, and H. Schultz, "Oberflachensegreghation von Sauerstoff in Niob," Z. Metall. 67, 189 (1976).

51. H. Hahn and H. Halama, "AES Depth Profile Measurements of Niobium for Superconducting Cavities," J. Appl. Phys. 47, 4629 (1976).

52. I. Lindau and W. Spicer, "Oxidation of Nb as studied by the UV-Photoemission Technique," F. Appl. Phys. 45, 3720 (1974).

53. H. Farrell and M. Strongin, "The Interaction of Oxygen and Nitrogen with the Niobium (100) Surface I," Surf. Sci. 38, 18 (1973).

54. T. Haas, A. Jackson, and M. Hooker, "Adsorption on Niobium (110), Tantalum (110), and Vanadium (110) Surfaces," J. Chem. Phys. 46, 3025 (1967).

55. R. Pantel, M. Bujor, J Bardolle, "Continuous Measurement of Surface Potential Variations during Oxygen Adsorption on the (100), (110), and (111) Faces of Niobium using Mirror Electron Microscope," Surf. Sci. 62, 589 (1977).

56. G. Albrecht, J. Richter, and P. Weber, "Properties of Niobium-Based Josephson Tunnel Elements in Junction Microstructures," J. Low Temp. Phys 48, 61 (1982).

57. J. Nordman, "Thin Film Josephson Junctions using Getter-Sputtered Niobium," J. Appl. Phys. 40, 2111 (1969).

58. K. Schulze, "Preparation and Characterization of Ultra-High-Purity Niobium," J. of Metals 33 (May 1981).

59. M. Tinkam, Introduction to Superconductivity, 77 (R. E. Krieger Pub. Co., Huntington, N.Y., 1980).

60. P. Kneisel, O. Stoltz, and J. Halbritter, "On Surface Preparation and Measurement of Niobium Used in High Frequency Cavities," J. Appl. Phys. 45, 2296 (1974).

61. C. Varmazis and M. Strongin, "Inductive Transition of Niobium and Tantalum in the 10 MHz Range," Phys. Rev. B 10, 1885 (1974).

62. W. DeSorbo, "Effect of Dissolved Gases on some Superconducting Properties of Niobium," Phys. Rev. 132, 107 (1963).

63. W. DeSorbo, "Size Factor and Superconducting Properties of some Transition Metal Solutions," Phys. Rev. 130, 2177 (1963).

64. M. Robinson and H. Roetschi, "AC Polarization in β-Modification Nb_2O_5 Single Crystals," J. Phys. Chem. Sol. 29, 1503 (1968).

65. E. Greener, D. Whitmore, and M. Fine, "Electrical Conductivity of Near Stoichiometric α-Nb_2O_5," J. Chem. Phys. 34, 1017 (1969).

66. J. Turneaure and N. Viet, "Superconducting Nb TM 010 Mode Electron-Beam Welded Cavities," Appl. Phys. Let. 16, 333 (1970).

67. P. Ceperley, I. Ben-Zvi, H. Glavish, and S. Hanna, "Superconducting Re-entrant Cavities for Heavy Ion Linacs," IEEE Trans. Nuc. Sci. NS22, 1153 (1975).

68. P. Kneisel, O. Stoltz, and J. Halbritter, "On the Breakdown of a Superconducting Cavity at S-Band," J. Appl. Phys. 45, 2302 (1972).

69. H. Martens, H. Diepers, and R. Sun, "Improvement of Superconducting Nb Cavities by Anodic Oxide Films," Phys. Lett. 34A, 439 (1970).

70. E. Fromm and H. Jenn, "Reactions of Nb and Ta with Gases at High Temperatures and Low Pressures," Vacuum 19, 191 (1969).

71. H. Farrell, H. Isaacs, and M. Strongin,"The Interaction of Oxygen and Nitrogen with the Niobium (100) Surface II," Surf. Sci. 38, 31 (1973).

72. T. Haas, "A Study of the Niobium (110) Surface using LEED Techniques," Surf. Sci. 5, 345 (1966).

73. H. Padamsee, "A New Purification Technique for Improving the Thermal Conductivity of Superconducting Nb Microwave Cavities," IEEE Trans. Mag. MAG-21, 1007 (1985).

74. D. Peterson, B. Loomis, and H. Baker, "Purification of Vanadium by External Gettering," Metall. Trans. 12A, 1127 (1981).

75. R. Pasternak and B. Evans, "Adsorption, Absorption, and Degassing in the Oxygen-Niobium System at Very Low Pressures," J. Elchem. Soc. 114, 452 (1969).

76. P. Kneisel, R. Vincon, and J. Halbritter, "First Results on Elliptically Shaped Cavities," Nuc. Inst. Meth. 118, 669 (1982).

77. Ames Laboratory, Elecro-deposited niobium was electron-beam melted and rolled to 0.02" sheet at Ames Laboratory, University of Iowa. The RRR of this material varied locally from 90 to 200.

78. P. Clausing, "The Flow of Highly Rarified Gases through Tubes of Arbitrary Length," J. Vac. Sci. Tech. 8, 636, (1971).

79. P. Kneisel, "Results of some LALA Calculations for Accelerator Cavities with Elliptically shaped cross-sections," internal report SRF-820703, Laboratory of Nuclear Studies, Cornell University, Ithaca, N.Y. (July, 1982).

80. K. Krafft, Ph.D. Dissertation, Cornell University, Ithaca N.Y. (1983).

81. P. Kneisel, "Surface Preparation of Niobium," Proceedings of the Workshop on RF Superconductivity, M. Kuntze ed., 27 (Kernforschungszentrum Karlsruhe, 1980).

82. P. Niederman, N. Sankarra, R. Noer, and O. Fischer, "Field Emission from Broad-Area Niobium Cathodes--Effect of High Temperature Treatment," J. Appl. Phys. 59, 896 (1986).

83. R. Kirby, F. Palmer, E. Garwin, F. King, and M. Tigner, to be published.

84. A. Phillip and J. Halbritter, "Investigation of the Gap Edge Density of States at Oxidized Niobium Surfaces by RF measurements," IEEE Trans. Mag. Mag-19, 999 (1983).

85. M. Bahl, "ESCA Studies of Some Niobium Compounds," J. Phys. Chem. Solids 36, 485 (1975).

86. H. Padamsee, "Influence of Thermal Conductivity on the Breakdown Field of Niobium Cavities," IEEE Trans. Mag. MAG-21, 149 (1985).

87. D. Rudman, R. Howard, D. Moore, R. Zubeck, and M. Beasly, "Fabrication and Barrier Diagnostics of Superconductive Tunnel Junctions on Nb-Sn and V-Si," IEEE Trans. Mag. MAG-15, 582 (1979).